Head and Bond Contributions to Anchorage of a Headed Reinforcing Bar

by

Andrew M. Blau

A Report Submitted to the Faculty of the

Milwaukee School of Engineering

in Partial Fulfillment of the

Requirements for the Degree of

Master of Science in Structural Engineering

Milwaukee, Wisconsin

June 2010

Abstract

Headed reinforcing bars are becoming more popular in the construction industry; however, there is relatively little known about the interaction of the head and bond in resisting loads. As such, the ACI 318-08 (the 2008 version being the current version) code equation governing headed reinforcing bars appears to be a gross generalization of the capacity of a headed bar. The purpose of this project was to study the contributions of the head and bond as they change with varying bond lengths, clear covers, and head bearing areas to determine if a better model can be developed to represent a headed bar. Twelve headed bar specimens were cast, each one with a unique combination of bone length, clear cover, and head bearing area, and loaded until failure. Two failure modes were observed: bar yielding and side blowout. The loads resisted by the head and bond throughout the loading of each specimen were analyzed for trends. It was determined that headed bars follow one of two patterns: head-dominated and bond-dominated, and is dependent on bond length. As such, different models should be used for the capacity of each pattern. The specimen capacities were compared to models proposed by others, and the current ACI 318-08 code equation. The ACI 318-08 code equation was found to be a good fit with a minor modification for the bond-dominated bars. It was determined to not be possible to develop a model for head-dominated bars from this test program and that additional testing must be conducted.

Acknowledgments

I would like to thank my advisor, Dr. DeVries, and my committee, Dr. Stahl and Prof. Raebel, for helping me conduct this research over the past year. Their support and guidance are greatly appreciated. I would also like to thank my family for always supporting me. Finally, I'd like to thank Allison for her support, understanding and encouragement throughout the course of this project.

Table of Contents

List of Figures

List of Tables

Glossary

Anchorage Length	The portion of the bond length that passes through the CCT node of the specimen (see Figure 37 on page 50).
Bond Length	The length of a bar that is exposed to concrete during casting and resists load through bearing between the ribs on the bar and the concrete (see Figure 37 on page 50).
CCT node	Compression-Compression-Tension node. The point where two struts and one tie come together in a strut and tie model (see Figure 37 on page 50).
Embedment Length	The distance along that headed bar from the head to the face of the concrete specimen where the headed bar extends out (see Figure 37 on page 50).
Head	The bar of steel attached to the end of the Headed bar that resists force in the bar through the concrete bearing against the surface of the head. In terms of load sharing, the percentage of the load on the headed bar that is resisted by the head.
Head Slip	The distance that the head moved in the direction of the tensile force being applied.

Headed Bar	A deformed reinforcing bar with a head on one end that is cast into the test specimen and will have a tensile force applied to it in this test.
Side Blowout	A failure mode where the concrete cover over a bar or head spalls, or breaks, off and occurs most commonly with large embedment depth to side cover ratios.
Stiffness	A value calculated for each specimen by dividing the load applied to the headed bar by the head slip.
Straight Bar	A deformed reinforcing bar with no head.

Chapter 1: Introduction

As concrete strengths rise, the amount of steel reinforcing required also increases, which can create congestion problems. Headed reinforcing bars are becoming increasingly advantageous to use where rebar congestion is a problem; however, there is little information available about the manner in which the head and bond work together to resist the load. Therefore, an accurate model of a headed reinforcing bar has yet to be developed. This project will analyze the contributions of the head and bond of a headed, deformed reinforcement bar in beam-end specimens to gain a better insight as to how each work together to resist load. Tests were conducted on twelve beam-end specimens with headed, deformed bars where the bond length, clear cover and head bearing area will be varied. The specimens were all repeatedly loaded except when they failed during the first load cycle. These test data were then compared to test data from straight deformed bars without a head having the same bond length and clear cover. The data from each of the specimens will be analyzed to find relationships between the bond length, clear cover and head bearing area and the contributions of the head and bond, and ultimately the capacity of the headed reinforcing bar.

Chapter 2: Background

Reinforced concrete design provides advantages when the reinforcing bars and concrete work in unison to resist the applied loads. The metal reinforcing bars that resist all of the tensile loads in the concrete member must be designed to transfer all of the tensile force to the concrete. In the case of standard deformed bars, the force transfer develops as a result of the bond between the concrete and the bar in which the concrete bears against the ribs of the steel bars (see Figure 1). With this method of force transfer,

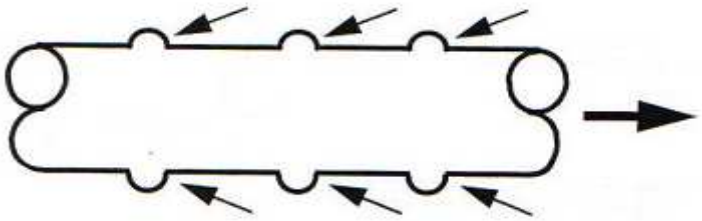

Figure 1: Force Transfer for Deformed Bars [1].

the amount of stress a bar can transfer to the concrete is a factor of the bond length of the bar. When required development length of a bar exceeds the available bond length, another method must be used to transfer the additional force. This has typically been done by bending a hook into the end of the bar which provides additional bearing area (see Figure 2). As the amount of steel in concrete structures keeps increasing, however, using hooks creates bad congestion problems. From this problem, headed reinforcing bars were developed in the offshore oil platform field where they are used to anchor longitudinal reinforcement bars in lieu of hook bars [1]. Headed bars have also been used in highway footings for added strength and in repairs [1]. Headed bars resist load much like hooked bars by providing additional bearing area but heads are much smaller than hook tails (see Figure 3). The use of headed reinforcing bars in the building construction industry, however, is still rather new and requires more research.

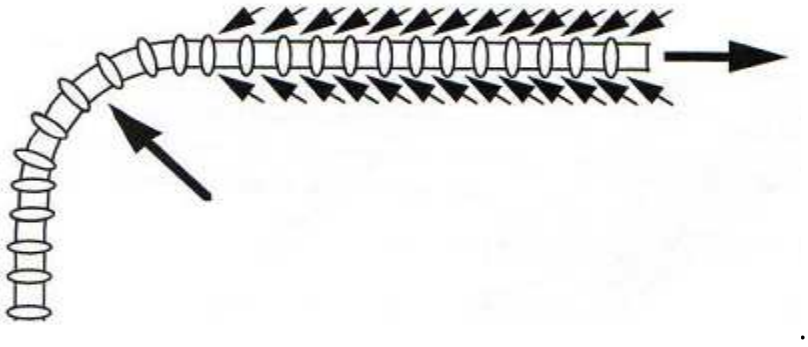

Figure 2: Force Transfer for a (90 Degree) Hooked Bar [1].

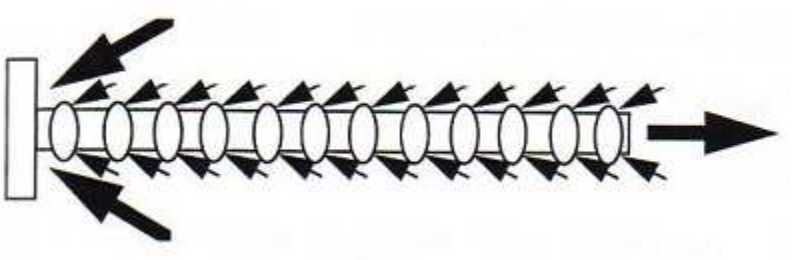

Figure 3: Force Transfer for a Headed Bar [1].

The other main reason that headed reinforcement bars are being considered in the design process more frequently now is that the manufacturing process has become more feasible and efficient from advancements in the industry [1]. Headed bars can be manufactured in multiple ways. Heads can be attached to bars with friction welding, arc or induction welding, forging or threaded onto the bar [2]. The friction welding process consists of spinning the bar while pressing the head against the end of the bar such that the friction creates great amounts of heat and welds the head to the bar [1]. When the heads are threaded onto the bar, parallel threads are cut into the head and the end of the bar. There are also several options for the head itself. Heads can be specially manufactured head pieces, or be cut from standard steel bar stock.

Chapter 3: Previous Tests

Headed bars have been studied by others in attempts to understand the contributions of the head and bond in order to develop better models. It is useful to review such tests to provide additional insight into the behavior of headed bars as well as different testing methods and strategies. The work of Zimdahl, Chun *et al.*, DeVries, and Thompson will be reviewed [3, 2, 1, 4, respectively].

3.1: Zimdahl

Zimdahl tested beam-end specimens to study the behavior of headed bars – more specifically, the manner in which the bond and head work together to resist a tensile load [3]. Zimdahl's specimen blocks represent the beam-end configuration found at the top of a beam-column (see Figure 4 and Figure 5), and therefore the cover over the bar and head are minimal. Zimdahl tested twelve specimens in which the variables were bond length

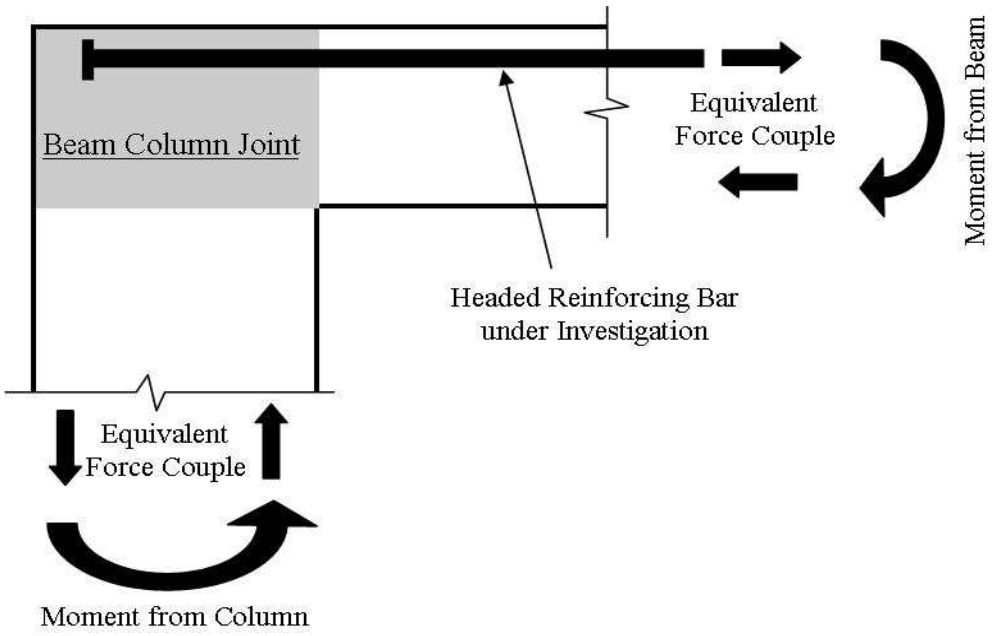

Figure 4: Origin of Zimdahl Specimen Block.

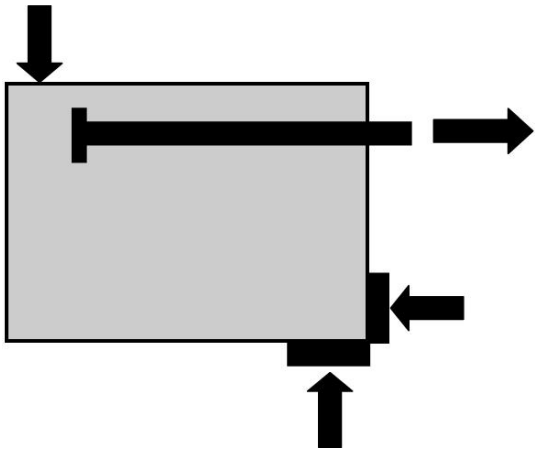

Figure 5: Zimdahl Specimen Block.

and clear cover in six unique combinations (see Table 1). Zimdahl used 4” x 2”x x0.75” plates for heads, which were friction welded to the bars (see Figure 6). The specimens measured 12” wide, 24” tall and 32” long (parallel to the headed bar) (see Figure 7) [3]. The specimen blocks were loaded into a test frame and a tensile load was applied to the headed bar via a hollow-core hydraulic cylinder (see Figure 8). For each unique variable combination, Zimdahl tested one specimen monotonically until failure, and the other specimen repeatedly [3]. During the tests, Zimdahl measured load on the headed bar,

Table 1: Zimdahl’s Variable Combinations [3].

ID	Clear Cover (inches)	Clear Cover (bar diameter, d_b)	Nominal Bonded Length (inches)
1HB00M	1	1	0
1HB00R	1	1	0
1HB08M	1	1	8
1HB08R	1	1	8
1HB16M	1	1	16
1HB16R	1	1	16
2HB00M	2	2	0
2HB00R	2	2	0
2HB08R	2	2	8
2HB08R2	2	2	8
2HB16R	2	2	16
2HB16R2	2	2	16

Figure 6: Headed Bar Specimen [3].

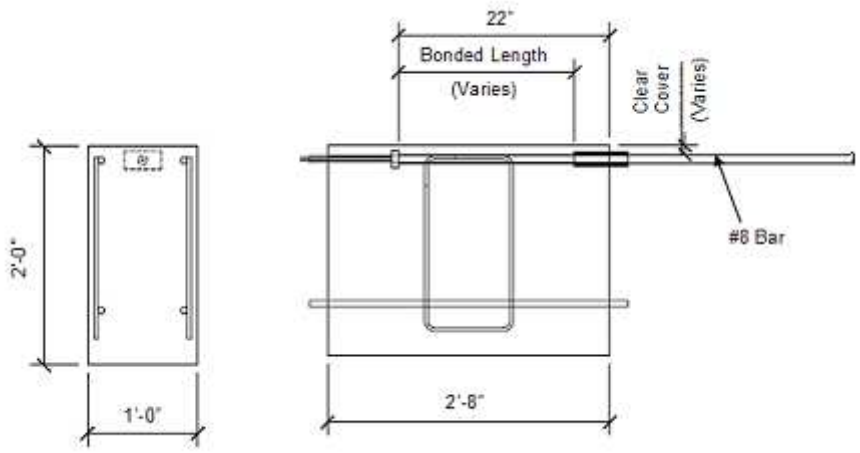

Figure 7: Beam End Specimen [3].

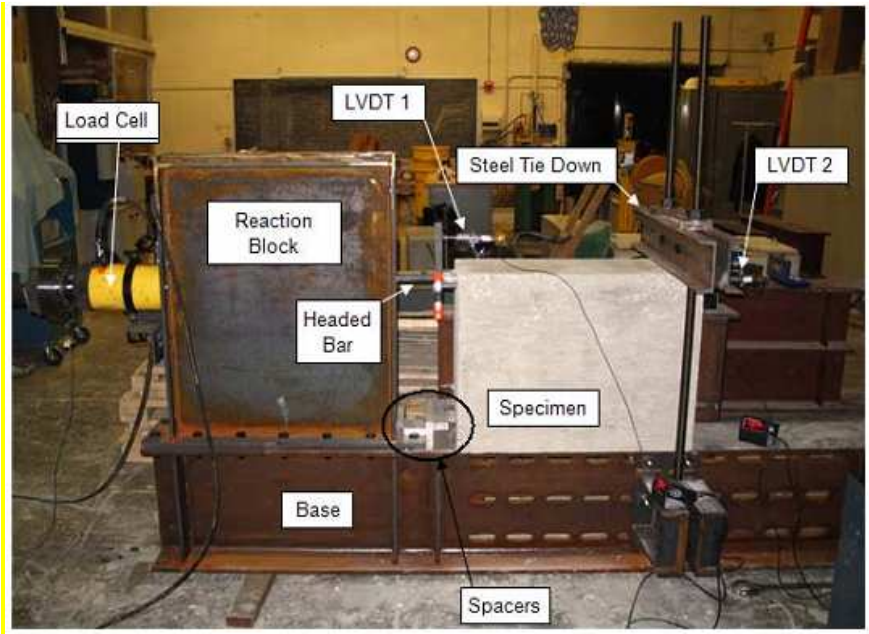

Figure 8: Test Frame Setup [3].

head slip, and lead slip of the bar. Zimdahl observed three different failure modes: tension yielding of the reinforcement bar (see Figure 9), side blow out of the concrete (see Figure 10 and Figure 11), and shear failure of the concrete (see Figure 12) [3]. Zimdahl based her analysis on a stiffness value that she calculated for each specimen because she did not have data on the contributions of the head and bond. The stiffness for a specimen was calculated from the head slip and the applied load. When analyzing

Figure 9: Typical Cracking Pattern of Specimens with Tension Yielding [3].

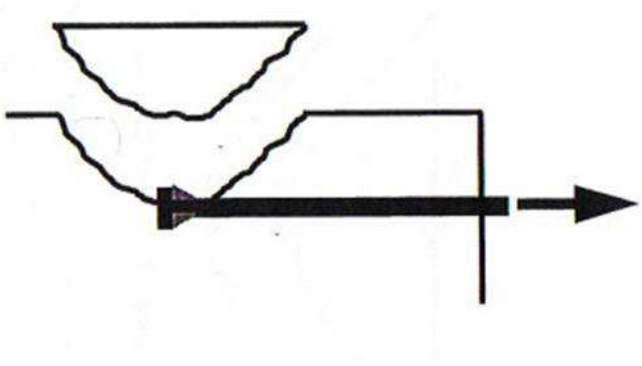

Figure 10: Side Blowout Mechanism [1].

the data she collected, Zimdahl found that there was no substantial difference between repeated loading and monotonic loading of the specimens [3]. More importantly, regarding her search for the roles of bond and head capacity, Zimdahl found that it is inaccurate to add a given bond length capacity to the capacity of a given head size to determine the capacity of a bar with that bond length and head size [3]. Rather, only a portion of each piece is used in the total capacity of the headed bar. Zimdahl also suggested that with less clear cover, a larger portion of the load is resisted by the head

Figure 11: Typical Cracking/Failure Pattern of Side Blowout [3].

Figure 12: Typical Cracking Pattern of Shear Failure [3].

of the bar [3]. Zimdahl also found that the stiffness of the headed bars with 16” of embedment length, both 1” and 2” of cover, was less than the straight bars with 16” of embedment length and the same cover [3]. Zimdahl used the stiffness value she had

calculated for each specimen (see Table A-1 in Appendix A) and Equation (1) to see if a consistent model could be created to predictably determine the capacity of the headed bar [3]:

$$\alpha k_{SB} + \beta k_{HB} = k_{TOTAL} \quad (1)$$

where,

α = the percentage of bonded length stiffness required,

k_{SB} = the stiffness of the average straight bar specimen,

β = the percentage of head stiffness required,

k_{HB} = the stiffness of the average headed bar with 0" bonded length,

and

k_{TOTAL} = the total stiffness of the headed bar.

Zimdahl tested five different combinations of values for the coefficients α and β (see Table 2). After analyzing each of the variable combinations against the measured stiffness of all of the specimens, Zimdahl found that none of these combinations can provide an accurate model. Zimdahl reported that it appeared that bond length has more of an effect on the α and β values than does the depth of clear cover [3]. Zimdahl concluded that an increase in clear cover has a positive relationship to stiffness as was anticipated and that bond length had a negative relationship with stiffness [3].

Table 2: Stiffness Equation Coefficient Combinations Analyzed by Zimdahl [3].

Theory	α	B
1	1.0	Measured stiffness set = to k_{TOTAL} and β solved for
2	Measured stiffness set = to k_{TOTAL} and α solved for	1.0
2.1	0.75	1.0
3	Measured stiffness set = to k_{TOTAL} and α solved for	Set equal to 0.3 by use of an equation derived by Thompson
4	0.5	0.5

3.2: Chun *et al.*

Chun *et al.* tested idealized exterior beam-column joints (see Figure 13) to evaluate the concrete contribution to the anchorage strength of headed bars [2]. Chun *et al.* tested thirty specimens with different combinations of the variables of embedment length and bar diameter (see Table 3). The column widths (B) were designed as six times the bar diameter and the entire embedment length was used as a bond length. The heads used were a new circular, screw-on system with an area equal to four times the bar area (see Figure 14). Chun *et al.*'s thirty specimens were modeled on the beam-end connection at mid column and tested both headed and hooked bars acting as CCT nodes [2]. The hooked bar tests (indicated with an "M" in the specimen designation in Table 3) will not be reviewed as they do not pertain to this test program.

Chun *et al.* surmised that when proper embedment and head geometry are used, beam-column connections will fail due to the joint shear mode, and they therefore focused on that type of failure [2]. Side blowout was not expected to control as in Zimdahl's tests due to the large amount of cover provided above the head by the column continuing upwards. To test the specimens, idealized beam flexure loads were applied to the column as a compression-tension force couple, and axial column loads were not

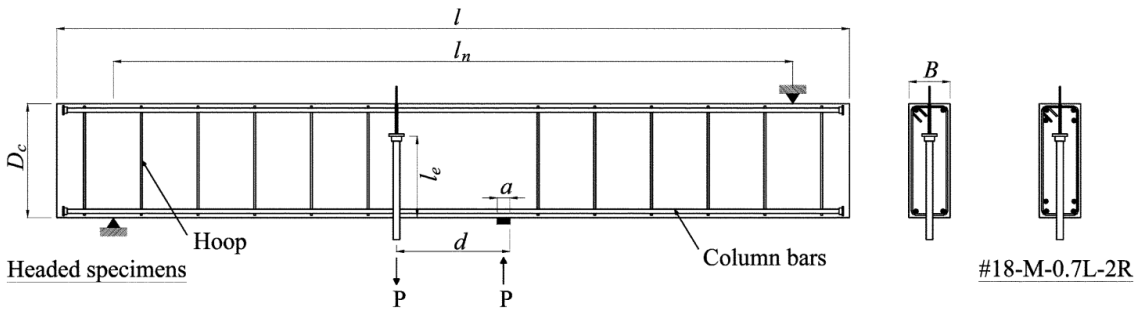

Figure 13: Details of Specimens [2].

Table 3: Chun *et al.*'s Variable Combinations [2].

Specimen ID*	l_e†, mm (in.)	Column bars	N‡	Details of specimens,§ mm (in.), MPa (ksi)
No. 18-H-0.9L	908 (35.7)	Four No. 11	1	B = 350 (13.8); a = 105 (4.1); l = 6708 (264.1); l_n = 5748 (226.3); $D_c = d$ = 958 (37.7); Hoop = No. 5 at 480 (18.9); f_c' = 24.2 (3.51); and f_y = 447.7 (64.92).
No. 18-M-0.9L	888 (35.0)	Four No. 11	2	
No. 18-M-0.7L	684 (26.9)	Four No. 11	2	
No. 18-M-0.7L-2R	684 (26.9)	Eight No. 11	2	
No. 18-M-0.5L	479 (18.9)	Four No. 11	2	
No. 18-H-0.5L	499 (19.6)	Four No. 11	1	
No. 11-H-0.9L	384 (15.1)	Four No. 8	1	B = 220 (8.7); a = 65 (2.6); l = 3044 (119.8); l_n = 2604 (102.5); $D_c = d$ = 434 (17.1); Hoop = No. 4 at 300 (11.8); f_c' = 24.6 (3.57); and f_y = 450.6 (65.34).
No. 11-M-0.9L	372 (14.6)	Four No. 8	2	
No. 11-M-0.7L	295 (11.6)	Four No. 8	2	
No. 11-M-0.7L-2R	295 (11.6)	Four No. 11	2	
No. 11-M-0.5L	217 (8.5)	Four No. 8	2	
No. 11-H-0.5L	229 (9.0)	Four No. 8	1	
No. 8-H-0.9L	273 (10.7)	Four No. 6	1	B = 160 (6.3); a = 45 (1.8); l = 2258 (88.9); l_n = 1936 (76.2); $D_c = d$ = 323 (12.7); Hoop = No. 3 at 200 (7.9); f_c' = 25.1 (3.64); and f_y = 454.8 (65.95).
No. 8-M-0.9L	264 (10.4)	Four No. 6	2	
No. 8-M-0.7L	212 (8.3)	Four No. 6	2	
No. 8-M-0.7L-2R	212 (8.3)	Four No. 8	2	
No. 8-M-0.5L	161 (6.3)	Four No. 6	2	
No. 8-H-0.5L	170 (6.7)	Four No. 6	1	

*No. ①-②-③L-④R: ① bar designation number; ② H-hooked bar, M-headed bar; ③ embedment length to column depth ratio; ④ "2R" denotes that the specimen was reinforced with twice the normal column reinforcements.
†l_e = embedment length.
‡N = number of specimens.
§Refer to Fig. 4.

Figure 14: Chun *et al.*'s Headed Bar Specimen [2].

applied as previous tests indicated that such loads tend to improve joint behavior [2]. Also, the effects of boundary conditions were reduced by using a longer specimen length [2]. Chun *et al.* found that as load was applied to the bars, the bar bond resisted all of the

load until the load reached the bond capacity for the bar, at which time the head began resisting the applied load (see Figure 15). Figure 15 shows the bond and head contributions for two different samples. Both bars were #18's with an embedment length of 35" and an embedment length to column depth ratio of 0.9. With the same embedment length, the hooked bar has less bond length due to the bend radius of the hook. The darker lines represent the headed bar and the lighter lines represent the hooked bar. Chun *et al.* found that the head bearing strength depends on the embedment depth in two ways. First, if the embedment depth is too shallow, the joint strut cannot confine the head and therefore strut and tie modeling cannot be used. Second, the head bearing cannot be fully developed in shallow embedment situations and is therefore proportional to the embedment length. From the data, Chun *et al.* found that when the embedment length was $0.7D_c$, the head bearing stress was equal to the effective compressive strength of the concrete and that the head bearing stress decreases linearly with shallow embedment and increases linearly with deep embedment longer than $0.7D_c$ (see Figure 16) [2]. Performing a linear regression on the data, Chun *et al.* developed Equation (2) to model head behavior:

$$P_{head} = \left[1 + 2.27\frac{(l_e - 0.7D_c)}{D_c}\right] 0.85 f_c' A_{nh} \quad \text{with } A_{nh} = A_h - A_b \tag{2}$$

where,

P_{head} = head capacity (kips),

l_e = embedment length (in),

D_c = column depth (in),

f'_c = compressive strength of concrete (ksi),

A_{nh} = net head area (in^2),

A_h = gross head area (in^2),

and

A_b = area of the bar (in^2).

In analyzing the bond strength, Chun *et al.* determined that interior CCT nodes (see

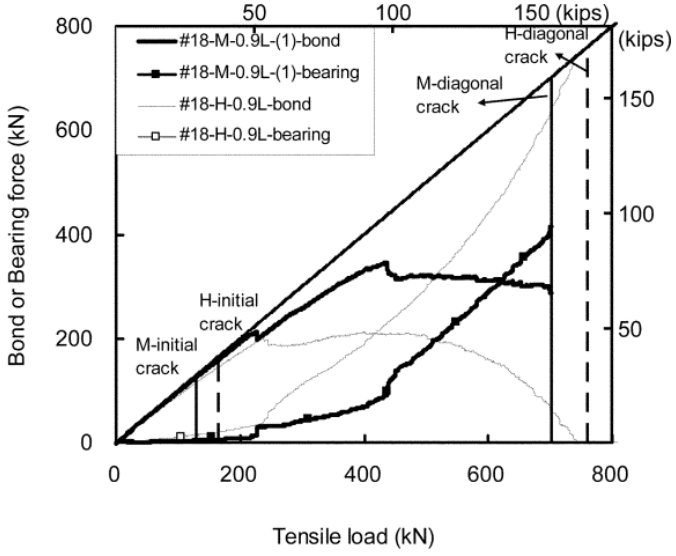

Figure 15: Bond and Head Bearing Contribution to Anchorage Strength [2].

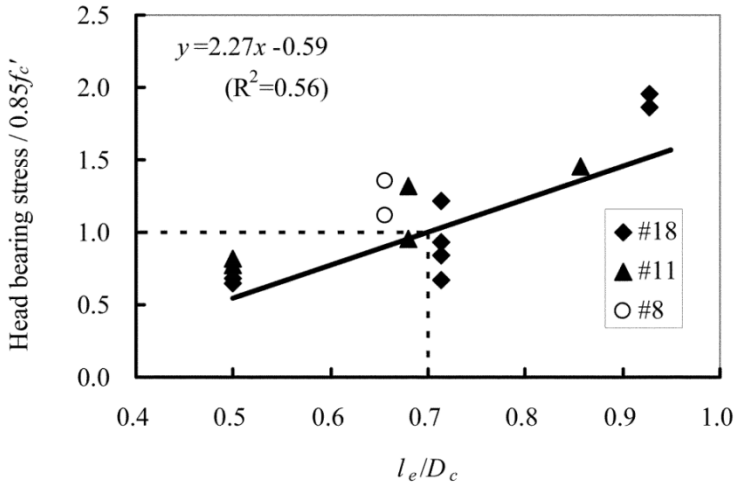

Figure 16: Relationship between Normalized Head Bearing and Normalized Embedment [2].

Figure 17b) may have a higher bond strength than the exterior CCT nodes (see Figure 17a) due to the directions of shear stresses of the concrete bond to the reinforcing bar. To analyze the bond stresses, strain gauges were applied along the entire embedment length of the bar at an equal spacing. The data showed that the stresses had no relationship with the embedment length [2]. Chun *et al.* developed Equation (3) to model the bond strength:

$$P_{bond} = 6.07\sqrt{f_c^{'}}\varphi_b\left(l_e - d_b\right) \tag{3}$$

where:

$\varphi_b = \pi d_b$,

and,

d_b = bar diameter.

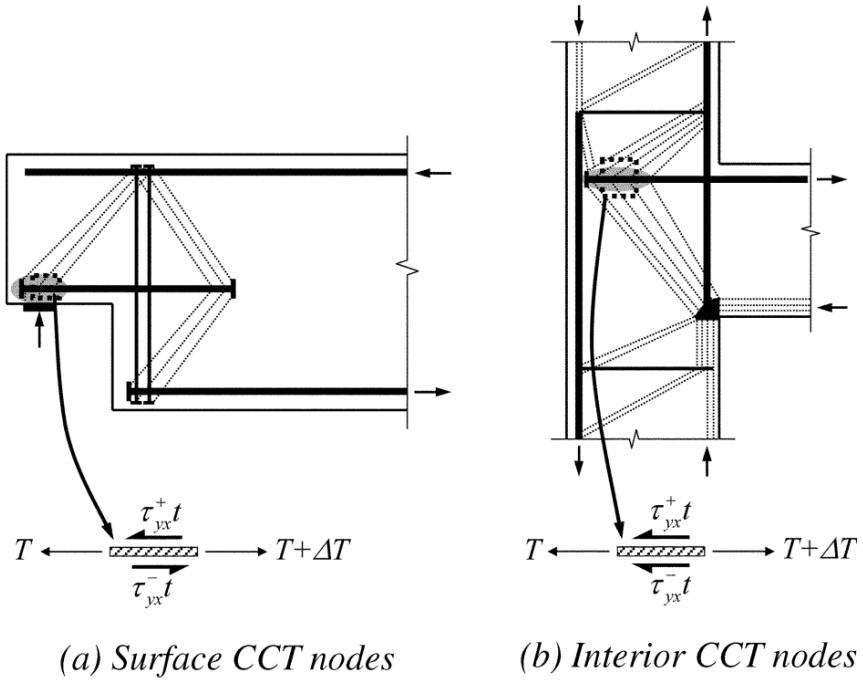

Figure 17: Shear Stress Distribution on Headed Bar [2].

Combining Equations (2) and (3) produces the anchorage capacity for headed reinforcing bars with at least $3d_b$ side cover measured to the center of the bar:

$$P = \left(P_{bearing} + P_{bond} \right),$$

$$P = \left[\left(1 + 2.27 \frac{l_e - 0.7 D_c}{D_c} \right) 0.85 f_c^{'} A_{nh} + 6.07 \sqrt{f_c^{'}} \phi_b \left(l_e - d_b \right) \right]. \quad (4)$$

To be used as a design equation, Equation (4) was adjusted to cover the 5% fractile:

$$P = n_{5\%} \left[\left(1 + 2.27 \frac{l_e - 0.7 D_c}{D_c} \right) 0.85 f_c^{'} A_{nh} + 6.07 \sqrt{f_c^{'}} \phi_b \left(l_e - d_b \right) \right] \quad (5)$$

where,

$n_{5\%}$ = the 5% fractile coefficient that adjusts the equation such that only 5% of the specimens fall below the design value; in this case, it was determined to equal 0.78.

Chun *et al.* concluded that due to the limitless design configurations and resulting failure modes, specific models should be used for various design conditions rather than a generalized design model for headed bars.

3.3: DeVries

DeVries performed pullout tests on over 140 headed reinforcing bars, testing variables including embedment depth, clear cover, close spacing, bar diameter, head size, head shape, head thickness, head orientation, transverse reinforcing in the anchorage zone of headed bars and additional development length [1]. DeVries studied both shallow embedment and deep embedment cases with a ratio of 5.0 of embedment depth to side cover as the dividing line. Further, DeVries tested edge and corner bars in each embedment case as well as single bars and bar groupings. Of the more than 140 bars that

were tested, only the 77 deep embedment, single edge bars will be reviewed as the shallow embedment, corner, and grouped bars do not apply to this test program.

As a result of locating bars near the edge of concrete specimens, the minimal clear cover causes pullout-cone or side blowout to be the governing failure modes of the anchorage strength as long as bar yield and fracture are designed adequately [1]. DeVries used eighteen blocks with four to twelve headed reinforcing bars cast around the perimeter for testing (see Figure 18). The bars were located in the blocks such that the anticipated failure surfaces would not interfere with each other [1]. The blocks each measured 36" deep and were either 36" by 36" square, or 48" by 48" square [1]. A standard head size was used for each bar size (see Table 4); however, non-standard head sizes were used for a few of the bars [1]. Bond lengths ranged from 0" to 24.0" and clear

Figure 18: DeVries's Specimen Block with Load Cylinder [1].

Table 4: Bar and Standard Head Sizes [1].

	Nominal Head Sizes (in)	
Bar Diameter (in)	**Square**	**Rectangular**
#6	2 x 2 x ½	2 ¾ x 1 $^{3}/_{8}$ x $^{5}/_{8}$
#8	2 ¾ x 2 ¾ x $^{5}/_{8}$	3 $^{1}/_{8}$ x 1 ½ x ¾
#11	3 ½ x 3 ½ x ¾	4 x 2 $^{1}/_{8}$ x 1

cover ranged from 0.75” to 5” [1]. The concrete mixes for the blocks were all standard mixes ranging in strength from 3,000 psi to 7,000 psi. DeVries tested each bar by using a hollow-core hydraulic cylinder to apply a tensile load monotonically until failure directly between the concrete block and the bars (see Figure 19). Because the hydraulic cylinder sat on top of the concrete directly adjacent to the test bar, strut and tie effects did not develop. To reduce or eliminate any shock loading effects, the load was applied in no less than 8 stages for each bar with ample time between each stage for the specimen to settle [1]. Measurements of load, deflection, strain and crack width as well as photographs were taken at each stage and upon failure. All 77 of the deep-embedment, single edge bars failed by side blowout (see Figure 10) [1].

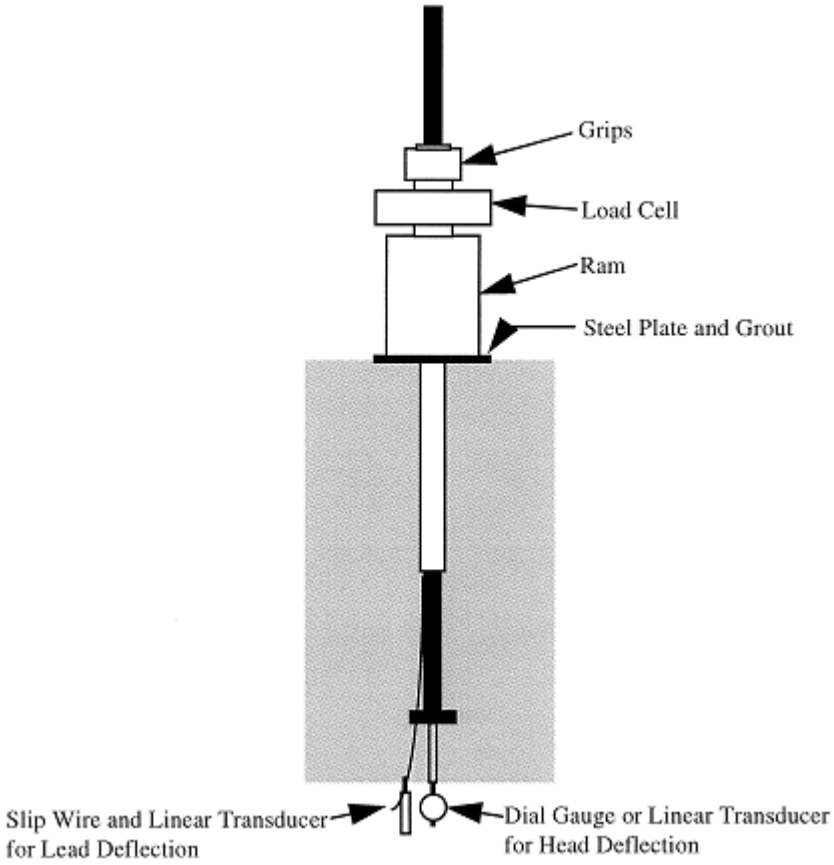

Figure 19: Test Equipment [1].

With the data collected, DeVries plotted the load versus head slip. For headed bars with no development length and no transverse reinforcement in the anchorage zone, DeVries found that head slip began immediately with load application and followed a slight curve up to bar capacity at which point side blowout occurred and deflection increased rapidly while the load decreased (see Figure 20) [1]. These bars also produced no cracking until just prior to failure [1]. With the loose cover removed after failure, the wedge which forms on the head that causes spalling, was visible in some of the specimens (see Figure 21). After the side blowout failure, some of the bars were subjected to additional deformations during which several of the bars yielded. DeVries, however, concluded from the unchanging head deflection and crack pattern that yielding had no impact on the blowout capacity of the anchorage [1].

Unlike bars with no development length, bars with development length, both with and without transverse reinforcement, developed a crack long before failure. The crack started at the beginning of the bond length nearest the load application and grew towards the head of the bar (see Figure 22). When comparing bars with similar head sizes, bar size, clear cover and concrete strength, Devries found that development length and

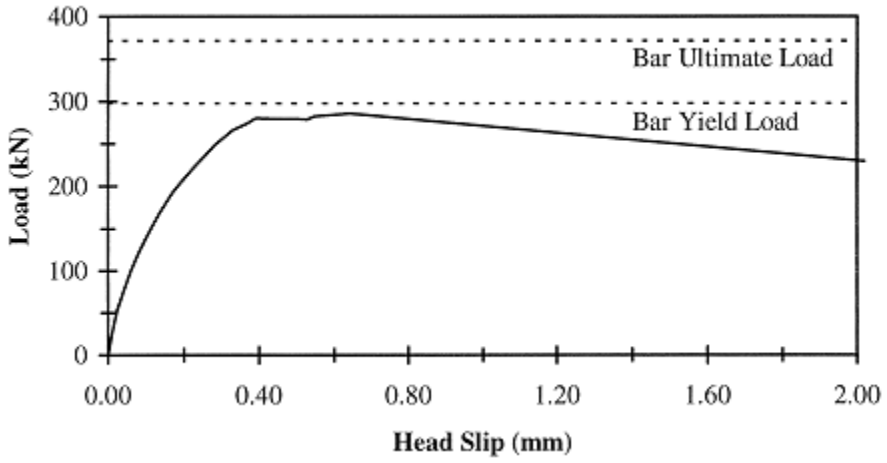

Figure 20: Load versus Head Slip for Headed Bar with no Development Length (Test ID: C19B5) [1].

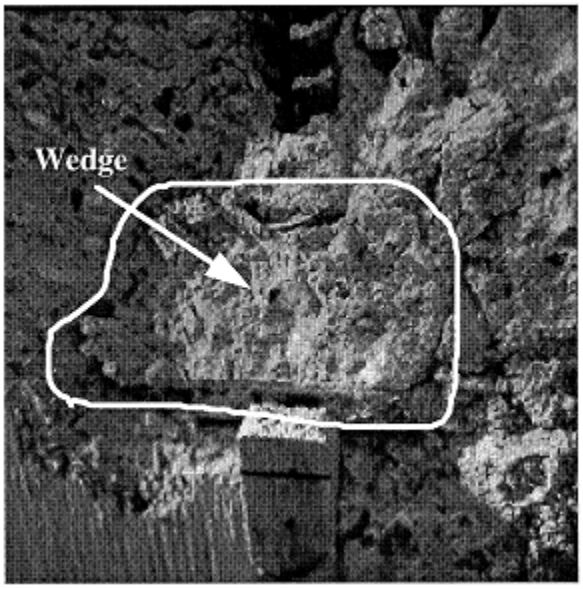

Figure 21: Wedge of Concrete Observed on Head After Failure [1].

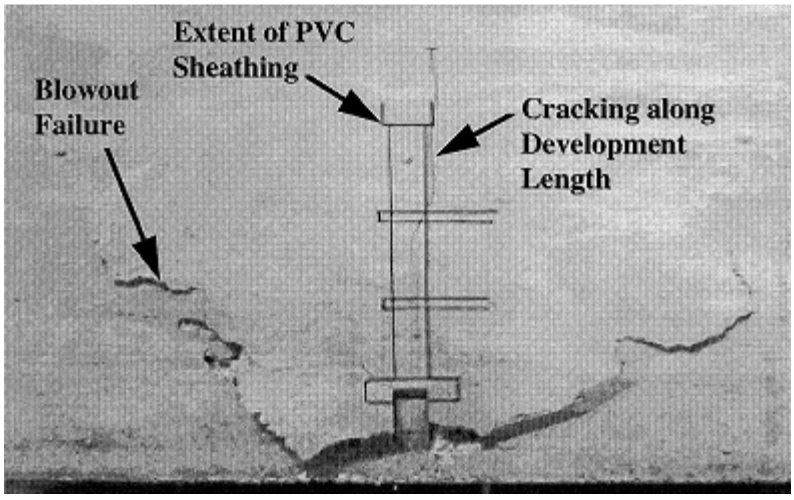

Figure 22: Cracking Along Development Length During Testing [1].

transverse reinforcement decreased head slip dramatically. Figure 23 shows the head slip comparison of three bars each with the same head size of 4" x 2 $^{1}/_{8}$" x 1". Development length is noted as l_d, and the amount of transverse reinforcing as A_{tr}.

From a series of 6 bar pairs in which the only difference between the two bars in the pair was head orientation, DeVries concluded that head orientation does not affect anchorage strength [1]. DeVries also concluded that development length does not have a

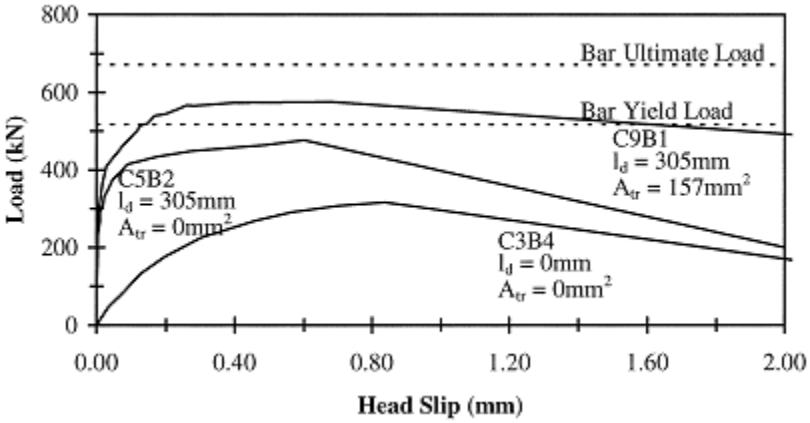

Figure 23: Load versus Head Slip for Various Deep-Embedment Tests [1].

big effect on anchorage capacity. In a series of 5 pairs of bars, even when the development length was doubled, the capacity only slightly increased.

Possibly the most relevant information to this test program from the DeVries analysis, however, were the results from a series of bars with strain gauges applied to the bar near the head. From those strain gauges, DeVries was able to determine the amount of load resisted by the head (see Figure 24). He found, initially, that the bond resisted most of the load, but as cracks form around the bar, load begins to transfer to the head. In Figure 24, the solid line is the force resisted by the head, while the dotted diagonal line is the total load applied to the bar. Had DeVries graphed the force resisted by the bond, the

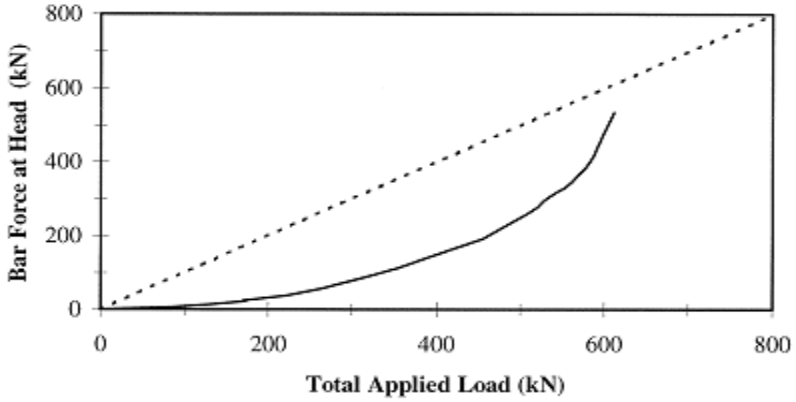

Figure 24: Head Contribution of Total Applied Load (Test ID: C9B3) [1].

graph would have looked very similar to what Chun *et al.* found (see Figure 15).

DeVries concluded that the three main contributing factors to anchorage capacity of a headed bar are head area, clear cover and concrete strength. DeVries found that all three factors had a positive relationship with anchorage capacity. In order to develop a capacity model, DeVries first performed a regression analysis to create a best fit equation (which has been calibrated to English units):

$$P_u = 60.2\left(C_1\right)^{0.609}\left(A_n\right)^{0.577}\left(f_c^{'}\right)^{0.671} \tag{6}$$

where:

P_u = capacity of headed bar (pounds),

C_1 = shortest edge distance (in),

A_n = net head area (in^2),

and

$f_c^{'}$ = compressive strength of concrete (psi).

DeVries then developed a model from the physical model (which has been calibrated to English units):

$$P_u = 55.4\left(C_1\right)^{1.33}\left(A_n\right)^{0.333}\left(f_c^{'}\right)^{0.667}. \tag{7}$$

Both models worked well; however, he reasoned that neither should be used for actual design situations due to the lack of development length variable in each equation. DeVries also noted that a design equation should be more conservative and include factors for corner placement and close spacing. With those goals in mind, DeVries developed this equation for design use which has been adjusted for the 5% fractile:

$$P_U = 151C_1\sqrt{A_n f_c^{'}}. \tag{8}$$

Note that the corner location and close spacing factors have been left off as they do not apply to this test program. The accuracy of Equation (6) is depicted in Figure 25. This equation is in an identical form to equations produced by others, including Furche and Eligehausen, noted DeVries. DeVries commented that development length does indeed increase anchorage strength (see Figure 23); however, it would be conservative to ignore the effects of development length. DeVries made this decision, noting that in many applications of headed reinforcement the available development length will likely be minimal. Further, the exclusion of development length in the model will provide reserve strength without increasing material cost appreciably [1].

3.4: Thompson

Thompson conducted tests on headed bars to study their uses in CCT nodes and lap splices as used in road construction per request of the Texas Department of Transportation (TxDOT); however, TxDOT also requested the specimens be designed as general as possible to allow the results to be used broadly [4]. The lap splice tests will not be reviewed as they do not pertain to this test program. Control tests were also conducted on straight and hooked bars to provide a basis for comparison. The general

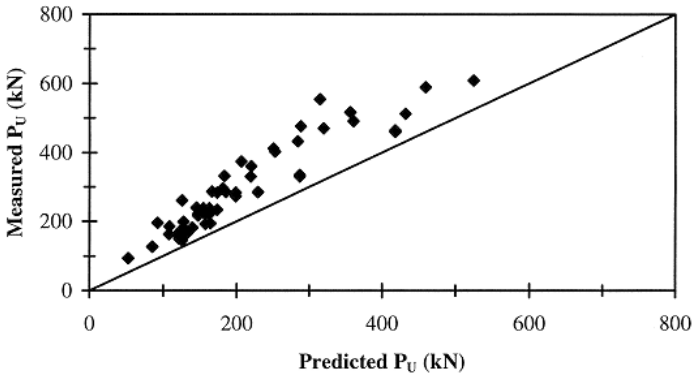

Figure 25: Comparison of Measured Capacities with Capacities Predicted by Characteristic Equation (Characteristic Equation: $P_u = 0.0125C_1A_n^{0.5}f_c^{0.5}$) [1].

focus of both tests was how the anchorage of the headed bars contributed to the strut-and-tie model of concrete design.

The CCT node test series was comprised of 64 specimens that were designed to test a single bar in a CCT node (see Figure 26). Variables tested included the angle of the compression strut, head size and shape (see Figure 27), bar size and presence of confinement reinforcement in the nodal zone. Thompson tested several different types of heads which resulted from different manufacturing techniques. Some heads were created by a forging process done to the end of the bar, while others were plates cut to size and welded to the reinforcing bars and other heads were threaded onto the bars. The specimens each measured 20” deep by 72” long while the width depended on the size of

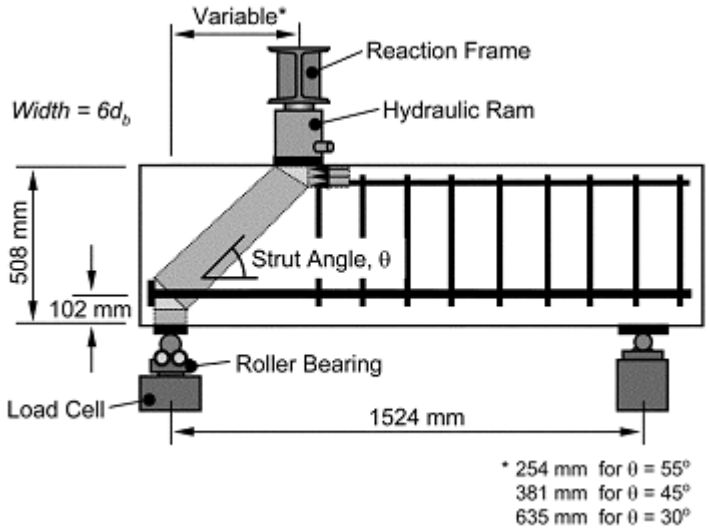

Figure 26: CCT Node Specimen and Test Setup [4].

Figure 27: Types of Heads Tested [4].

the headed bar and were 6” for a #8 bar and 8.5” for a #11 bar. The headed bar was centered and held 4” from the bottom of the specimen. Strut angles of 30°, 45°, and 55° were tested.

Fifty-nine of the specimens were cast without confinement in the node zone and therefore the hoop ties stopped where the load was applied (see Figure 26). Strain gauges were applied to the portions of the headed bars within the node zone to calculate stress, linear potentiometers were used to measure head slip, and a load cell was used to monitor load applied to the specimen. As in the case of the tests conducted by DeVries, the load was applied in steps, initially about 3-5 kips, and once cracking began, about 1-2 kips to avoid dynamic loading conditions.

Thompson’s most noteworthy conclusion concerned bond length used in strut and tie modeling. Thompson determined that it is more important to consider the length of bar that passes through the node and struts, which he called the anchorage length, than the full embedment length from the critical section to the head (see Figure 28 and Figure 29). Thompson explained that only the anchorage length should be used because it is only along the anchorage length that tension force gets transferred from the struts to the bar.

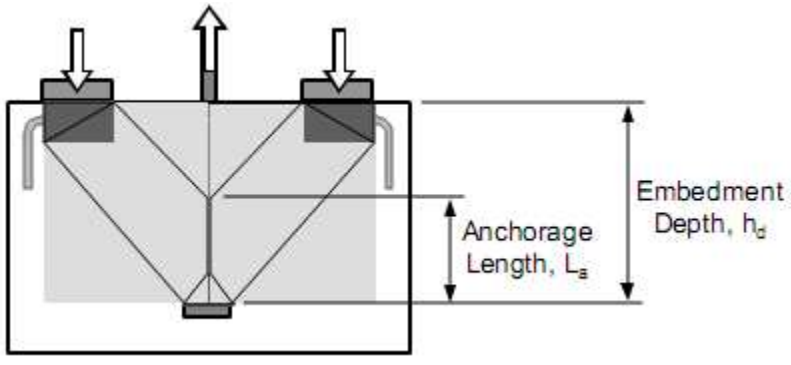

Figure 28: Anchorage Length Compared to Embedment Length [4].

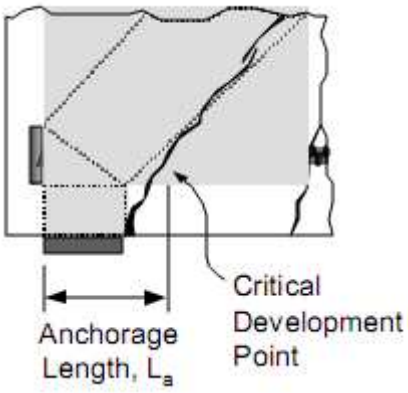

Figure 29: Anchorage Length as it Occurred in Thompson's Specimens [4].

Thompson's other findings largely corroborated DeVries' findings including the sudden and brittle failure typical of the specimens and the bond behavior [4]. Thompson found that shallower strut angles provided for better anchorage strength because shallower angles cause the CCT node to expand, which increased the anchorage length. Also, it was determined that the larger #11 bars resisted the load in a similar fashion to the smaller #8 bars. Similar to DeVries' findings, Thompson also found that the bar load was initially resisted primarily by bond, but as the load got closer to the bond capacity, the bond started to fail and the load became increasingly resisted by the head bearing. Thompson's plot of bond and head behavior (see Figure 30) is very similar to DeVries' (see Figure 24), where the head resists most of the maximum load and the bond resists less load than it had at a lower total bar load. Regarding head slip, Thompson found that larger heads decreased overall slip and also delayed initial head slip till higher loads. The specimens exhibited three different failure modes: pullout of the bar from the CCT node, rupture of the concrete strut, and yielding of the headed bar [4]. Bar pullout was limited to non headed bars, and rupture of the strut failure occurred in all specimens where bar yield did not appear.

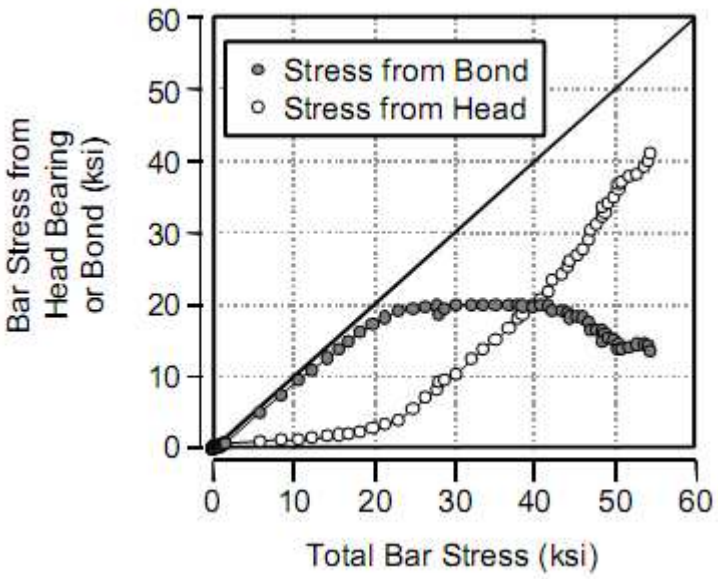

Figure 30: Components of Bar Stress Provided by Bond and Head Bearing [4].

In developing his model for head bearing capacity, Thompson concluded that the most important factors included concrete strength, head bearing area and clear cover. When analyzing the bond capacity, Thompson found a result interestingly opposite: the larger head sizes caused a decrease in the peak bond forces. This action may have resulted from the larger heads not allowing as much slip which may have not allowed optimum bond from occurring. Thompson noted that the ACI bond strength equation will not work in the strut and tie model as tested in this program because of the compressive force of the strut.

Thompson developed the following equations for headed bars with at least $6d_b$ of anchorage length and greater than a 2.5 anchorage length to cover ratio:

$$f_{s-head} = 1.4 f_c' \left(\frac{c_1}{d_b} \right) \sqrt{\frac{A_{nh}}{A_b}} \Psi \quad , \tag{9}$$

$$\text{with } \Psi = 0.6 + 0.4 \frac{c_2}{c_1} \leq 2.0 \quad , \tag{10}$$

where:

f_{s_head} = the capacity of the head (ksi),

c_1 = minimum cover dimension (in),

c_2 = secondary cover dimension (the smallest cover dimension measured perpendicular to the minimum cover) (in),

and,

Ψ = radial disturbance factor.

Thompson explained that the ACI bond strength equation will not work for headed bars used in strut and tie models for several reasons. First, at the total capacity for the headed bar, the bond portion is significantly reduced from that of just a straight bar because the bond starts to deteriorate as the head resists more of the load. Second, due to the designed location of the head in the strut region, the extra compressive force provided by the strut helps to increase bond capacity. Therefore, in a design scenario, it is necessary to first establish the size and location of the strut in order to determine the anchorage length. The development length that a straight bar would require to resist the load then needs to be calculated from the ACI provisions. Finally, the bond contribution in a headed bar can be calculated as

$$f_{s-bond} = \chi f_y \left(\frac{l_a}{l_d} \right), \tag{11}$$

$$\text{with } \chi = 1 - 0.7 \frac{A_{nh} / A_b}{5} \geq 0.3, \tag{12}$$

where:

f_y = yield strength of the bar (ksi),

l_a = anchorage length determined from strut size and location (in),

and,

l_d = required development length of straight bar of same diameter (in).

Equations (8) and (10) are then added together to find the total anchorage capacity for a headed bar:

$$f_{s-headed\,bar} = 1.4 f_c^{'} \left(\frac{c_1}{d_b} \right) \sqrt{\frac{A_{nh}}{A_b}} \Psi + \chi f_y \left(\frac{l_a}{l_d} \right). \quad (13)$$

3.5: Current Code Model

The current model provided in the ACI 318-08 code treats a head bar similar to a hooked bar [5]. The equation simply reduces the required development length if a head meeting minimum requirements is added:

$$l_{dt} = \left(\frac{0.016 f_y}{\sqrt{f_c^{'}}} \right) d_b \quad (14)$$

.

This equation is applicable for bars not greater than #11, normal weight concrete, heads with net bearing area greater than four times the bar area, clear cover of at least two bar diameters, and clear spacing between bars of at least four bar diameters. Lastly, l_{dt} must be larger than six inches and eight bar diameters. This equation does not respond at all to different sized heads.

3.6: Summary

Table 5 summarizes the variables tested in each of the programs and segregates the variables that are relevant for this test program. As different as each of the tests were, three of them all produced similar results in terms of the behavior of bond and head bearing to resist tensile loads in the bar (see Figure 31). Each of the four test programs

Table 5: Variables Tested in Each Program.

Variables	Zimdahl	Chun *et al.*	DeVries	Thompson
Variables Also Tested in this Program				
Bond Length	X			
Clear Cover	X		X	
Head Size			X	X
Head Shape			X	X
Variables Not Tested in this Program				
Embedment Length		X	X	
Bar Diameter		X	X	X
Head Orientation			X	
Transverse Reinforcing in Anchorage Zone			X	X
Close Spacing			X	
Head Thickness			X	
Additional Development Length			X	
Angle of Compression Strut				X
Head Type				X
Lap Length				X
Lap Configuration				X
Bar Spacing				X

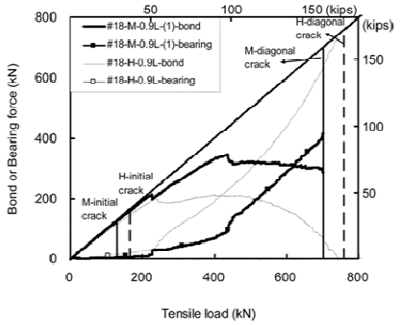

Chun
Solid diagonal is total bar load
Dark lines represent a headed bar
Light lines represent a hooked bar

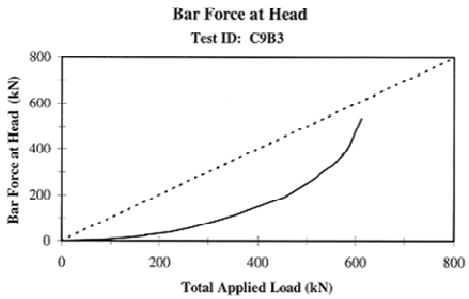

DeVries
Dashed diagonal is total bar load
Solid curve is head bearing

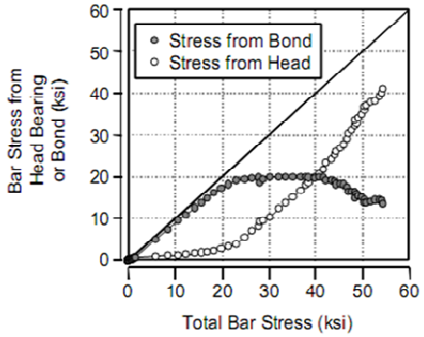

Thompson
Solid diagonal is total bar load

Figure 31: Comparison of Head versus Bond Graphs from 3 Test Programs.

observed that bond initially resists the load and as the bond deteriorates, the head bearing resists a greater proportion of the load.

Chapter 4: Methods

Twelve beam-end specimens with headed deformed bars were constructed. The specimens consisted of pairs of specimens to compare the effect of one manipulated variable while the other variables where held constant. The variables tested include bond length, clear cover and head bearing area. The specimens were cast, cured and tested to analyze headed bar behavior.

4.1: Specimen

Each specimen block was 12” wide, 24” tall and 32” long, with a tolerance of plus or minus ¼”. Each specimen contained one headed deformed #8 bar, and four corner bars running parallel to the headed bar which were used to hold the specimen together after failure and for moving the specimen during testing. The specimens also had two number 3 ties tied to the corner bars to provide shear reinforcement. The heads were threaded onto the bars and set into the specimens with an embedment depth of 22” for all specimens (see Figure 32). The bar continued out behind the head through a hole in the formwork to positively locate the bar in the specimen and to provide a way to measure

Figure 32: Headed Bar with Strain Gauge Attached.

the head-slip during testing with a LVDT. The length of bar behind the head and directly inside the front of the form were sheathed in a piece of PVC pipe to keep concrete from bonding to the bar. The length of the PVC sheath in the front of the specimen was varied to control the bond length of the specimen. All ends of the PVC sheaths were then sealed with caulk to prevent concrete from leaking into the sheath and bonding to the bar while still being flexible to not resist deflection of the specimen. The headed bar extended out of the specimen about four feet at the opposite side from the head so that tension could be applied to the bar. The bars were also outfitted with a strain gauge located just in front of the head to analyze how the head and bond behaved individually. Figure 33 shows a beam-end specimen and Figure 34 shows a photograph of the formwork prior to concrete placement. Specimens were designed such that there would be multiple series to compare the result of changing one variable while the other variables were constant.

4.1.1: Specimen Naming Designation

The specimen designation is derived from the three manipulated variables. The first number designates the size of the head in bar diameters; the second number

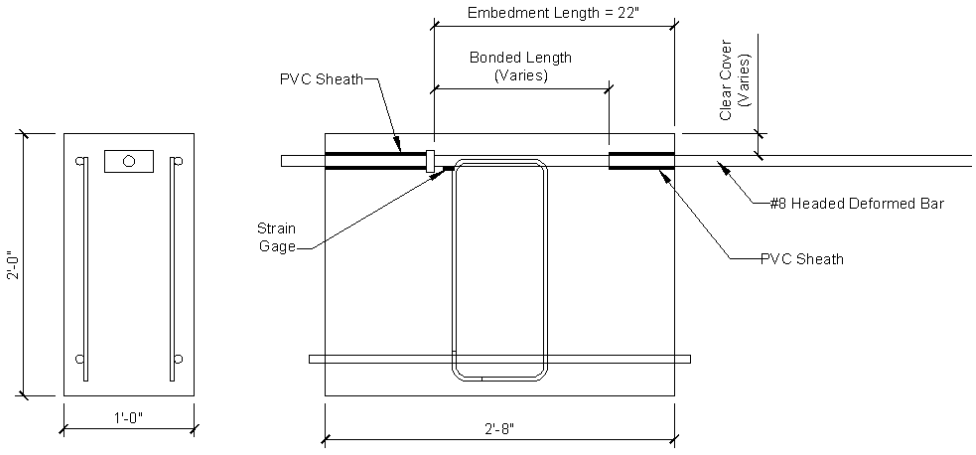

Figure 33: Beam-End Specimen.

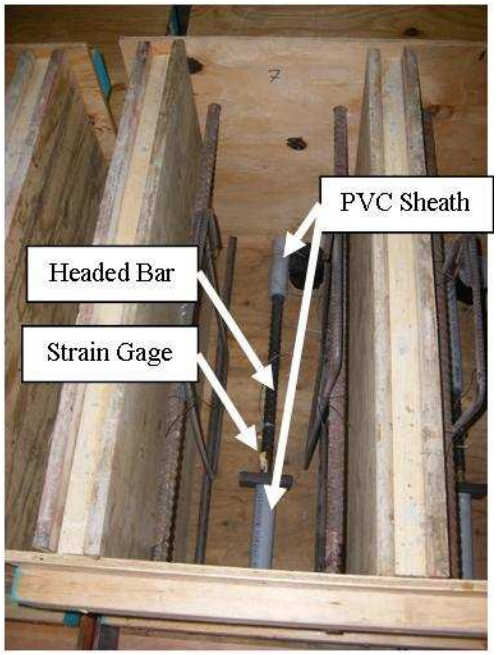

Figure 34: Photograph of Empty Formwork.

designates the bond length in inches; and the third number designates the cover in bar diameters. Table 6 features the specimen names and variable combinations.

4.2: Formwork

The formwork for the specimens was constructed using plywood, 2"x4" lumber, nails and screws. Two sets of forms were constructed for six specimens each. Holes

Table 6: Specimen ID's and Manipulated Properties.

Specimen ID	Head Size (in x in)	A_{brg}/A_{bar}	Bond Length (in)	Clear Cover (in)	Clear Cover (bar diameter, d_b)
9-16-1	4 x 2	9	16	1	1
9-16-2	4 x 2	9	16	2	2
9-8-1	4 x 2	9	8	1	1
9-8-2	4 x 2	9	8	2	2
6-16-1	2.75 x 2	6	16	1	1
6-16-2	2.75 x 2	6	16	2	2
6-8-1	2.75 x 2	6	8	1	1
6-8-2	2.75 x 2	6	8	2	2
3.5-16-1	1.75 x 2	3.5	16	1	1
3.5-16-2	1.75 x 2	3.5	16	2	2
3.5-8-1	1.75 x 2	3.5	8	1	1
3.5-8-2	1.75 x 2	3.5	8	2	2

were drilled in the forms to run the headed bar and each of the four corner bars through to ensure precise location of each of the bars.

4.3: Materials

The concrete used in the specimens was a 4,000 psi mix ordered from a local ready-mix company. Compressive strength tests were conducted on multiple six inch cylinders at three days, seven days, fourteen days, twenty-one days and twenty-eight days. An extra set of cylinders were tested at twenty-eight days simply to get more samples. Table 7 shows the break test data for each of the cylinders and Figure 35 shows

Table 7: Concrete Compressive Strengths.

Day	Break Test Result (lbs)				Strength (psi)
	Cylinder 1	Cylinder 2	Cylinder 3	Average	
3	56500	56100	X	56300	**1991**
7	94100	84700	84200	87667	**3101**
14	120900	127100	121100	123033	**4351**
21	130600	137700	136200	134833	**4769**
28	146000	124700	126000	137683	**4870**
28 (v2)	130100	147600	151700		

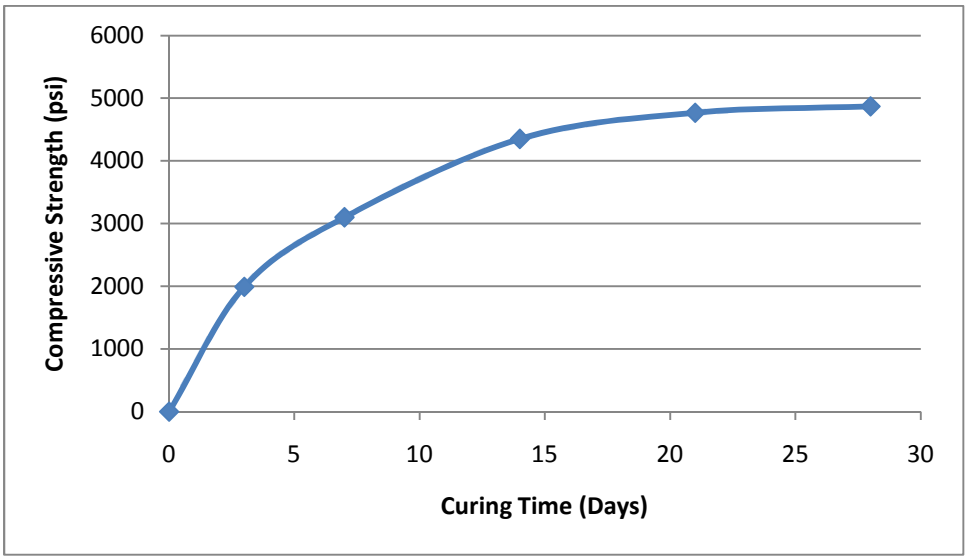

Figure 35: Compressive Strength of Cylinders over Time.

the strength growth over time of the concrete. The headed deformed bar at the center of this investigation was a #8 bar with rectangular head three-quarters of an inch thick, two inches tall, and varied widths. The heads were threaded onto the bar on cold-formed threads cut into the bars and heads.

4.4: Casting

The specimens were cast using the chute of the ready-mix concrete truck in three lifts per specimen. The initial lift was poured over a shovel in an attempt to eliminate any damage or movement caused by the impact of the concrete after freefall from the chute. The specimens were vibrated after each lift and trowel finished. During casting, the slump was measured and six inch test cylinders were cast for testing later.

4.5: Test Frame

The test frame was constructed using a W-shape as the base. On to that were attached a steel reaction block which held the hydraulic cylinder, and the tie-down wings which worked with a pair of tie-down rods and channels to hold down the rear end of the specimen during testing. Figure 36 illustrates the forces that the test frame was designed to apply to the specimen and Figure 37 shows the internal strut and tie elements of the specimen and defines the various reinforcing ar lengths. Figure 38 shows a specimen in the test frame. The specimens were loaded into the frame by moving it along the length of the base while guiding the exposed length of the headed bar through the reaction block and then through the hollow-core hydraulic cylinder. The front of the specimen was placed tight up against spacers which were tight against the reaction block. Once in place, the tie-down system was installed and clamped down on the rear end of the block and the LVDT sensors were positioned to measure Head-slip (see Figure 39) and

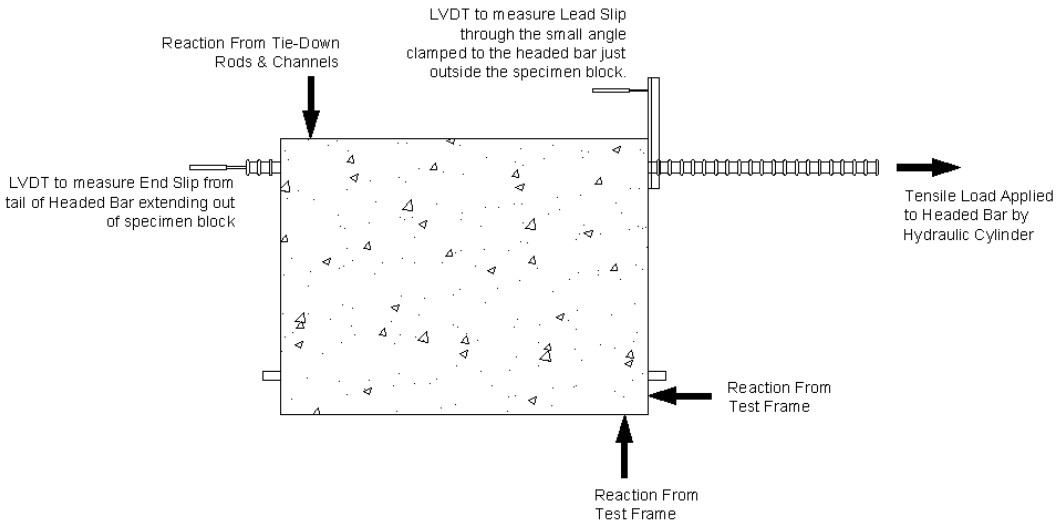

Figure 36: Free Body Diagram of Specimen.

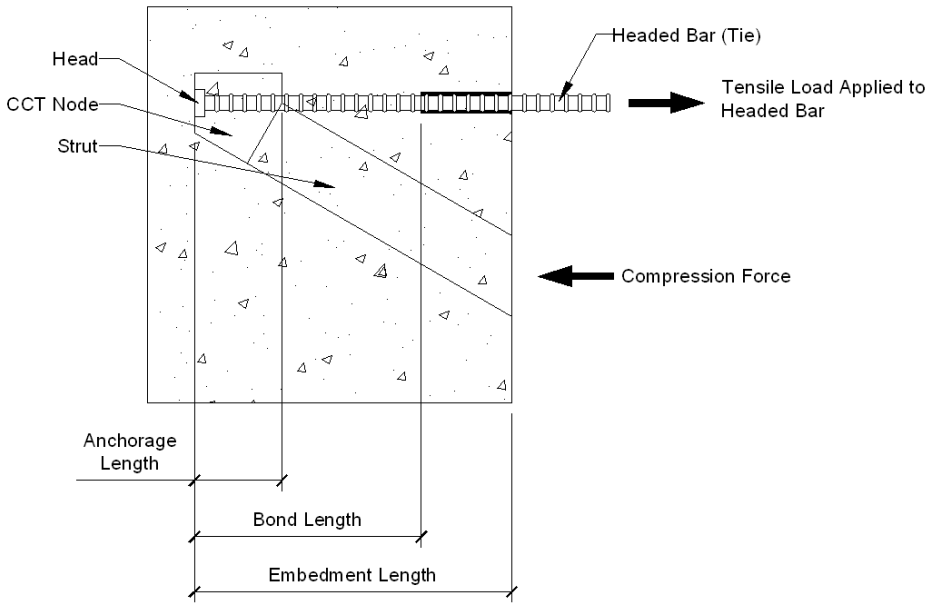

Figure 37: Strut and Tie Model of Specimen with Rebar Lengths Defined.

Lead-slip (see Figure 40). To measure lead slip, a small steel angle was clamped to the headed bar just outside the specimen which the LVDT then measured. Washer-like spacers were then placed over the end of the head bar, and a ¾" thick plate (similar to a nut) was screwed onto threads cut into the exposed end of the headed rod. The hydraulic cylinder and load cell pushed against the spacers which pushed against the threaded plate

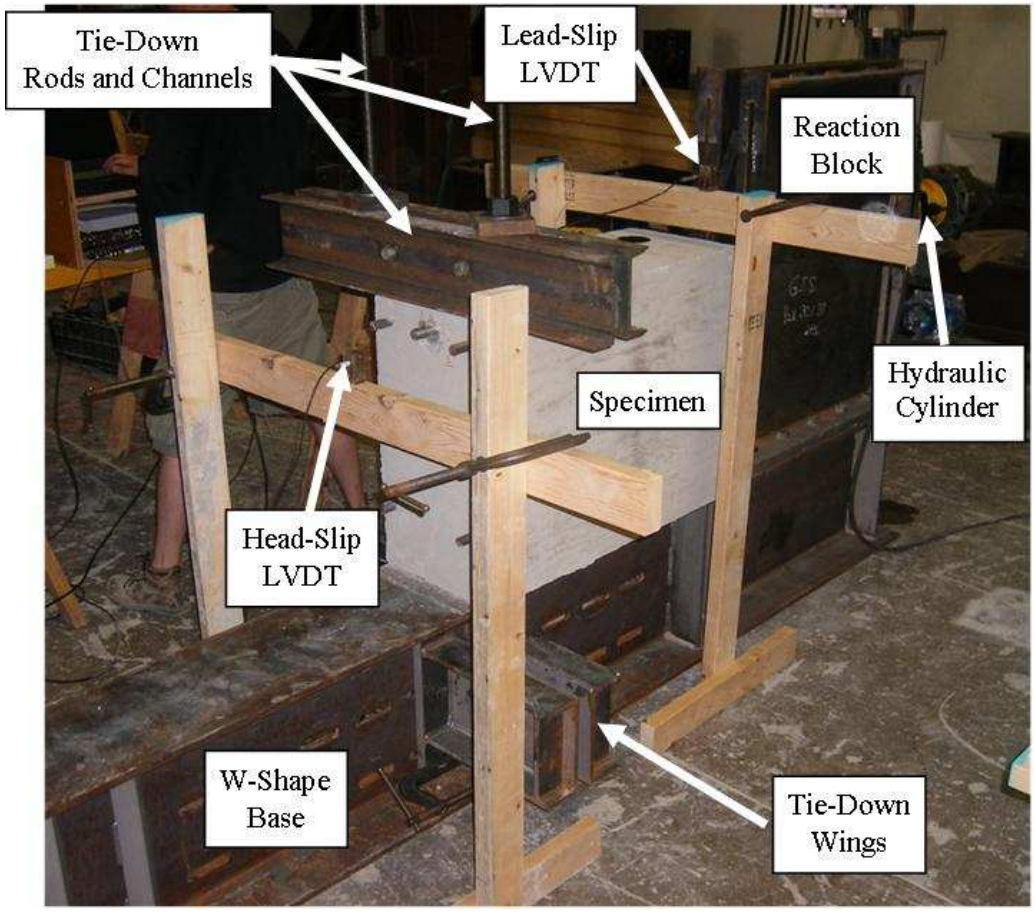

Figure 38: Test Frame Setup.

Figure 39: Head Slip LVDT.

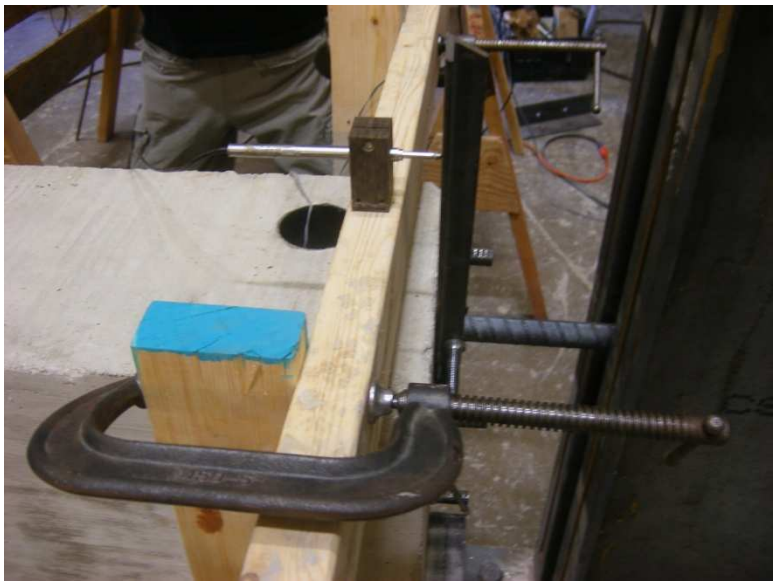

Figure 40: Lead Slip LVDT.

to apply load to the bar. The load cell, LVDT's, and the strain gauge were then all connected to a computer running a program to record the load, displacements and strain experienced by the specimen throughout loading.

4.6: Testing

Testing began on the twenty-seventh day after casting and finished on the twenty-eighth day. After each specimen had been loaded into the test frame, the headed bar was loaded in direct tension by the hydraulic cylinder. Each of the specimens were loaded repeatedly through five cycles. Load was applied in approximately 5,000 pound increments to avoid any dynamic loading implications. The bar was loaded up to about 50,000 pounds and released down to 5,000 pounds for each of the first four cycles. For the fifth cycle, the bar was loaded until yielding was observed in the bar, or there was a concrete failure. Four of the twelve specimens failed from side blowout while the other eight specimens failed by bar yield. Some of the specimens which failed by side blowout failed at a load less than 50,000 pounds and therefore were loaded less than five cycles.

Specimen 3.5-8-2, was the first specimen to be tested. It was initially tested with only one threaded plate screwed onto the exposed end of the bar. During the first load cycle, the threads in the threaded plate failed resulting in an abrupt removal of tension from the specimen. This may have caused some shock loading effects and will be examined later. Specimen 3.5-8-2 was then re-tested using 2 threaded plates to transfer force form the hydraulic cylinder to the headed bar. Two threaded plates were then used on all of the remaining specimens.

Chapter 5: Data Reduction

The focus of the testing was to examine the contributions of the head and the bond as load was applied in order to create a model to predict the capacity of a headed bar. Because the specimens failed by different mechanisms – side blowout and bar yielding – it would not be accurate to compare all twelve specimens to each other using only the failure load. Therefore, the specimens were analyzed using the head and bond contributions at several load levels as well as stiffness. As mentioned previously, the head and bond contributions will be calculated from the strain gauge data. The specimen stiffness values will be calculated from load and head slip data collected from the load cell and the head slip LVDT, respectively.

The head and bond contributions were graphed for each specimen (see Figure 41). The horizontal axis represents the total force applied to the bar by the hydraulic cylinder. The vertical axis plots the force resisted by the head, the bond, and the diagonal line is the sum of the head and bond forces which is therefore equal to the total far force. Figure 41 is typical of all the specimens in that the head and bond contributions were very similar between the first and last load cycle. The last load cycle will be used for head and

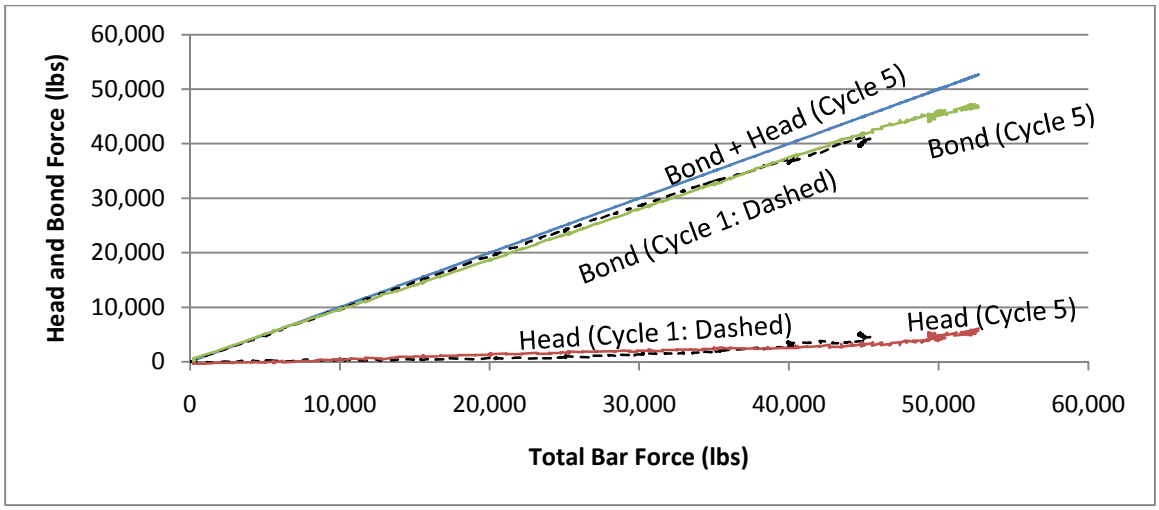

Figure 41: Comparison of Head and Bar Forces over Loading Cycles (Specimen 9-16-1).

bond contribution graphs as they provide the most data. The capacity of a straight bar with the same cover and bond length was then plotted on the graph for comparison. The values for the straight bar capacity were taken from a test conducted by Bolda using a similar setup as this test [6]. Figure 42 is a typical graph of specimens where the head did not add capacity and Figure 43 is typical of specimens where the head did add capacity. The head and bond contributions were also plotted against head slip (see Figure 44).

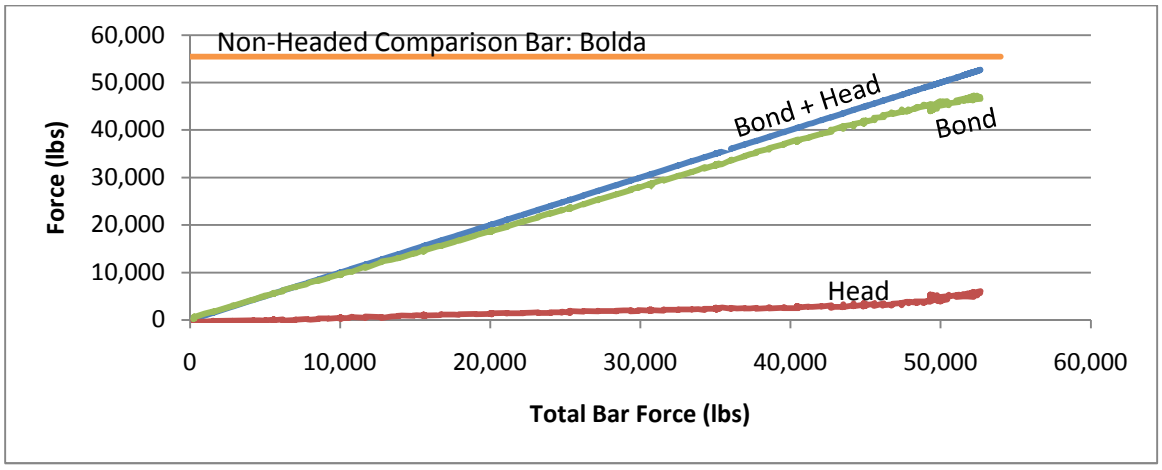

Figure 42: Typical Bond and Head Forces Graph where Head did not Add Capacity (Specimen 9-16-1).

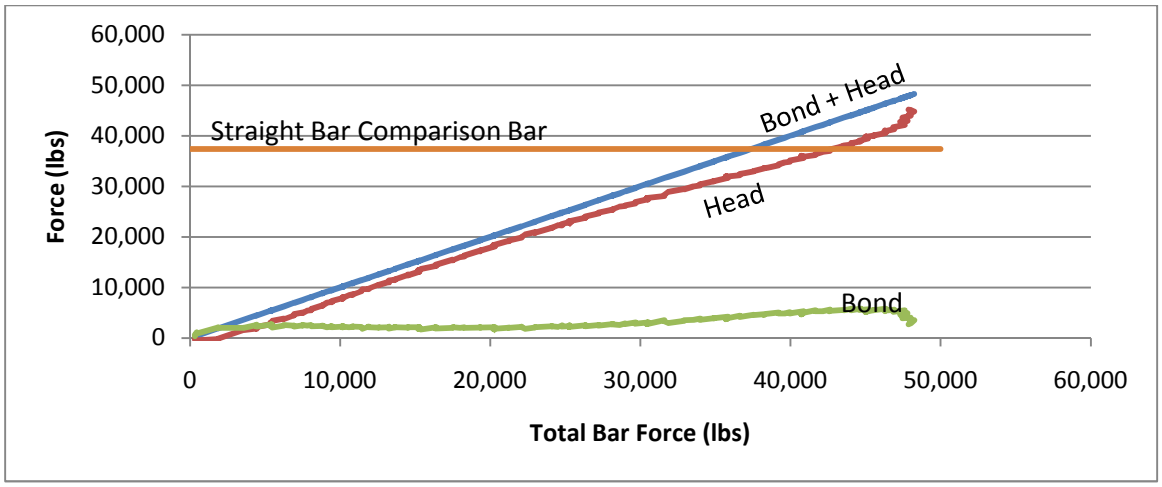

Figure 43: Typical Bond and Head Forces Graph where Head Added Capacity (Specimen 9-8-1).

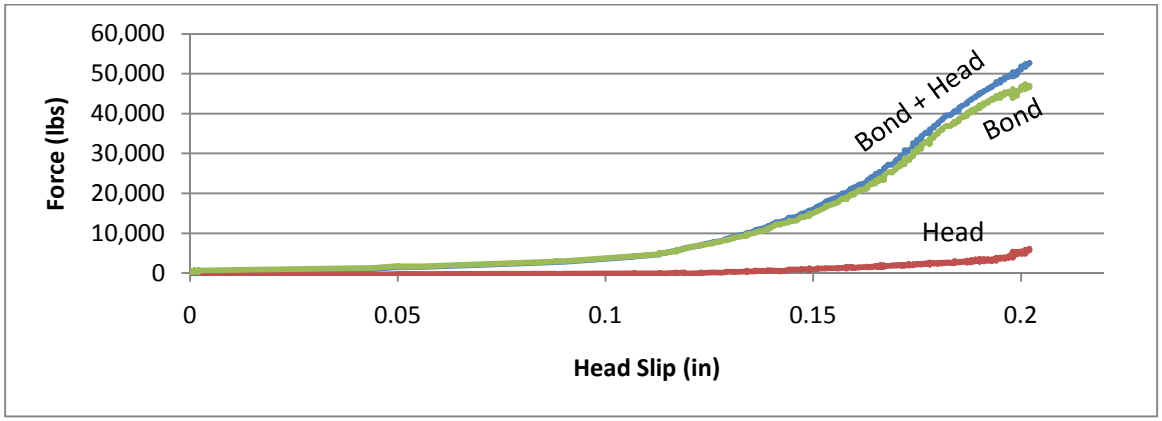

Figure 44: Typical Bond and Head Contribution Graph plotted against Head Slip (Specimen 9-16-1).

To determine the stiffness, the head slip was plotted for the each of the five load cycles for each specimen. The stiffness of the specimen is then the slope of the graph. After the initial load cycle, the remaining cycles all had approximately the same stiffness (see Figure 45). Therefore, the stiffness for each specimen will be determined from the last load cycle (in cases where the specimen failed due to concrete blowout, this may not be the fifth cycle) because the last load cycle was typically loaded further than the previous cycles and thus should be the best representation of the specimen. Using the last load cycle also makes sense because structures are subjected to Live Loads which are applied and removed and would thus have similar stiffness reactions. The graphs were

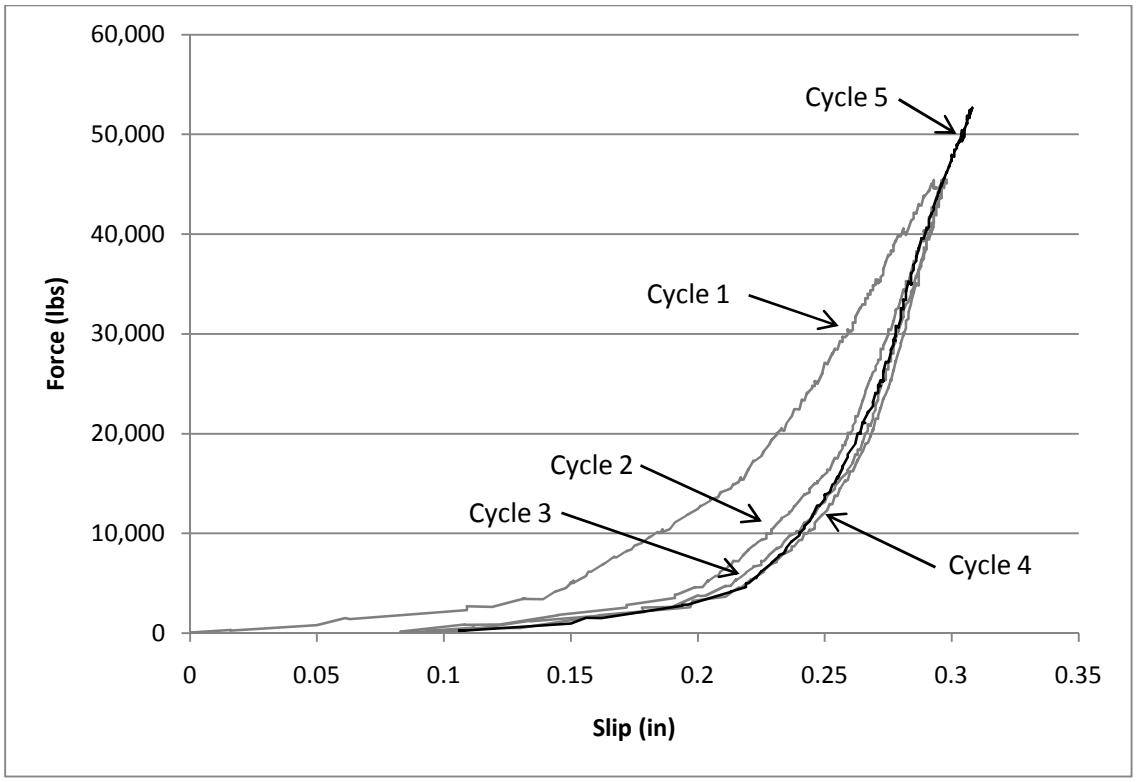

Figure 45: Typical Comparison of Head Slip for each Load Cycle (Specimen 9-16-1).

then reduced to just the last cycle (see Figure 46). The bottom portion of the graph, including the more-horizontal line and the transitioning curve, was attributed to the specimen settling in the test frame, and therefore, was discarded (see Figure 47). The stiffness value for each specimen was then calculated from the remaining data points which were shifted to the origin of the graph for easier comparison. The LVDT sensors

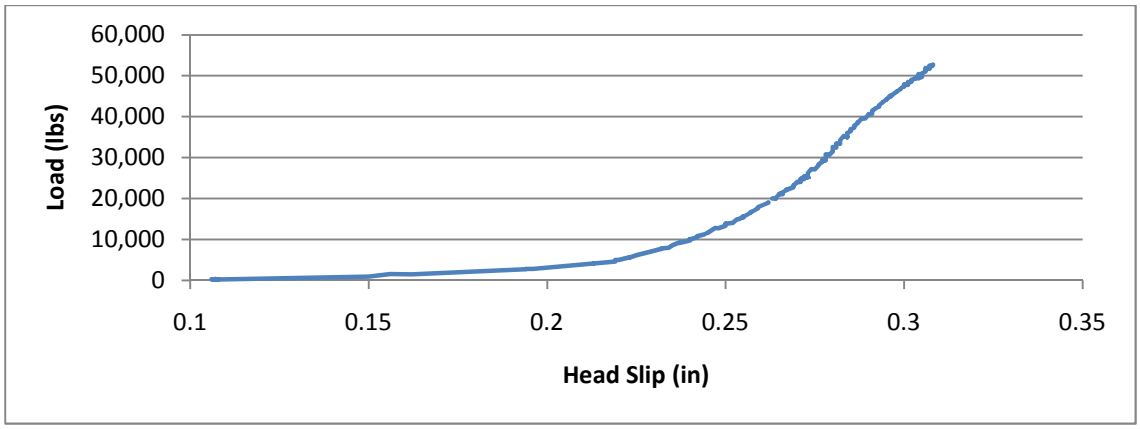

Figure 46: Typical Specimen Stiffness from the Last Load Cycle (Specimen 9-16-1).

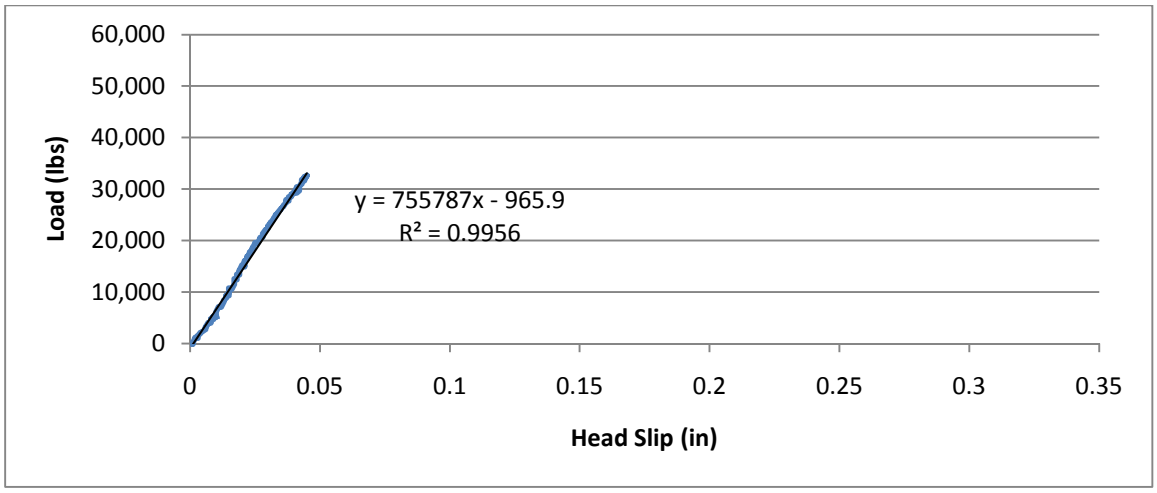

Figure 47: Typical Final Specimen Stiffness Graph (Specimen 9-16-1).

used to measure slip were accurate to 1% of their stroke. The measured slip along the portion of the graph used to calculate stiffness was compared to the stroke of the LVDT. The measured head slips of all twelve specimens ranged between 4.8% and 14.2% of the stroke, making the slip measurements reliable. It may, however, be unreasonable to draw completely accurate conclusions from stiffness analyses because of the assumptions made in the process of reducing the data to determine the stiffness.

Chapter 6: Summary of Results

6.1: Tabulated Results

Table 8 lists the failure mode, failure load, contribution of the head in resisting the load, specimen stiffness, and a comparison to a straight bar.

6.2: Specimen Graphs

On the following pages, in Figures 48 through 83, bond and head contributions versus total bar force, bond and head contributions versus head slip, and stiffness are each graphed for each specimen. The three graphs for each specimen are presented together and appear in the same order that the specimens are listed in Table 8.

Table 8: Summary of Specimen Test Data.

Specimen	Failure Mode	Failure Load (lbs)	Head Contribution at: **			Contribution Switch (%) †	Stiffness (lbs/in)	Straight Bar Failure Load (lbs)	Vs. Straight Bar ‡
			Failure Load (%)	90% Failure Load (%)	45,000 pounds (%)				
9-16-1	Yield	52,661	12	7	7	N/A	755,787	55,469	D
9-8-1	Blowout	47,852	94	79	87	6	1,427,452	37,354	I
6-16-1	Blowout	52,393	49	17	17	N/A	1,325,479	55,469	D
6-8-1	Blowout	51,123	85	72	79	3	1,135,804	37,354	I
3.5-16-1	Yield	53,223	15	8	8	N/A	1,036,177	55,469	D
3.5-8-1	Blowout	45,605	83	61	78	33	322,155	37,354	I
9-16-2	Yield	46,729	4	4	4	N/A	1,316,505	46,680	I ‡‡
9-8-2	Yield	54,883	69	57	63	7	674,357	43,994	I
6-16-2	Yield	45,459	3	3	2	N/A	1,110,272	46,680	D
6-8-2	Yield	45,557	63	56	60	8	784,875	43,994	I
3.5-16-2	Yield	45,557	4	4	4	N/A	1,012,538	46,680	D
3.5-8-2*	Yield	53,223	62	54	59	7	1,492,959	43,994	I

* Specimen experienced an abrupt removal of the tensile load applied to the headed bar which may have caused shock loading effects (see section 4.6 for further explanation).

** Values are the percentage of the total load on the headed bar that was resisted by the head at the given load. 45,000 pounds was used as a comparison point because it was the highest load all specimens reached.

† The Contribution Switch is the percentage of the failure load of the headed bar where the head began resisting more of the load than the bond. As such, this does not apply to the specimens where the bond resisted most of the total load for the entire test.

‡ The failure load for the specimen was compared to the failure load of a bar tested by Bolda [6] with the same bond length and clear cover. "D" indicates that the addition of the head decreased the failure load of the bar, while "I" indicates that the addition of the head increased the failure load of the bar.

‡‡ This increase is so small, that it may in fact be due to the irregularities inherent of concrete and if a duplicate specimen was tested, could very well result in a decrease which would fit the pattern.

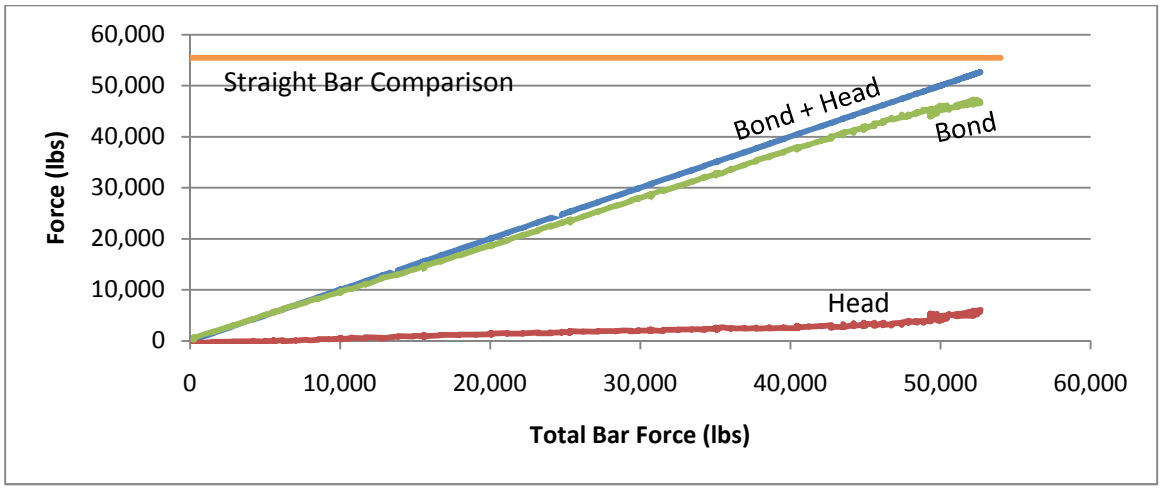

Figure 48: Specimen 9-16-1 Bond and Head Contributions versus Total Bar Force.

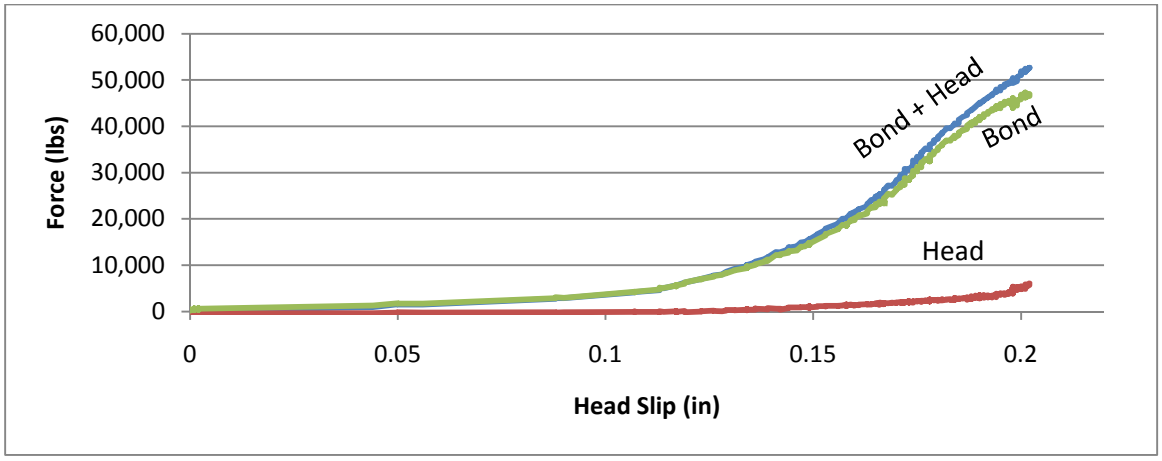

Figure 49: Specimen 9-16-1 Bond and Head Contributions versus Head Slip.

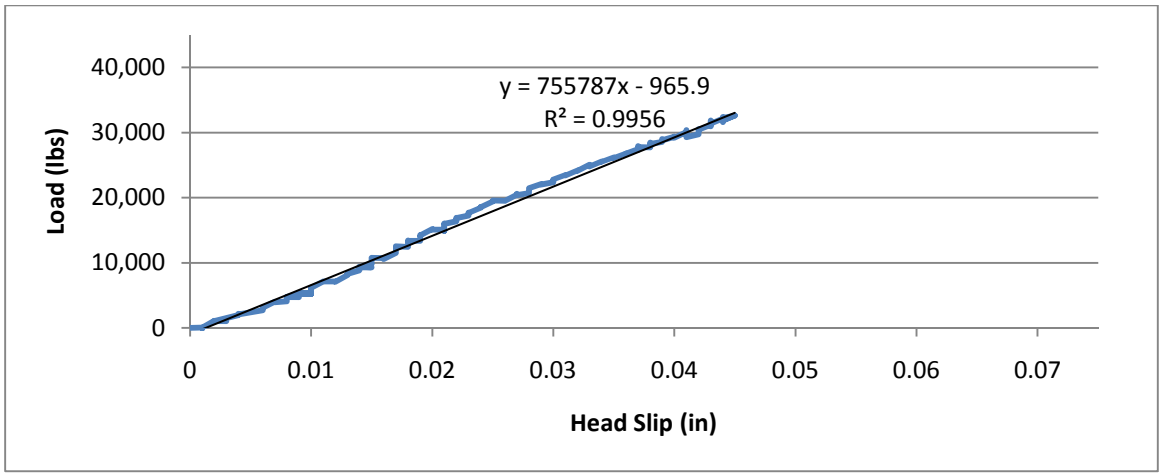

Figure 50: Specimen 9-16-1 Stiffness.

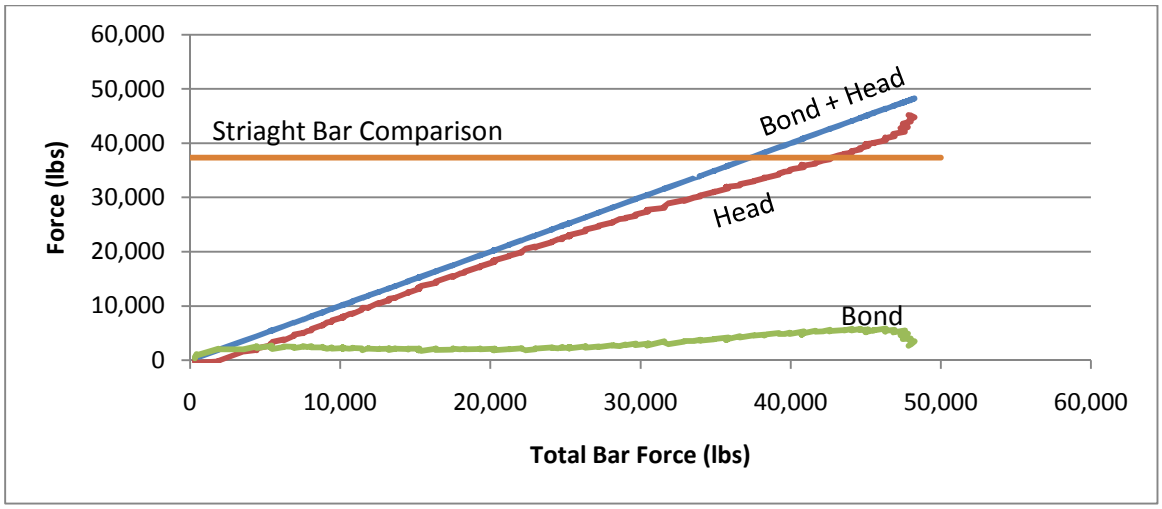

Figure 51: Specimen 9-8-1 Bond and Head Contributions versus Total Bar Force.

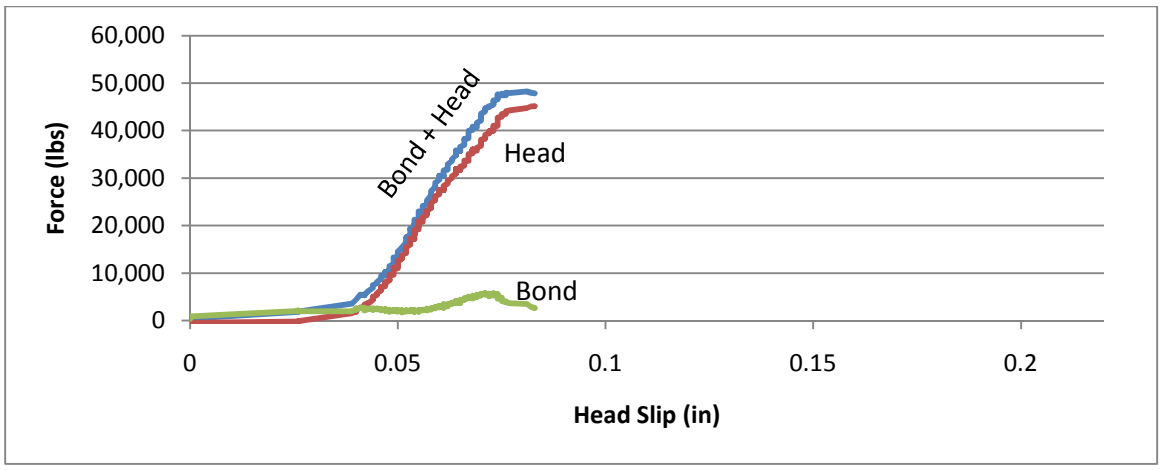

Figure 52: Specimen 9-8-1 Bond and Head Contributions versus Head Slip.

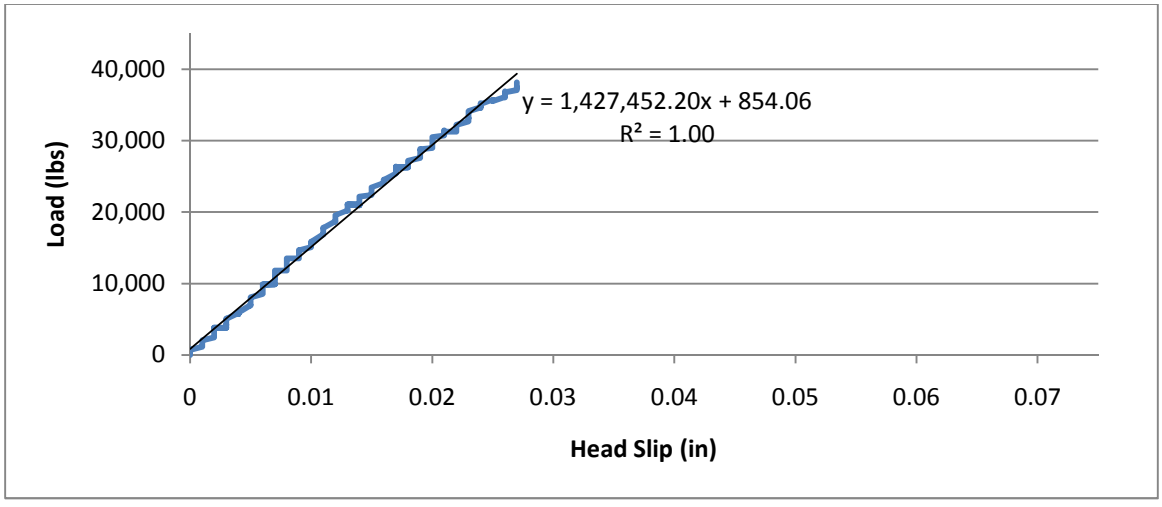

Figure 53: Specimen 9-8-1 Stiffness.

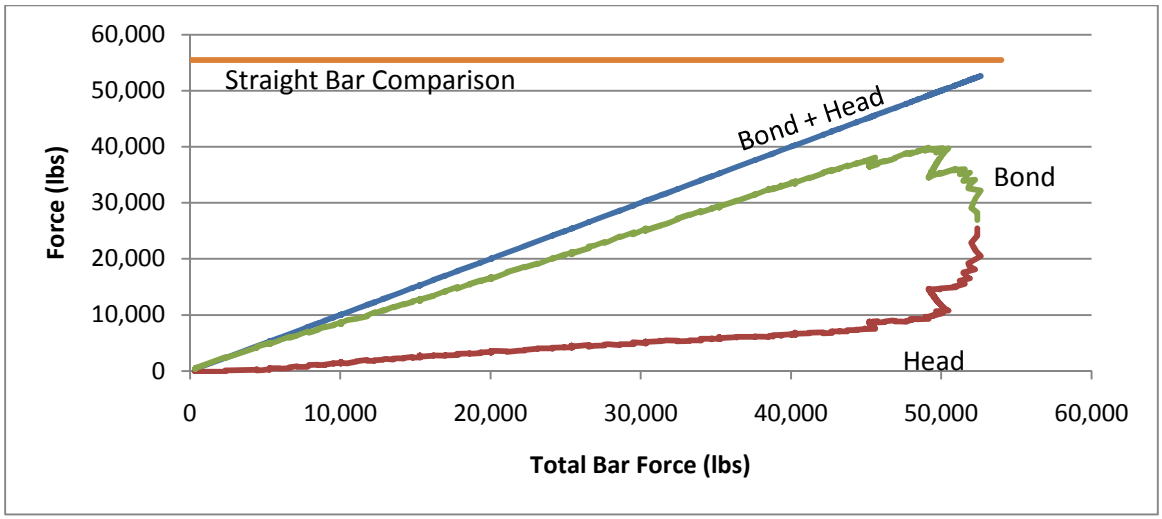

Figure 54: Specimen 6-16-1 Bond and Head Contributions versus Total Bar Force.

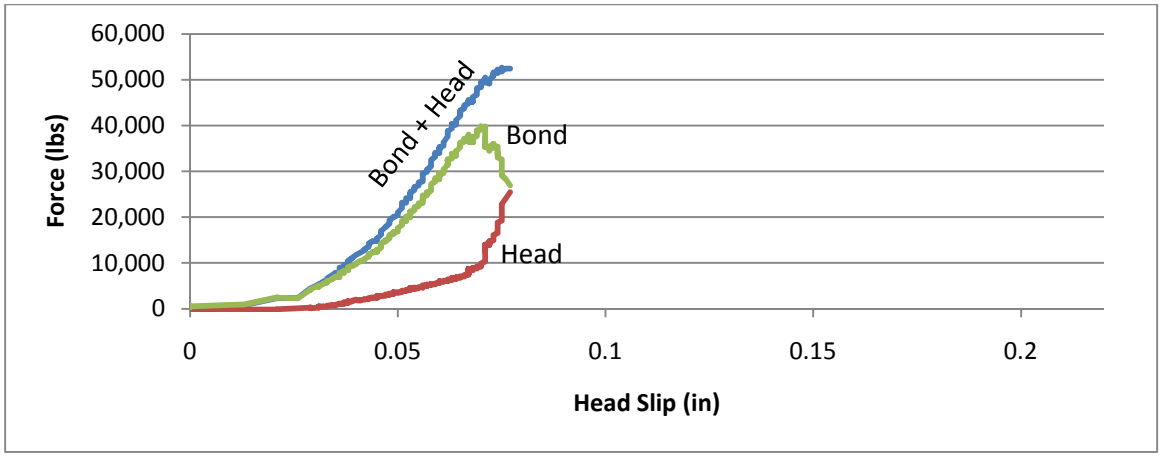

Figure 55: Specimen 6-16-1 Bond and Head Contributions versus Head Slip.

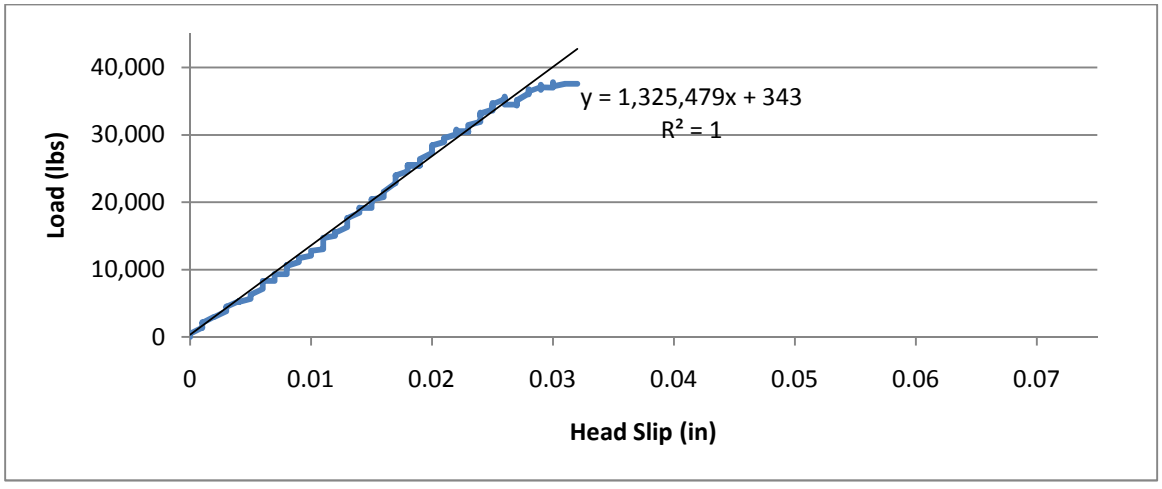

Figure 56: Specimen 6-16-1 Stiffness.

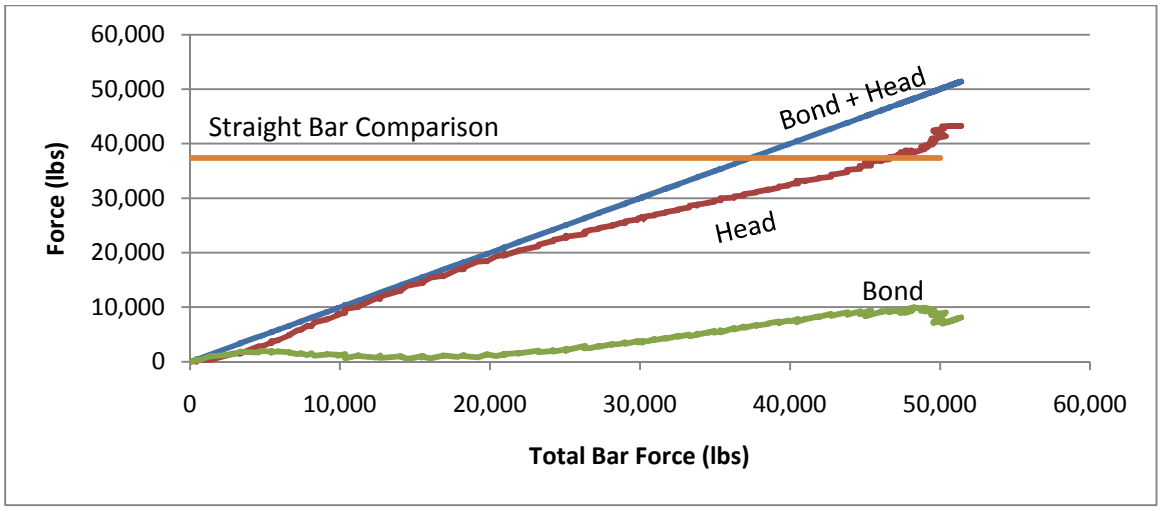

Figure 57: Specimen 6-8-1 Bond and Head Contributions versus Total Bar Force.

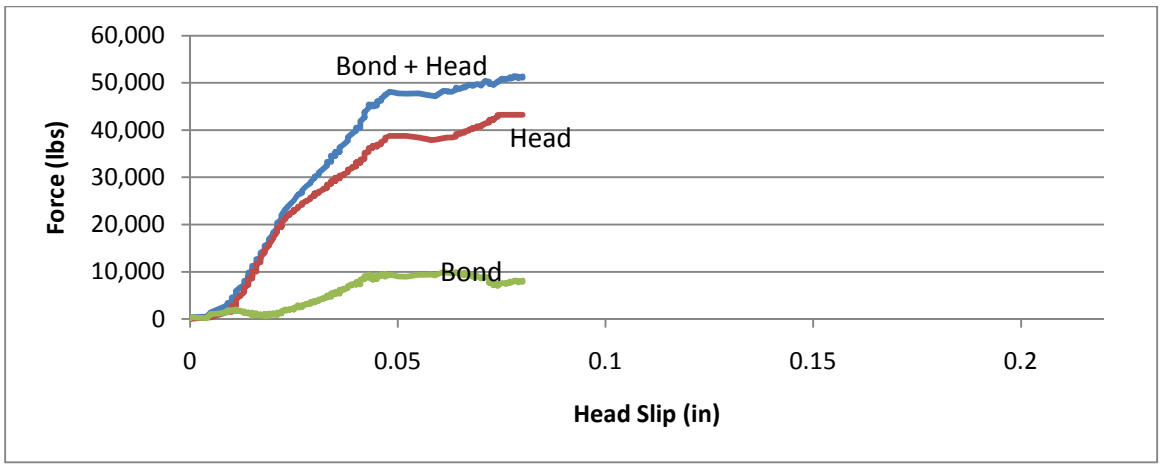

Figure 58: Specimen 6-8-1 Bond and Head Contributions versus Head Slip.

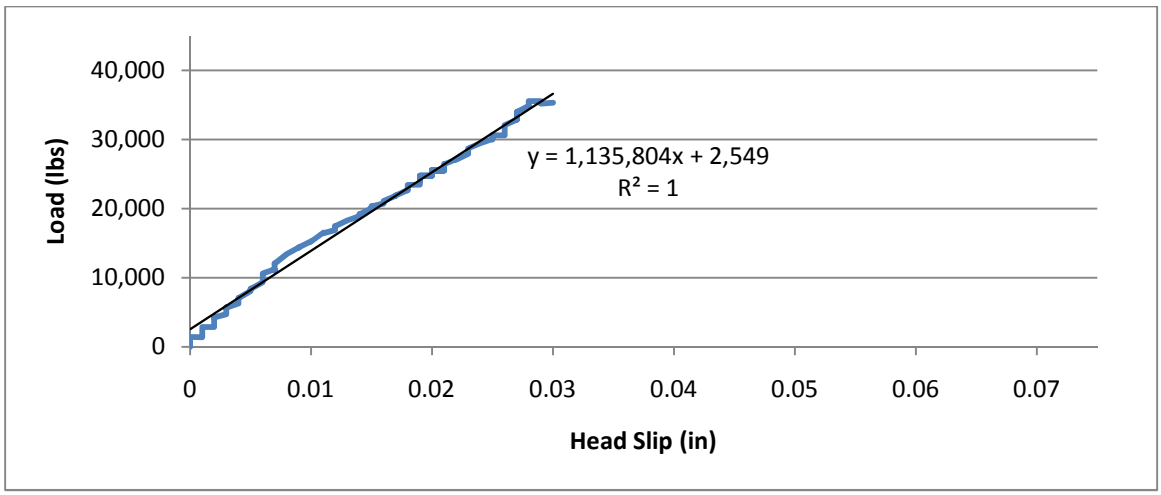

Figure 59: Specimen 6-8-1 Stiffness.

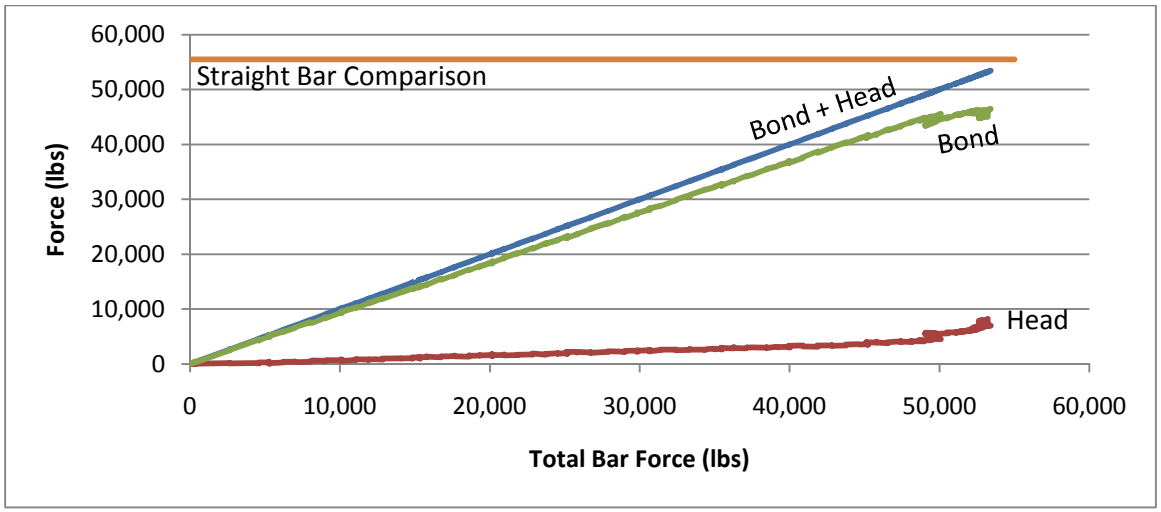

Figure 60: Specimen 3.5-16-1 Bond and Head Contribution versus Total Bar Force.

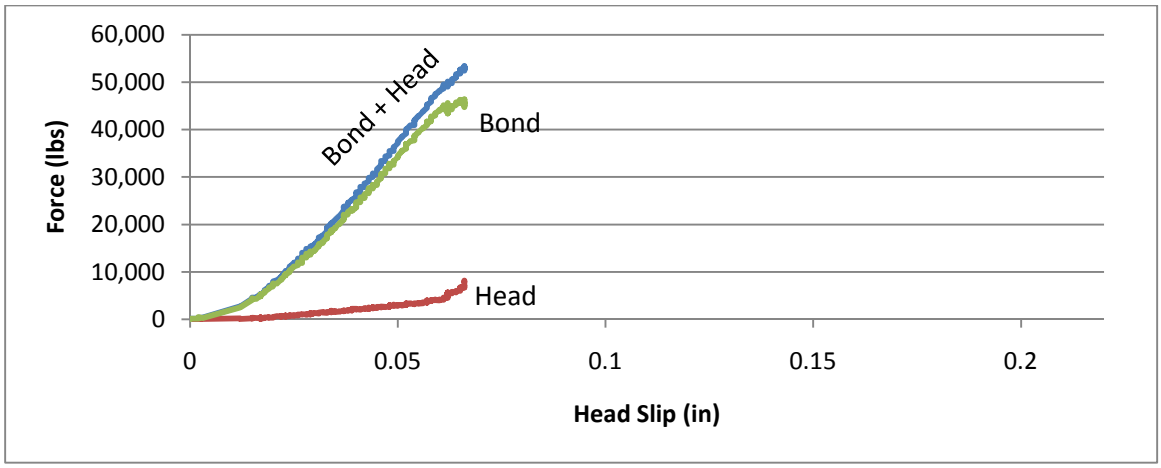

Figure 61: Specimen 3.5-16-1 Bond and Head Contributions versus Head Slip.

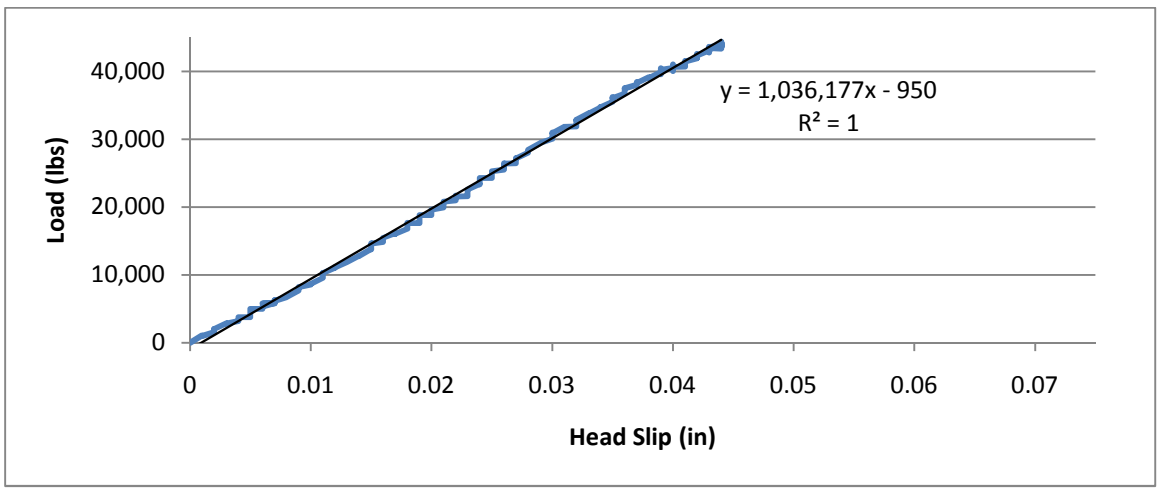

Figure 62: Specimen 3.5-16-1 Stiffness.

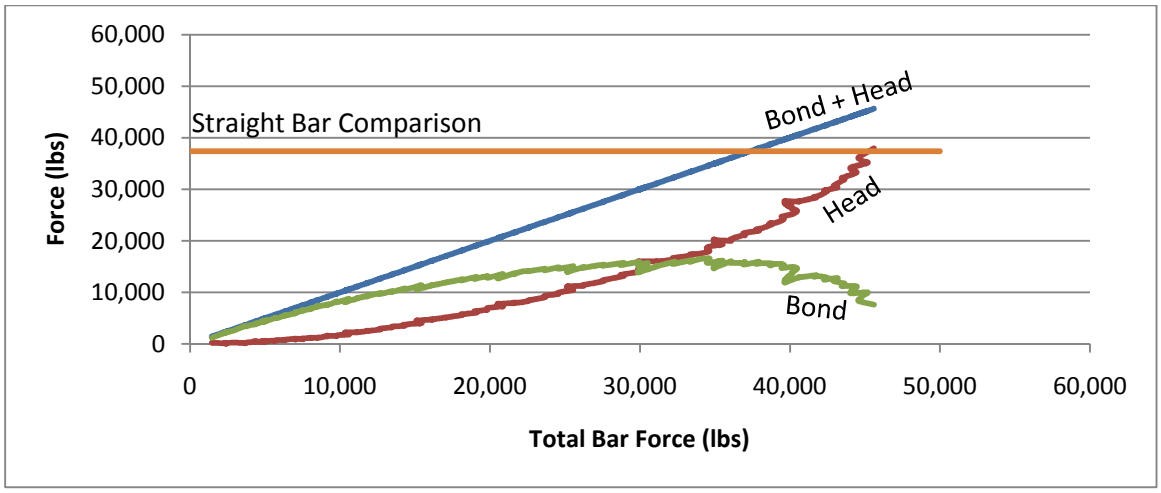

Figure 63: Specimen 3.5-8-1 Bond and Head Contributions versus Total Bar Force.

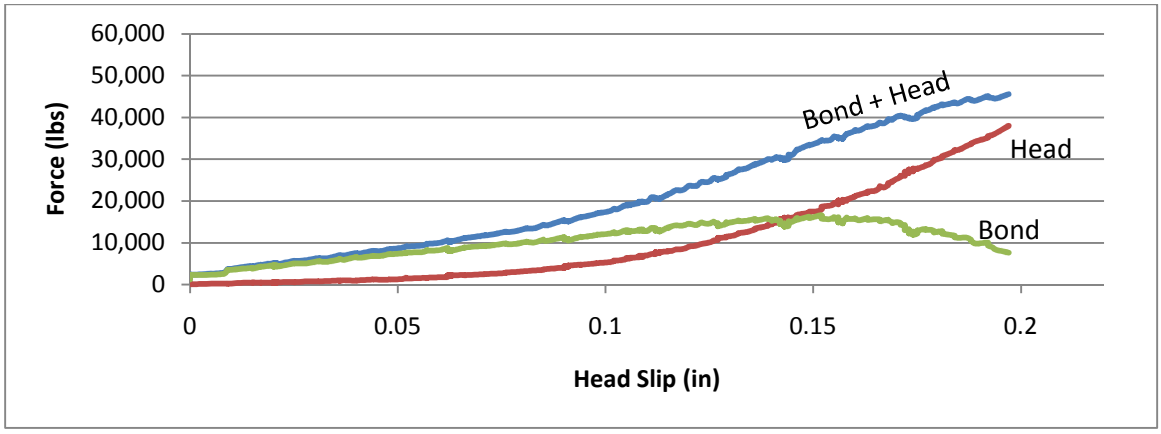

Figure 64: Specimen 3.5-8-1 Bond and Head Contributions versus Head Slip.

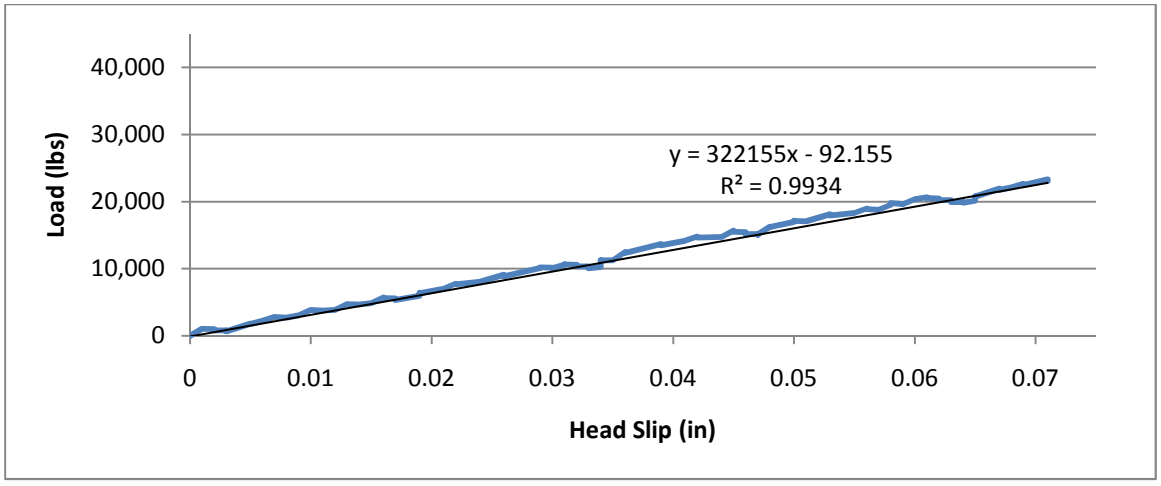

Figure 65: Specimen 3.5-8-1 Stiffness.

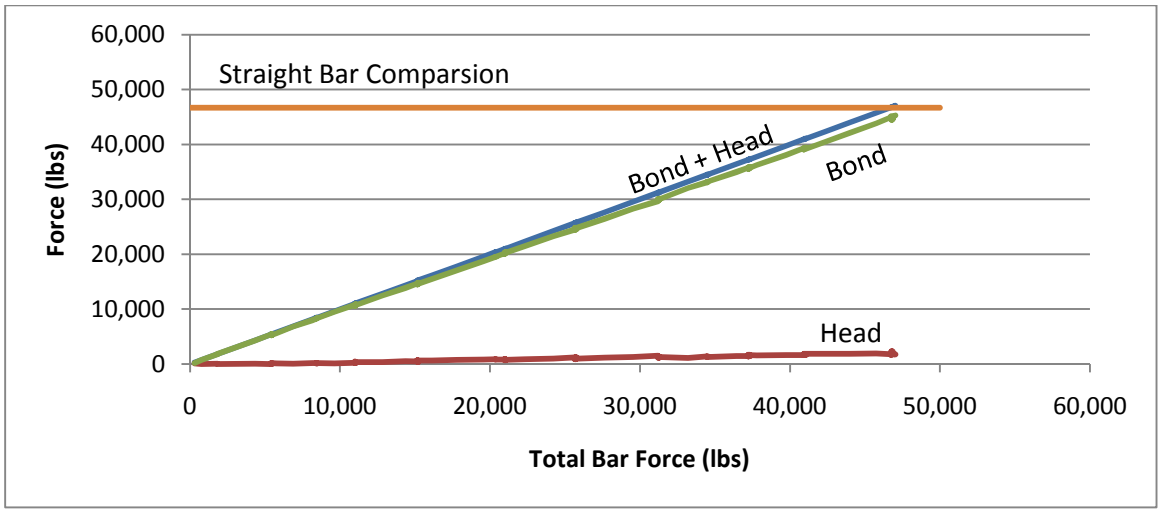

Figure 66: Specimen 9-16-2 Bond and Head Contributions versus Total Bar Force.

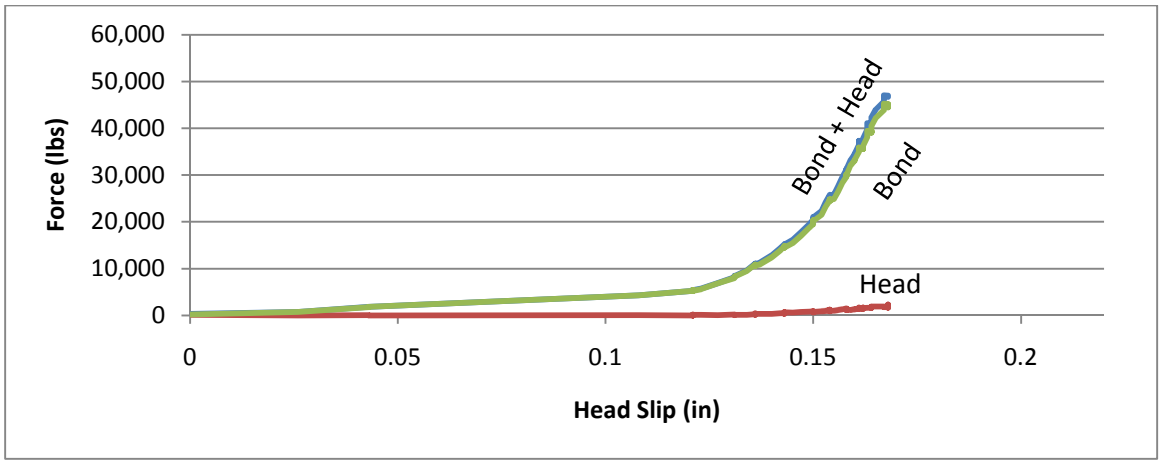

Figure 67: Specimen 9-16-2 Bond and Head Contributions versus Head Slip.

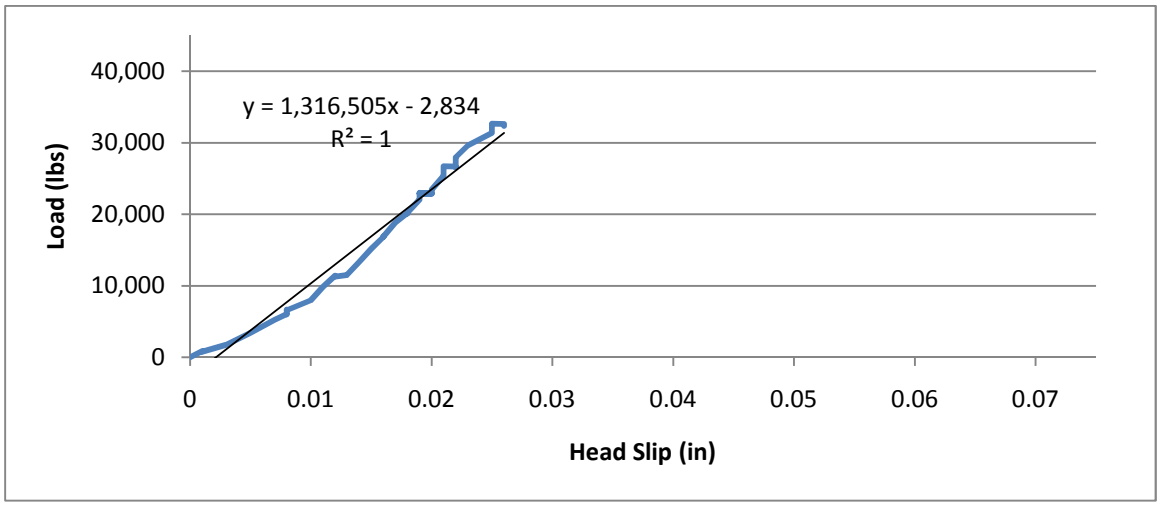

Figure 68: Specimen 9-16-2 Stiffness.

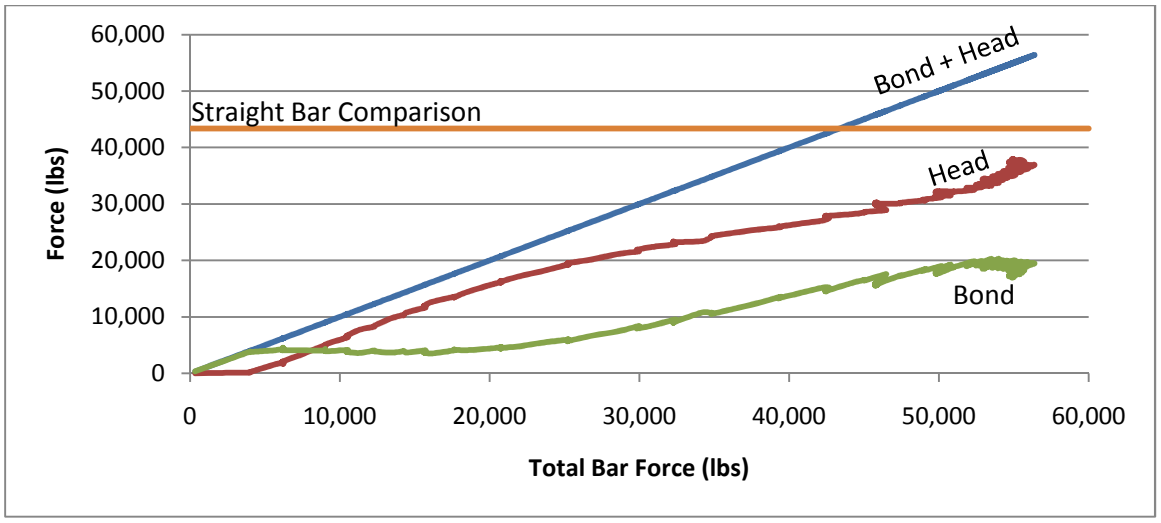

Figure 69: Specimen 9-8-2 Bond and Head Contributions versus Total Bar Force.

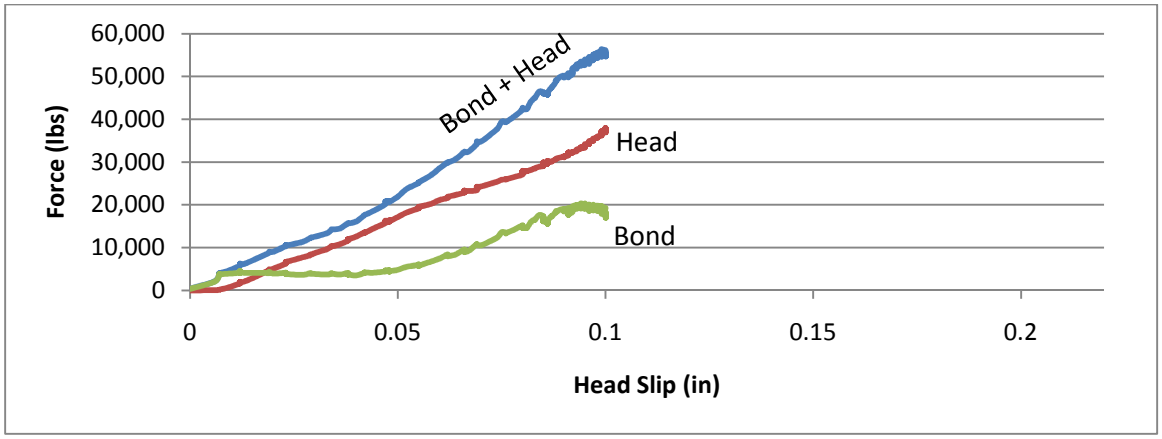

Figure 70: Specimen 9-8-2 Bond and Head Contributions versus Head Slip.

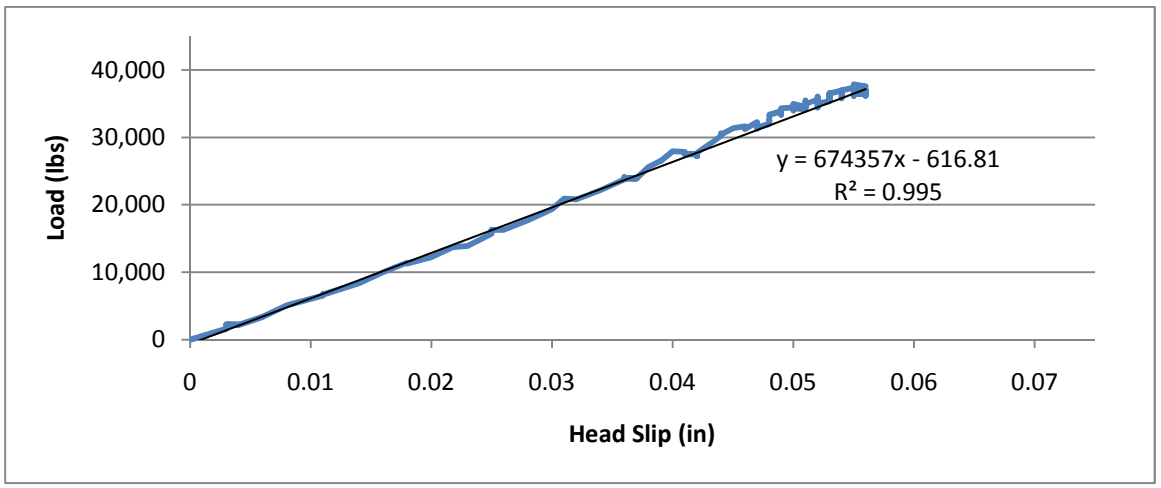

Figure 71: Specimen 9-8-2 Stiffness.

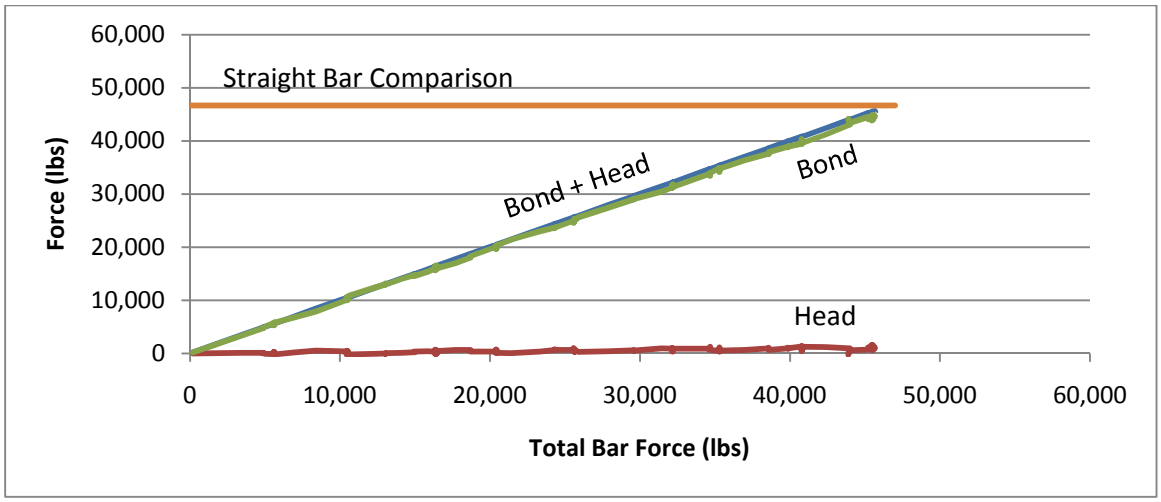

Figure 72: Specimen 6-16-2 Bond and Head Contributions versus Total Bar Force.

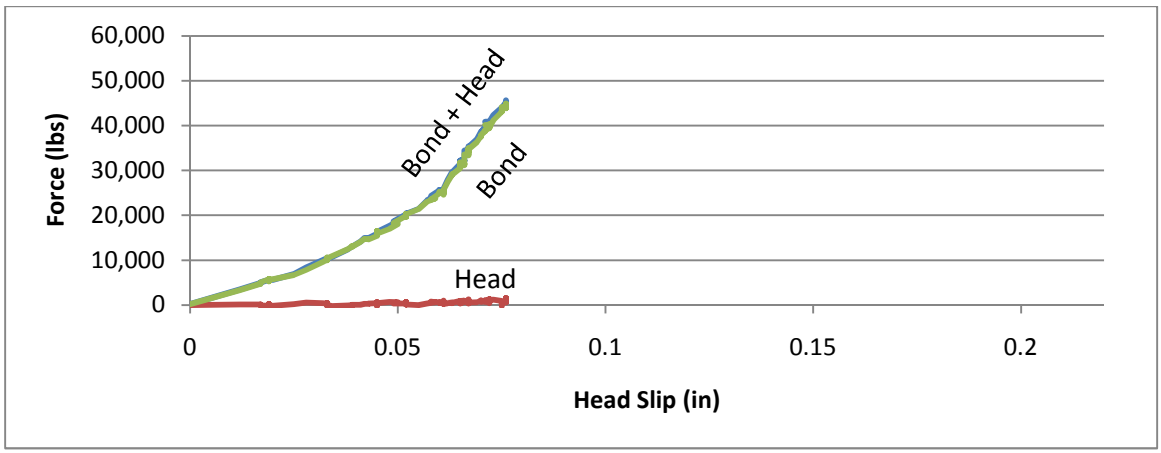

Figure 73: Specimen 6-16-2 Bond and Head Contributions versus Head Slip.

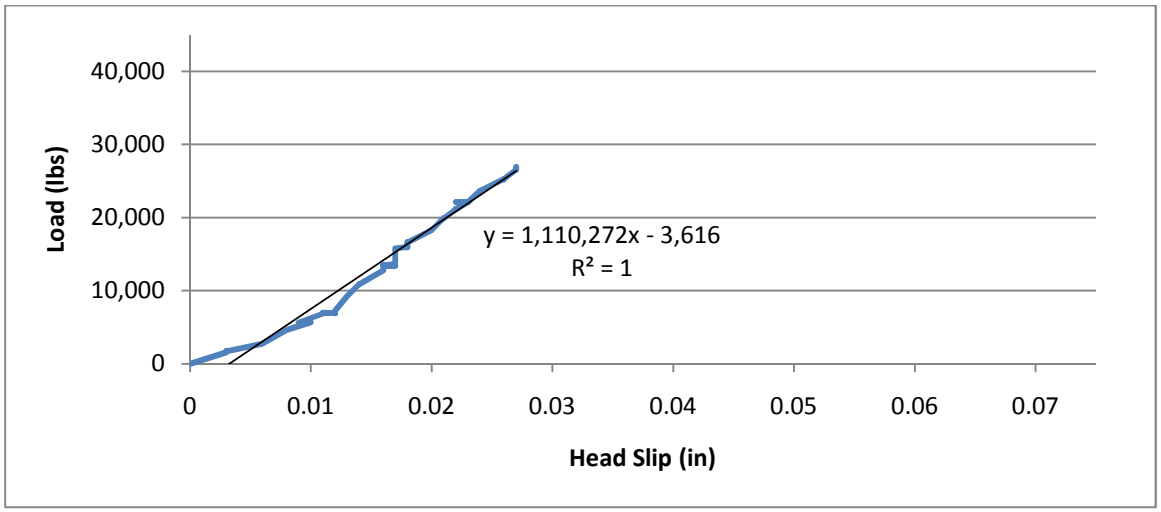

Figure 74: Specimen 6-16-2 Stiffness.

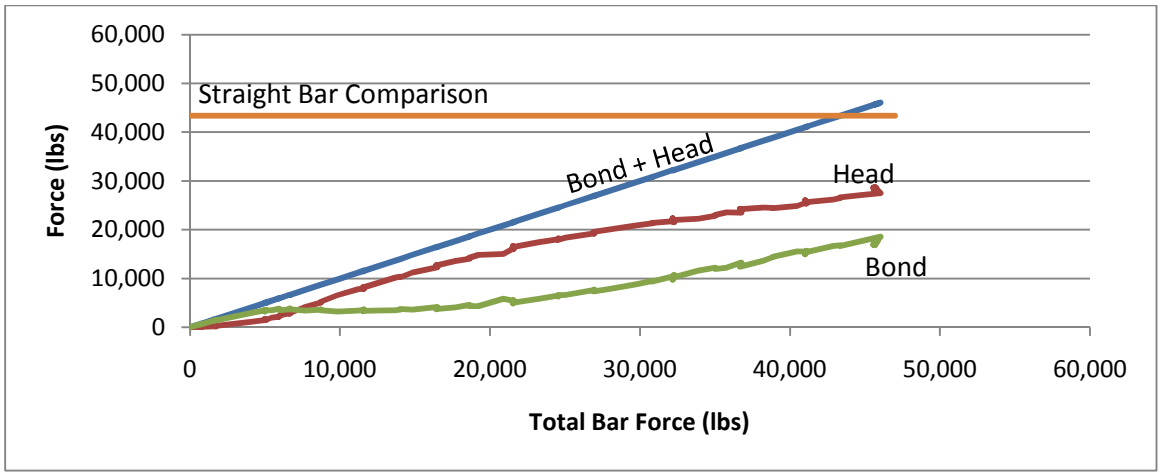

Figure 75: Specimen 6-8-2 Bond and Head Contributions versus Total Bar Force.

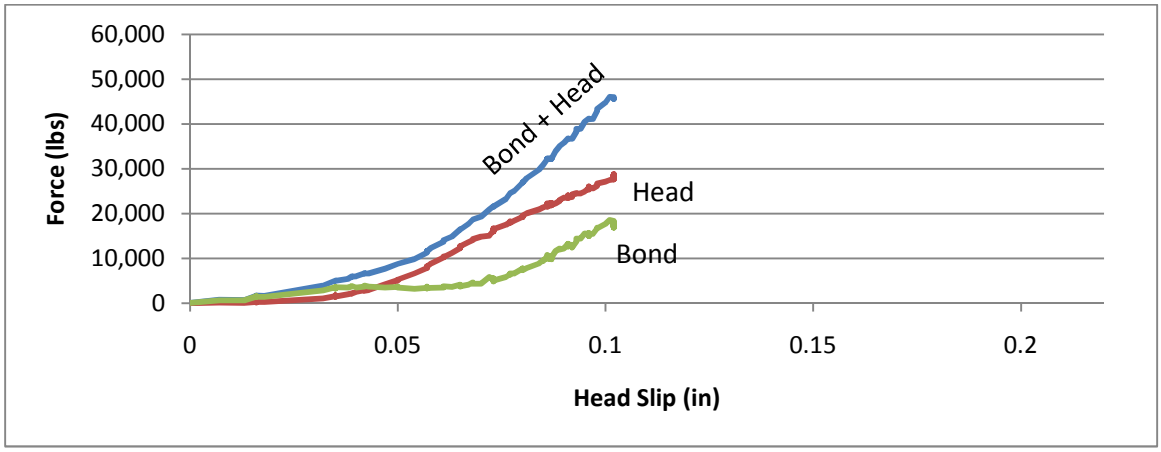

Figure 76: Specimen 6-8-2 Bond and Head Contributions versus Head Slip.

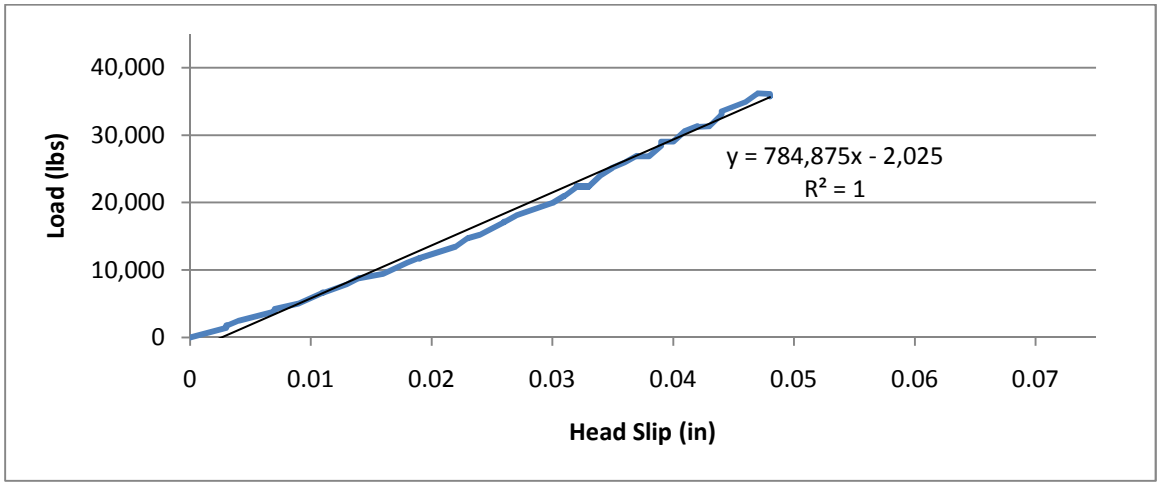

Figure 77: Specimen 6-8-2 Stiffness.

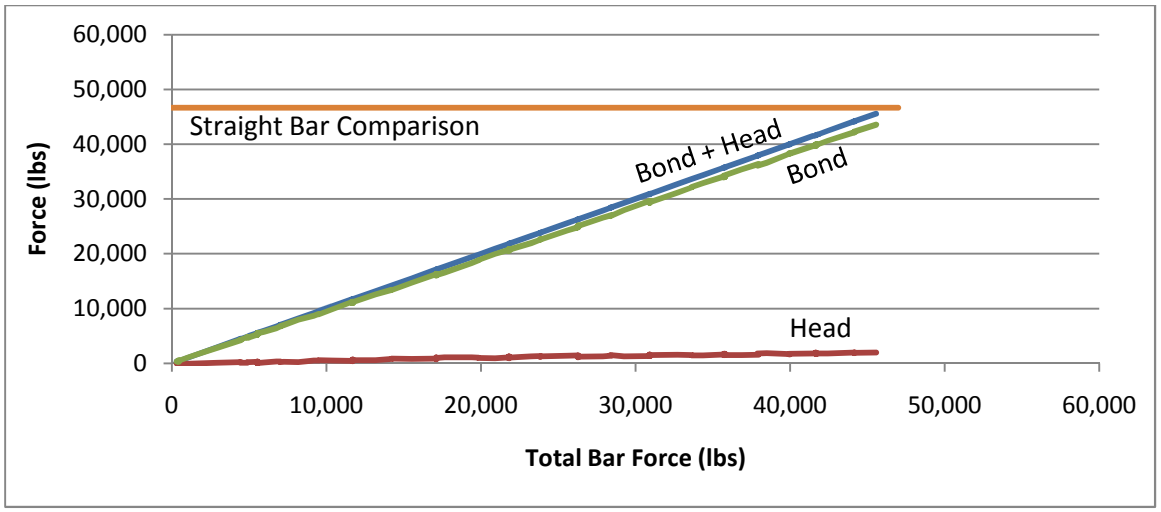

Figure 78: Specimen 3.5-16-2 Bond and Head Contributions versus Total Bar Force.

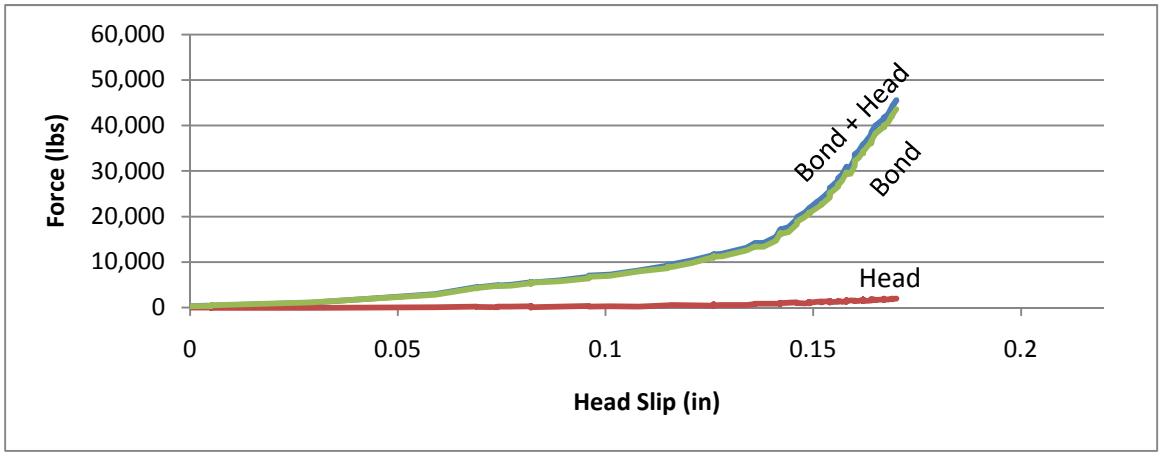

Figure 79: Specimen 3.5-16-2 Bond and Head Contributions versus Head Slip.

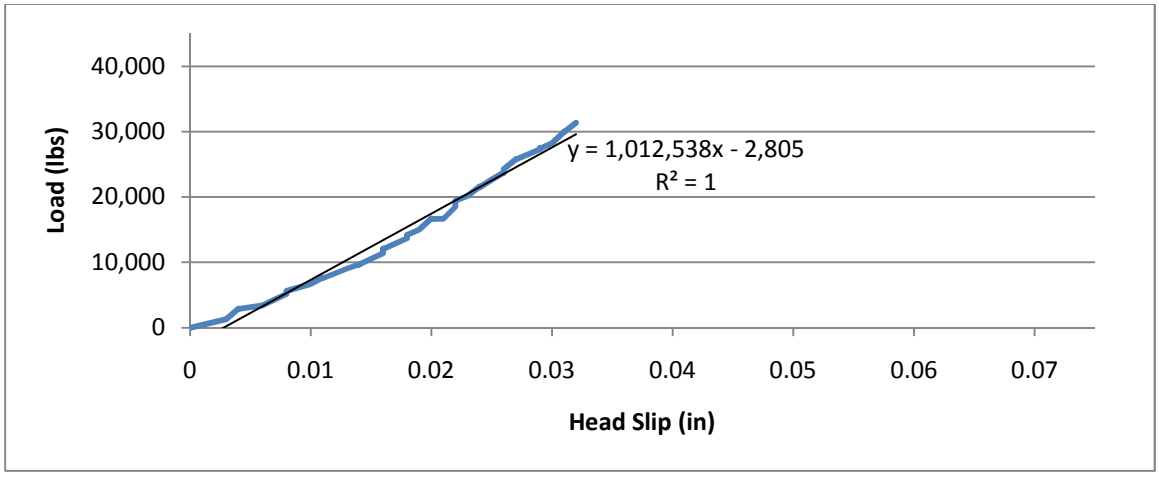

Figure 80: Specimen 3.5-16-2 Stiffness.

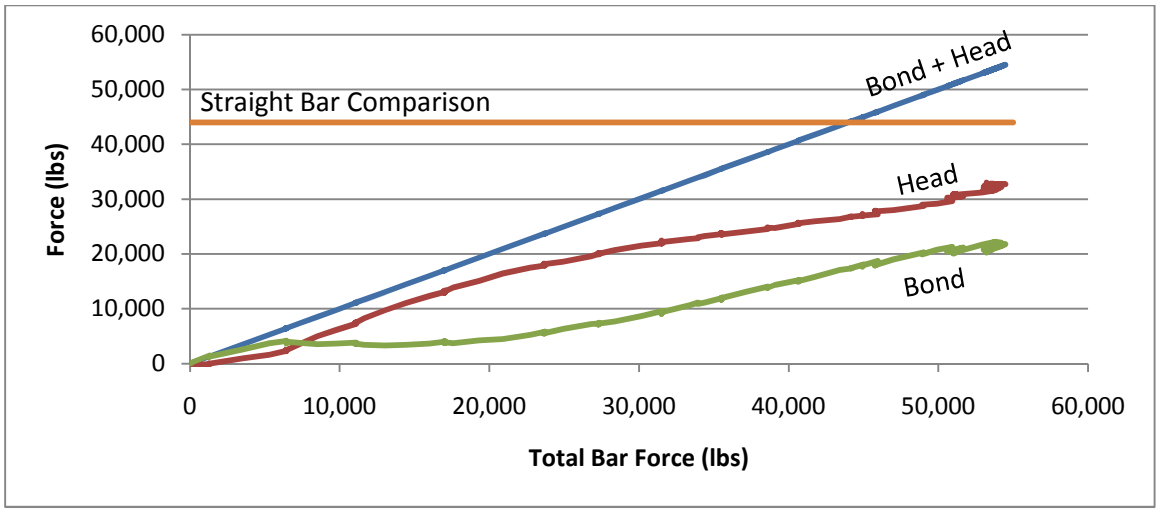

Figure 81: Specimen 3.5-8-2 Bond and Head Contributions versus Total Bar Force.

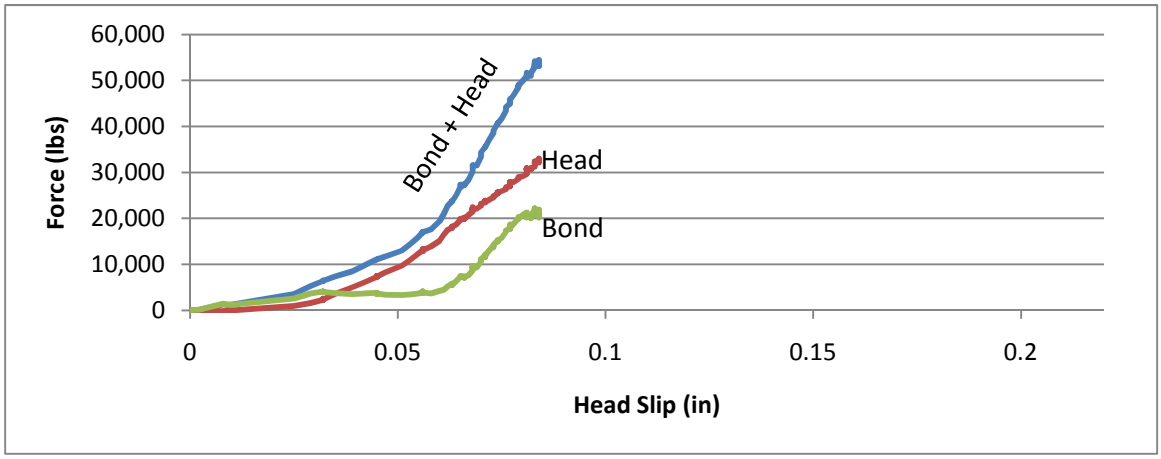

Figure 82: Specimen 3.5-8-2 Bond and Head Contributions versus Head Slip.

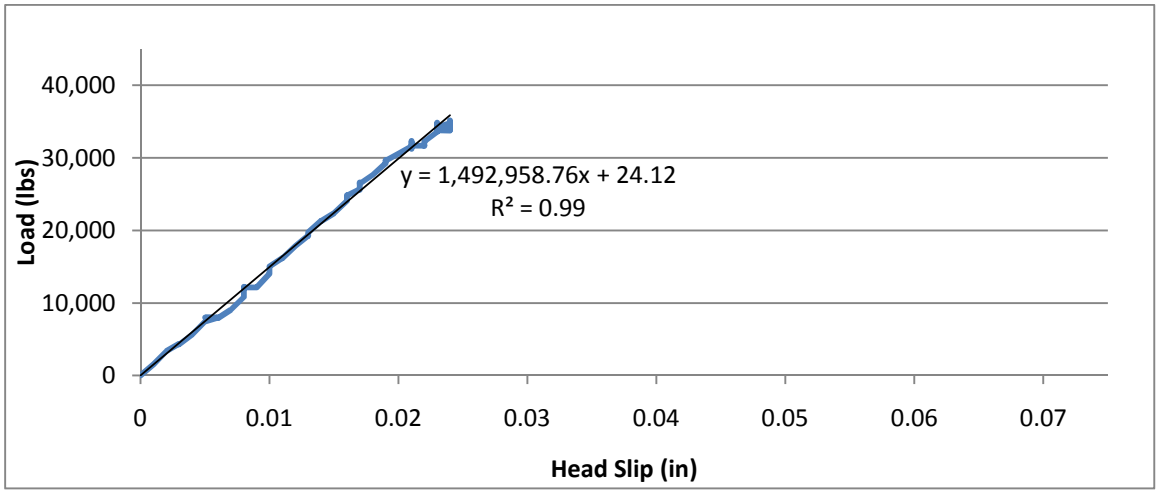

Figure 83: Specimen 3.5-8-2 Stiffness.

Chapter 7: Trends Among the Specimens

7.1: Contributions of Head and Bond

The three variables studied in this test program each had different effects on the degree of head and bond contributions in the specimens.

7.1.1: Effects of Bond Length on Head and Bond Contributions

The bond length of the headed bar had a very consistent effect on the contributions of the head and bond in resisting the total bar load. In all six specimens with sixteen inches of bond length, the bond resisted most of the load. Specimen 9-16-1 (see Figure 48) is typical of these six specimens. In the other six specimens, each with a bond length of eight inches, the load was initially resisted primarily by the bond, but rather quickly was resisted primarily by the head. The total load at the point where the head began resisting more load than the bond was less than 10% of the failure load for five of these six specimens. Specimen 9-8-1 (see Figure 51) is typical of the six specimens where the head resisted most of the failure load. This contribution pattern is very similar to the results found by Chun *et al.*, Thompson, and DeVries (see Figure 31). Figure 84, Figure 85, and Figure 86 compare the head contribution of the six bond length

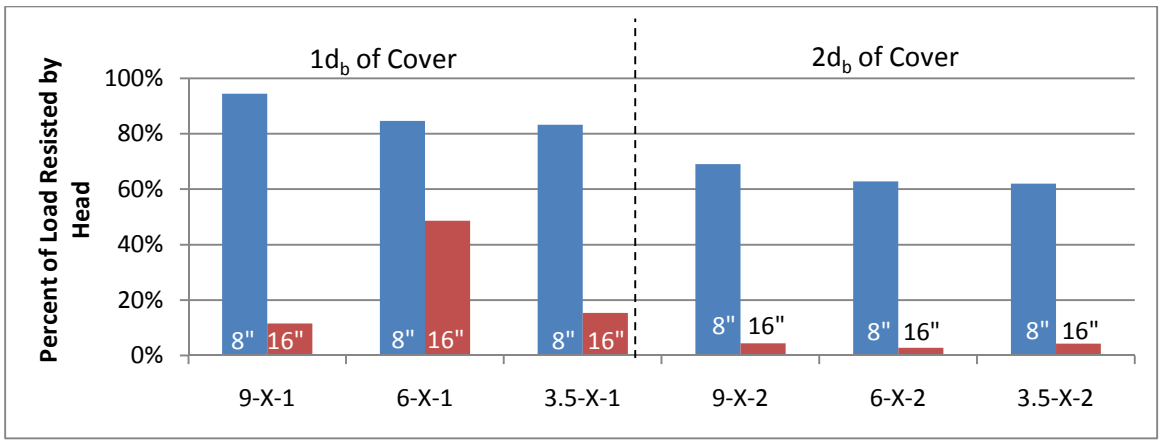

Figure 84: Comparison of Head Contribution at Failure Load Between Specimens with 8" Bond and 16" Bond.

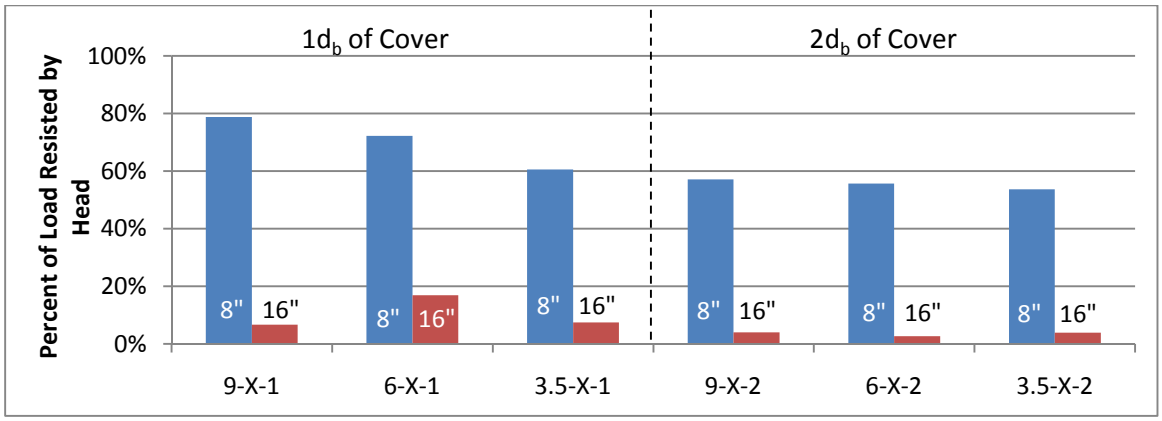

Figure 85: Comparison of Head Contribution at 90% Failure Load between Specimens with 8" Bond and 16" Bond.

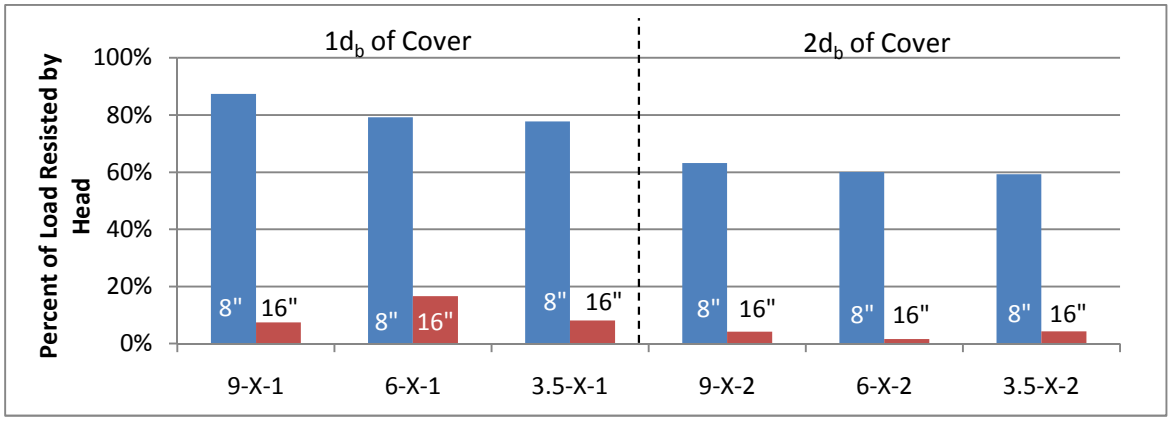

Figure 86: Comparison of Head Contribution at 45,000 lbs load between Specimens with 8" Bond and 16" Bond.

specimen pairs at the three different load levels. Specimen 6-16-1 (see Figure 54) is the lone specimen that doesn't follow the pattern of bond resisting most of the load in specimens with 16" of bond length and heads resisting most of the load in specimens with 8" of bond length. At failure, the head in specimen 6-16-1 resisted 49% of the load (see Figure 84). Up until about the last 3,000 pounds of load, however, the head behaved similarly to the other specimens with 16" of bond length. This specimen was also the only specimen with 16" bond length to fail by side blowout. The irregular head contribution and failure mode might be indicating that a discontinuity from casting may have caused the blowout failure. It is also possible that the strain gauge malfunctioned

and the head may have actually behaved as the rest of the heads in specimens with 16" bond length.

7.1.2: Effects of Cover on Head and Bond Contributions

The depth of clear cover over the bars also had a very consistent impact on the contributions of the head and bond in resisting the load applied to the headed bar. In all six of the pairings where the cover was the only changed variable, the head resisted a higher percentage of the load in the specimens with only one inch of clear cover (see Figure 87, Figure 88, Figure 89). This pattern is rational because stress always goes to the stiffest element available. As the cover decreases, the bond becomes less stiff,

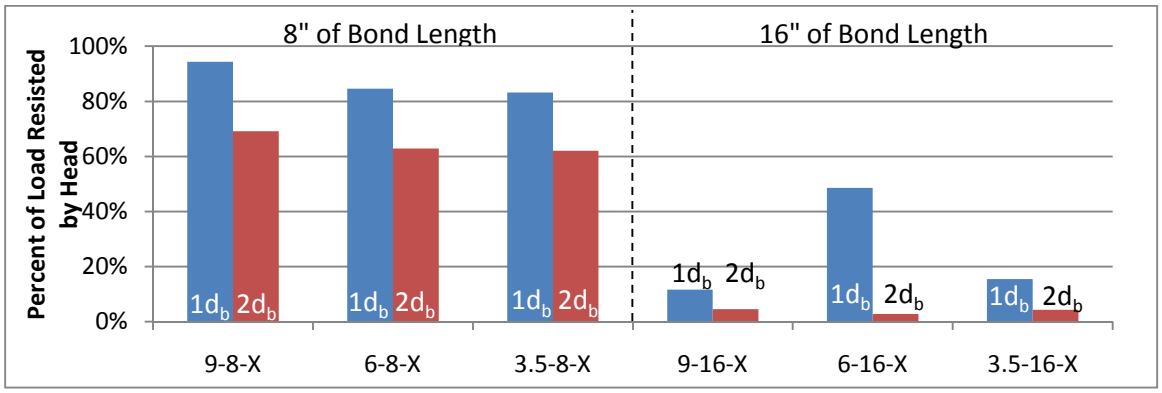

Figure 87: Comparison of Head Contribution at Failure Load between Specimens with $1d_b$ Cover and $2d_b$ Cover.

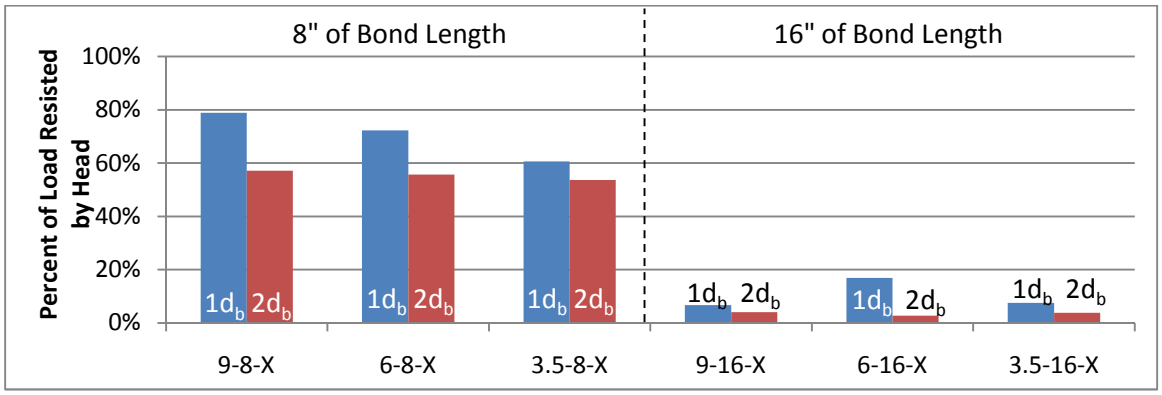

Figure 88: Comparison of Head Contributions at 90% Failure Load between Specimens with $1d_b$ Cover and $2d_b$ Cover.

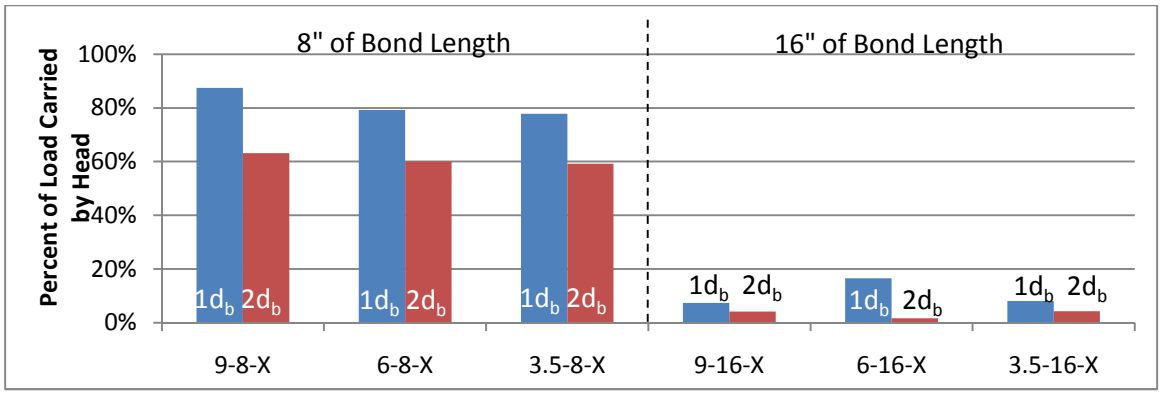

Figure 89: Comparison of Head Contributions at 45,000 lbs load between Specimens with $1d_b$ Cover and $2d_b$ Cover.

making the head relatively stiffer compared to the bond. As the head becomes relatively stiffer, it would naturally assume more load. This suggests that the use of a head provides greater benefit in cases where there is less cover available to help the bond resist the load. Besides being less stiff, the code equations dictate that a bar with less cover has less capacity. So again, the addition of a head might result in a larger capacity increase for a bar with less cover.

7.1.3: Effects of Head Bearing Area on Head and Bond Contributions

The size of the head does not have as consistent of an impact on the Head contribution as the other two variables. Where the bond length is shorter (8") and the head resists the majority of the load at failure, an increase in the head size does increase the amount of load that the head resists (see Figure 90, Figure 91, Figure 92). Whereas the bars with longer bond (16") in which the head resists very little of the load, a larger head does not result in larger loads resisted by the head. However, even for the bars with the shorter bond length, increasing the size of the head doesn't have a drastic impact on the head contribution. The head contribution in the specimen series with eight inches of bond length and one inch of cover at the failure load, for example, increased only 2.4%

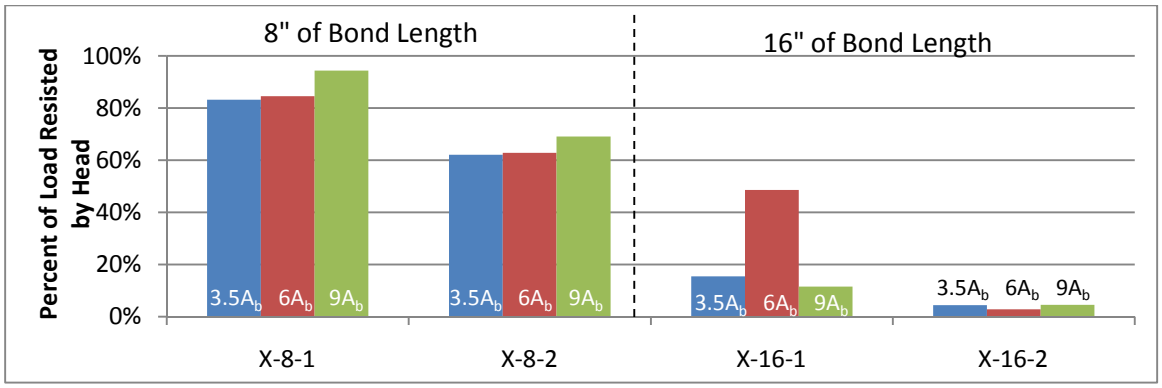

Figure 90: Comparison of Head Contribution at Failure Load between Specimens of 3.5, 6, and $9A_b$ Head Bearing Areas.

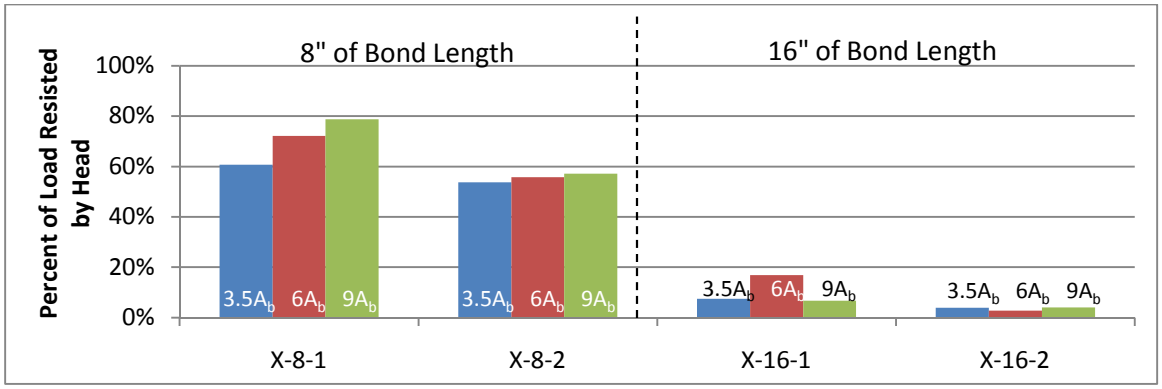

Figure 91: Comparison of Head Contribution at 90% Failure Load between Specimens of 3.5, 6, and $9A_b$ Head Bearing Areas.

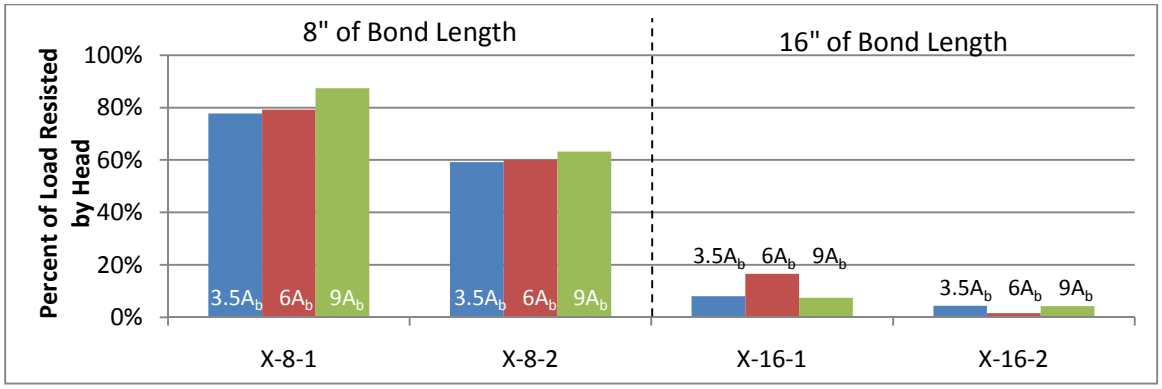

Figure 92: Comparison of Head Contribution at 45,000 lbs load between Specimens of 3.5, 6, and $9A_b$ Head Bearing Areas.

with a 74% head size increase ($3.5A_b$ to $6A_b$) and only 13.5% with a head increase of 165% ($3.5A_b$ to $9A_b$). The specimen with eight inches of bond and two inches of cover resulted in even smaller head contribution increases with increased head bearing area.

Both the specimen series with 16” bond length and 1” cover and the series with 16” bond length and 2” cover also showed very little changes in head contributions due to head bearing area changes excluding specimen 6-16-1. As mentioned in section 7.1.1, specimen 6-16-1 may be an anomaly. These very minor increases in head contributions suggest that the presence of a head on the bar has much more effect on the contributions of the head and bond than does the size of the head. Simply stated, where there was less bond length, the heads resisted most of the load, and where there was more bond length, the heads resisted very little of the load.

Another interesting trend that suggests that the presence of the head is more important than the size of the head is that head size doesn’t have a large impact on the Contribution-Switch load. The Contribution-Switch load is the load at which the head begins to resist more load than the bond. The heads in the specimen group with 8” bond length and $2A_b$ cover all began resisting most of the load between 3,460 lbs and 4,112 lbs or between 7% and 8% of the bar failure load (see Figure 69, Figure 75, Figure 81). This consistency suggests that it might be possible to determine the Contribution-Switch load. Beyond that load on the bar, the head would dominate the capacity equation, while below that point the bond would dominate the capacity equation for the bar. In the specimen group with 8” bond length and $1A_b$ cover, the Contribution-Switch loads for the two larger heads were again very low: between 3% and 6% of the failure load (see Figure 51, Figure 57). The specimen with the small head didn’t begin resisting most of the load until 33% of the failure load, however, it did resist 83% of the failure load of the bar (see Figure 63). The high Contribution-Switch load of specimen 3.5-8-1 could be explained as a result of the bond being much stiffer than the very small head; however, specimen

3.5-8-1, which would have an even stiffer bond from more cover, had a Contribution-Switch load of 7%. This is another place where duplicate specimens would have been beneficial.

7.2: Specimen Stiffness

The stiffness analysis produced trends of varying consistencies with the variables; however, as noted in Chapter 5, it may not be reasonable to make explicit conclusions on the stiffness data. One trend that showed up across all three variables was that the stiffness behaves closer to expectations as a variable is increased or decreased when the other two variables are proportional to each other. For example, specimens with short bond length with small head tend to behave closer to expectations than specimens with short bond length with large head.

7.2.1: Effects of Bond Length on Specimen Stiffness

An increase in bond length results in an increase in specimen stiffness in four of the six specimen pairing where the head size and clear cover were held constant (see Figure 93). The two pairings that didn't result in an increase in stiffness were the pairing

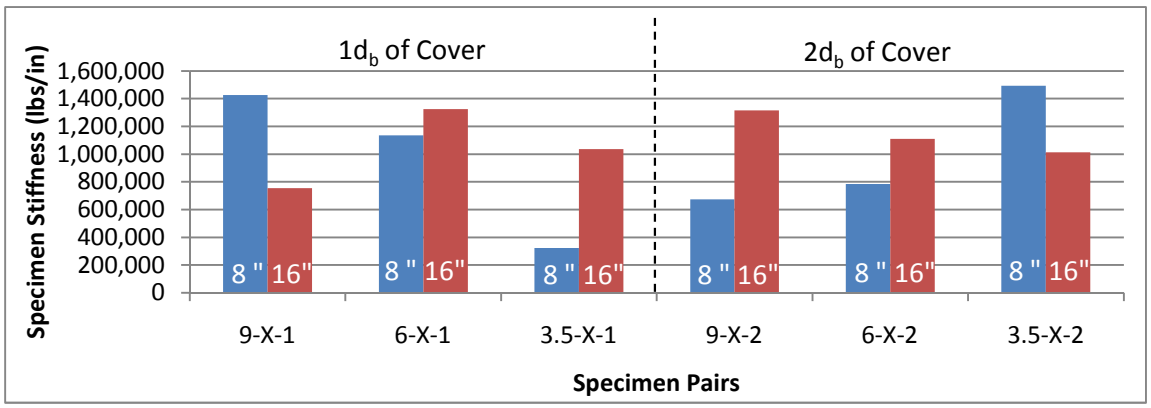

Figure 93: Comparison of Specimen Stiffness between Specimens with 8" and 16" of Bond Length.

with the largest head and one inch of cover, and the pairing with the smallest head and two inches of cover.

7.2.2: Effects of Cover on Stiffness

Increasing the cover over the bar only increased the stiffness of the specimen in two of the six pairings (see Figure 94). Interestingly, the increases in stiffness occurred in specimen pair 3.5-8-X (having the smallest head and short bond length) and pair 9-16-X (having the largest head and long bond length).

7.2.3: Effects of Head Bearing Area on Specimen Stiffness

Finally, increasing the head size only increased the stiffness of the specimen in two of the four groupings: X-8-1 and X-16-2 (see Figure 95). Similar to the pattern of how

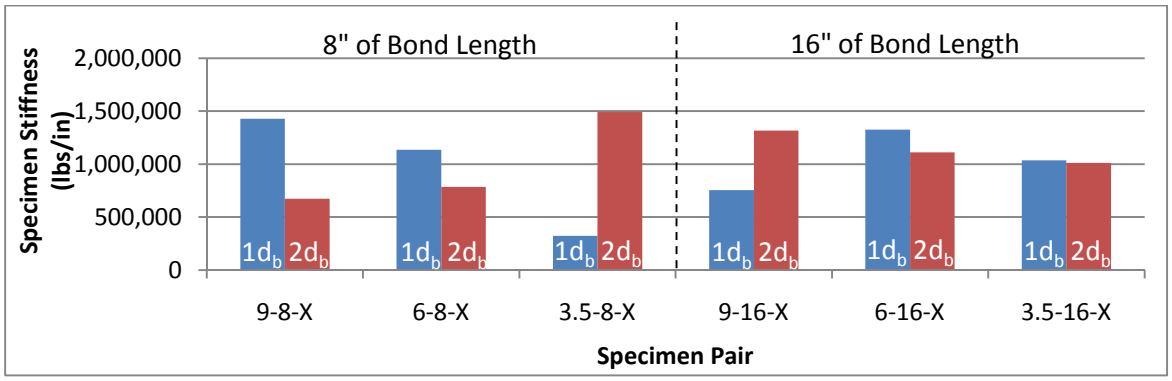

Figure 94: Comparison of Specimen Stiffness between Specimens with $1d_b$ and $2d_b$ Clear Cover.

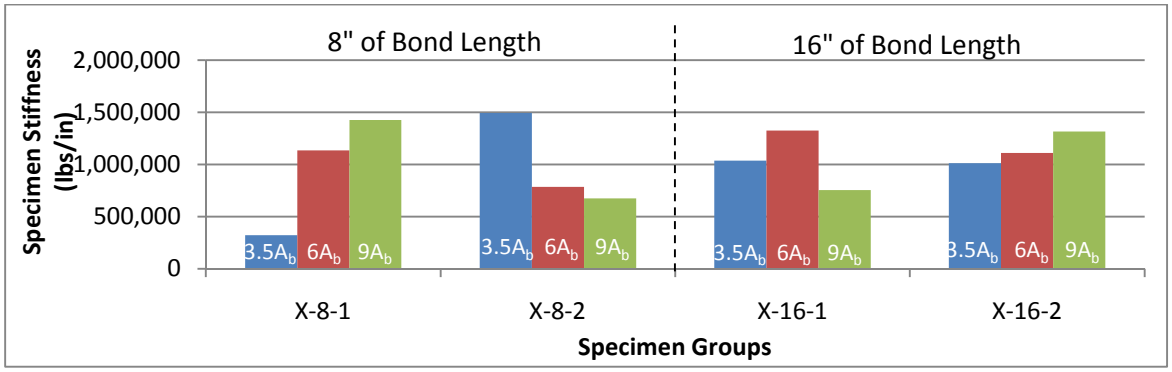

Figure 95: Comparison of Specimen Stiffness between Specimens with 3.5, 6, and $9A_b$ Head Bearing Areas.

cover affects stiffness, increased head bearing area produced increased stiffness in the grouping with short bond length and less cover and the grouping with long bond length and more cover.

7.3: Addition of a Head

A very interesting trend was that in five of the twelve specimens, the addition of a head actually decreased the capacity of the bar (see Figure 96). All five bars that experienced a decrease in capacity compared to a straight bar had 16" of bond length. The sixth bar with 16" bond length exhibited a very small increase in capacity which could have easily been a result of the high variability of concrete in either the headed or straight bar specimen.

7.4: Failure Mode

Whereas it was inappropriate to compare specimen capacities earlier across all twelve specimens due to the different failure modes, this section will compare the

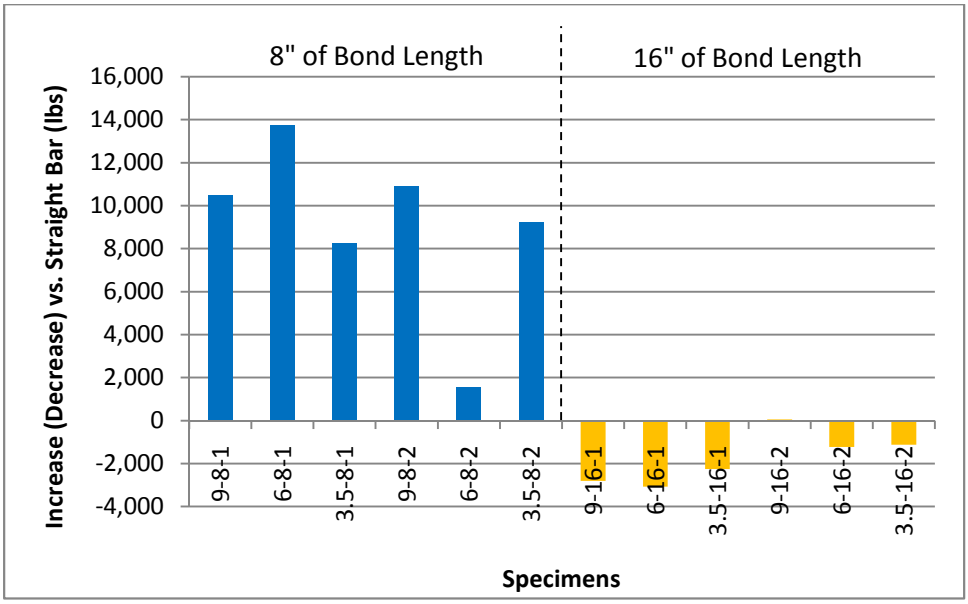

Figure 96: Failure Loads of Specimens Compared to Straight Bars.

capacities of specimens with similar failure modes. In general, the failure mode did not have a noticeable impact on the capacity of each specimen. The capacities of specimens failing from both failure modes cover approximately the same range (see Figure 97).

To analyze the capacities of the specimens for possible trends associated with the variables, it is necessary to only study specimen pairs or groups in which all specimens failed by the same failure mode. Further, the specimen pairs or groups in which the specimens failed by bar yield will not be analyzed because the capacity was dependent on the material strength of the bar only. The range of the specimen capacities only represent the range of the material strength and not the interactions of the head and bond anchoring to the concrete.

7.4.1: Effects of Bond Length on Capacity

In the one bond length pair that failed from side blowout, the capacity increased slightly as the bond length increased (see Figure 98). Because there is only one pairing to

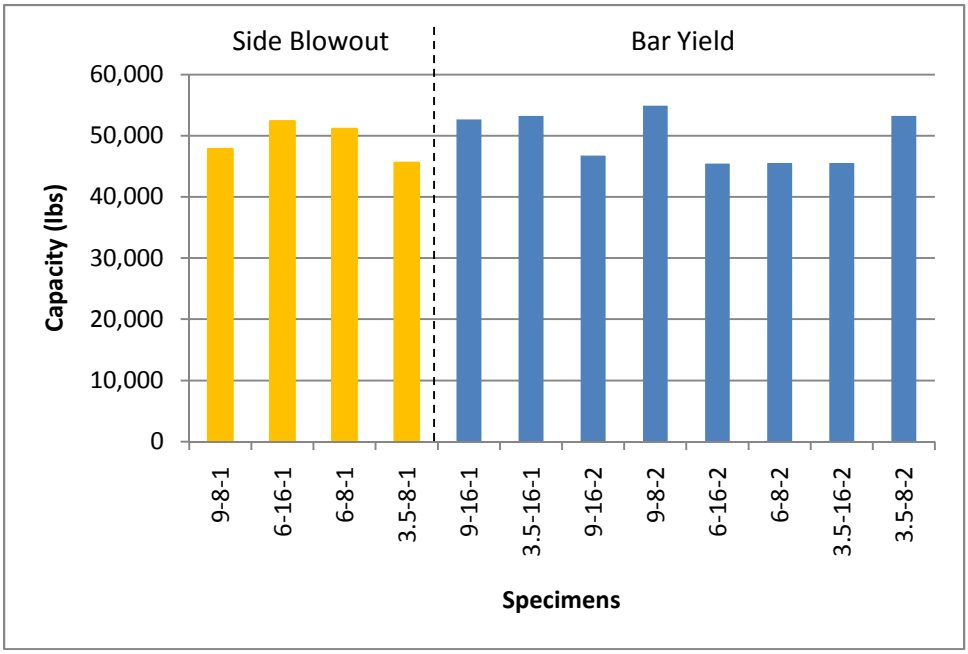

Figure 97: Comparison of Specimen Capacities by Failure Mode.

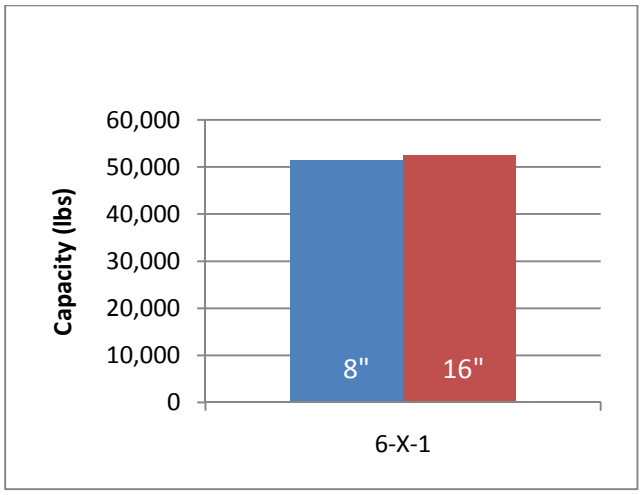

Figure 98: Comparison of Capacity between specimens with 8" and 16" Bond by Failure Mode.

analyze and the capacity increase was so small, it is difficult to conclude the actual impact that bond length has on capacity.

7.4.2: Effects of Cover on Capacity

There were no specimen pairs in which both specimens failed by side blowout therefore, the effects of cover cannot be analyzed.

7.4.3: Effects of Head Bearing Area on Capacity

In the one specimen grouping in which all three specimens failed by side blowout, the capacities of the specimens did not consistently increase or decrease as the head size increased (see Figure 99). This supports the finding from section 7.1.3 that the inclusion of the head is more important than the size of the head.

7.5: Shock Load Effects

Under the assumption that shock loading effects would negatively impact the specimen, it appears that shock loading effects did not result from the testing process for specimen 3.5-8-2. In the head contribution analysis, specimen 3.5-8-2 seems to fit the bond length trend where the head resists much more load where there is only 8” bond

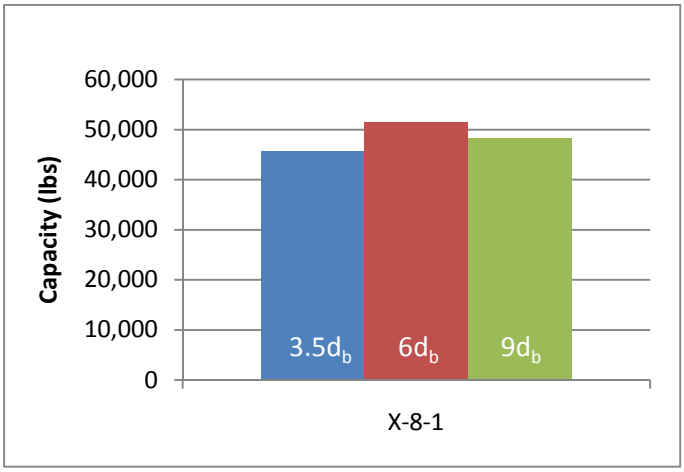

Figure 99: Comparison of Capacity between Specimens with $3.5d_b$, $6d_b$, and $9d_b$ Head Area by Failure Mode.

length (see Figure 84); the cover trend where the head resists more load where there is less cover (see Figure 87); and the head size trend where the head resists more load as the head increases (see Figure 90). In the stiffness analysis, specimen 3.5-8-2 does not seem to fit the bond length trend where stiffness increases with bond length (however, it may be noted that only four of the six pairings behave that way) (see Figure 93); the cover trend where stiffness decreases with cover (however, it may be noted that only four of the six pairings behave that way) (see Figure 94); and there is no clear trend about how head size affects stiffness. Specimen 3.5-8-2 does follow the trend that the head increases the capacity over a straight bar when there is 8" of bond length (see Figure 96). It also appears to fit within the range of capacities of specimens that failed by bar yield (see Figure 97).

Chapter 8: Analysis

8.1: Contributions of Head and Bond

The contributions of the head and bond are heavily influenced by the bond length and clear cover over the bar and only minimally influenced by the bearing area of the head. In the six specimens with a capacity substantially higher than that of a straight bar (all specimens with 8" bond length), the head resisted at least 62%, and as much as 94%, of the failure load of the specimen. In the six specimens with a capacity not substantially higher than that of a bar without a head (all specimens with 16" bond length), the head only resisted up to 15%, and as little as 3%, of the failure load of the specimen. The capacity of specimen 6-16-1 was less than that of a bar without a head, but the head resisted 49% of the failure load. The head and bond contributions analysis indicates that the bond length is the most important variable.

8.2: Specimen Stiffness

The stiffness of a specimen seems to be most consistently influenced by bond length and cover. In four of the six pairings, an increase in bond results in an increase in stiffness; however, the increase in stiffness does not occur at a 1:1 ratio with bond length. The cover also seems to have a strong influence on the stiffness. Four of the six pairs behave similarly; however, the stiffness in those four pairs actually decreases as cover increases. The specimen stiffness analysis confirms that bond length is the most important variable, but also suggests that cover is very important as well.

8.3: Addition of a Head

As was discussed earlier, stress goes to the stiffest element first and these results show where there are sixteen inches of bond, the bond is stiffer than the head. It would be reasonable that the bond should resist all of the load up to the failure load of the straight comparison bar at which point the head would begin resisting most of the load to increase the capacity of the system. This is not the case, though, because even with no head, the sixteen inches of bond was enough to fully develop the bars (even though the code equation requires much more than sixteen inches to fully develop a #8 bar). Further, the data indicated that even though the bond was enough to fully develop the yield strength of the bar, the head did still resist some of the load, which may have ultimately interfered with the bond and been the reason for the decrease in capacity of the bar. This raises an interesting issue: the code requires more than sixteen inches to fully develop a #8 bar which would then require a hook or a head on the bar; however, adding a head actually decreased the capacity of the bar so adding the head doesn't provide any benefit. It could be argued that an even larger head might increase the capacity of the bar; however, as this test showed, large increases in head size provided relatively small increases in the contribution of the head. The analysis of adding a head indicates that the presence of a head is more important than the head itself. This implies that it may be acceptable to not consider the size of the head in a design equation and simply require a minimum head size.

8.4: Failure Mode

As a result of only comparing specimen groups in which all specimens failed by side blowout, there was almost no data to analyze. Increased bond length produced a

very small increase in capacity and head bearing area did not show any consistent pattern. In both cases, the very small amount of data inhibits the ability to make any conclusions.

8.5: Comparison of Other Models

Several models will be compared with respect to the measured capacity of the test specimens. The models include Equation (4) developed by Chun *et al.*, Equations (6), (7), and (8) developed by DeVries, Equation (13) developed by Thompson, and the current code equation, Equation (14). Table 9 features each specimen's test-capacity as a percentage of the model-capacity. The test-capacity to model-capacity ratio for a conservative model should be greater than 100% and a model that closely fits the test results should have a low standard deviation. Chun *et al.*'s model appears to fit the test data the closest with the lowest standard deviation and an average fairly close to 100%. DeVries's Equation (6) model and Thompson's model are somewhat close to a good fit while DeVries's other two models and the code model have extremely high standard deviations. As was determined earlier in this report, however, there is a big difference in

Table 9: Comparison Test-Capacity to Model-Capacity.

Specimen	Chun *et al.*	DeVries			Thompson	Code
		Eq. (6)	Eq. (7)	Eq. (8)		
9-16-1	92%	94%	171%	186%	120%	96%
9-8-1	85%	86%	157%	171%	104%	175%
6-16-1	112%	120%	197%	230%	147%	95%
6-8-1	110%	117%	192%	225%	134%	187%
3.5-16-1	138%	167%	240%	308%	182%	97%
3.5-8-1	117%	143%	205%	263%	150%	165%
9-16-2	83%	55%	61%	83%	65%	85%
9-8-2	99%	66%	73%	100%	75%	205%
6-16-2	97%	68%	68%	100%	77%	83%
6-8-2	98%	69%	68%	101%	74%	167%
3.5-16-2	117%	94%	81%	131%	100%	83%
3.5-8-2	140%	112%	97%	157%	113%	198%
Average	**107%**	**99%**	**134%**	**171%**	**113%**	**136%**
Standard Deviation	**18%**	**33%**	**63%**	**70%**	**37%**	**48%**

the way the head and bond perform in relationship to the bond length. Because all of these models were developed for bars in which the head resists a significant portion of the load, it might be useful to examine the head-dominated (bond length of 8") and bond-dominated (bond length of 16") specimens separately to see if the bond-dominated specimens inflated the averages or standard deviations (see Table 10 and Table 11). With the bond-dominated specimens removed (see Table 10), the average test-capacity to model-capacity ratios stayed about the same or decreased slightly, while the standard deviations decreased for all but one model. From just the six head-dominated specimens, Chun *et al.*'s model still appears to be the most accurate, but Thompson's model also appears to be very accurate. It is very interesting that DeVries's Equation (6) model still appears accurate, considering the fact that his model was developed from a pull-out limit

Table 10: Comparison of Test-Capacity to Model-Capacity for Head-Dominated Specimens.

Specimen	Chun *et al.*	DeVries			Thompson	Code
		Eq. (6)	Eq. (7)	Eq. (8)		
9-8-1	85%	86%	157%	171%	104%	175%
6-8-1	110%	117%	192%	225%	134%	187%
3.5-8-1	117%	143%	205%	263%	150%	165%
9-8-2	99%	66%	73%	100%	75%	205%
6-8-2	98%	69%	68%	101%	74%	167%
3.5-8-2	140%	112%	97%	157%	113%	198%
Average	**108%**	**99%**	**132%**	**169%**	**108%**	**183%**
Standard Deviation	**18%**	**28%**	**55%**	**60%**	**28%**	**15%**

Table 11: Comparison of Test-Capacity to Model-Capacity for Bond-Dominated Specimens.

Specimen	Chun *et al.*	DeVries			Thompson	Code
		Eq. (6)	Eq. (7)	Eq. (8)		
9-16-1	92%	94%	171%	186%	120%	96%
6-16-1	112%	120%	197%	230%	147%	95%
3.5-16-1	138%	167%	240%	308%	182%	97%
9-16-2	83%	55%	61%	83%	65%	85%
6-16-2	97%	68%	68%	100%	77%	83%
3.5-16-2	117%	94%	81%	131%	100%	83%
Average	**107%**	**100%**	**136%**	**173%**	**117%**	**90%**
Standard Deviation	**18%**	**37%**	**70%**	**78%**	**43%**	**6%**

state test and didn't include any strut and tie analysis. When removing the head-dominated specimens (see Table 11), the averages increased or stayed relatively the same for five of the six models, and surprisingly decreased dramatically for the code model. The standard deviations also increased or stayed relatively the same for the same five models while the standard deviation for the code model drastically decreased. As for the first five models, this indicates that the models do fit better the specimens that are dominated by the head. As for the code equation, the low standard deviation and average close to 100% suggests that it is a good fit for headed bar applications where the bond is expected to dominate.

These results certainly suggest that there are two behavior patterns that headed bars will follow – head-dominated and bond-dominated – and that each pattern should be defined by different models.

8.6: Model Development

If there are to be two models for headed reinforcement, it is necessary to have a cut-off point to determine which model to use. Because bond length seems to have the most impact regarding whether the bar will be head-dominated or bond-dominated, the cut-off point should depend on bond length. In the design process, once the size of the reinforcing bar is determined, the required development length can be determined for that size bar. The required development length is then compared to the available embedment length to determine if a straight bar can full develop or if something extra such as a hook or head is needed. It seems reasonable that the cut-off point could be determined from the required development length and the available embedment length. The required development length was calculated for a #8 bar as used in this test using the code

equations. The required development length from section 12.2.2 of ACI 318-08 [5] for bars that meets the minimum spacing and cover dimensions is

$$l_d = \left(\frac{f_y}{20\sqrt{f_c'}} \right) d_b \quad , \tag{15}$$

and the required development length for bars that don't meet the minimum spacing and cover dimensions is

$$l_d = \left(\frac{3 f_y}{40\sqrt{f_c'}} \right) d_b \quad , \tag{16}$$

and the general equation for required development length from section 12.2.3 is

$$l_d = \left(\frac{3}{40} \frac{f_y}{\sqrt{f_c'}} \frac{1}{\left(\frac{c_b + K_{tr}}{d_b} \right)} \right) d_b \quad , \tag{17}$$

$$K_{tr} = \frac{40 A_{tr}}{sn} \quad ,$$

where:

A_{tr} = area of transverse reinforcing (in^2), in this case is zero,

s = the spacing of the transverse reinforcement,

and

n = the number of transverse reinforcing bars.

Table 12 reports the required development lengths calculated from Equations (15), (16), and (17) as found in the ACI 318-08 code [5]. Table 13 features the bond length present in the test specimens as a percentage of the required bond length for a #8 bar which was used in the tests. If a cut-off ratio of available embedment length as a

Table 12: Code Required Development Lengths.

Code Equation	$1d_b$ Cover	$2d_b$ Cover
Section 12.2.2 (with spacing & Cover Minimums)	47”	
Section 12.2.2 (“Other Cases”)	71”	
Section 12.2.3 (Equation 12-1)	47”	28”
Minimum	47”	28”

Table 13: Bond Length of Test Specimens as a Percentage of the Required Bond Length for a #8 Bar.

	$1d_b$ Cover	$2d_b$ Cover
16” Bond	34%	57%
8” Bond	17%	29%

percentage of required development length of 30% was used, that would put all of the specimens with 8” bond length in the head-dominated range and all the specimens with 16” bond length in the bond-dominated range. With the distinction between head-dominated and bond-dominated specimens set, design equations are needed.

8.6.1: Bond-Dominated Bars

As discussed earlier, the ACI 318-08 [5] code equation for a headed bar, Equation (14), appears to fit the bond-dominated, tested specimens well with a standard deviation of only 6% which is very low for the high-variability nature of concrete. The average test-capacity to model-capacity percentage is only at 90%, but should absolutely be higher than 100%. Further, it should be significantly higher than 100% to offer a factor of safety. If the coefficient is increased from 0.016 to 0.022, the equation becomes

$$l_d = \left(\frac{0.022 f_y}{\sqrt{f_c'}} \right) d_b \quad . \tag{18}$$

Recalculating the model capacity produces new test-capacity to model-capacity percentages (see Table 14). The standard deviation remains very low while the average percentage increases to 123% which is much better and the percentage of test-capacity to

Table 14: Comparison of Test-Capacity to Model Capacity for Bond-Dominated Specimens using the Modified Code Equation.

Specimen	Modified Code Equation (18)
9-16-1	131%
6-16-1	131%
3.5-16-1	133%
9-16-2	117%
6-16-2	114%
3.5-16-2	114%
Average	**123%**
Standard Deviation	**9%**

model-capacity for all the specimens is above 100%. Changing the coefficient to 0.022, however, may not be an optimal solution. Heads should be a better option than hooked bars and thus require a shorter development length. The current coefficient in the ACI 318-08 [5] model for hooked bars is 0.02:

$$l_d = \left(\frac{0.02 f_y}{\sqrt{f_c'}} \right) d_b \quad , \tag{19}$$

which results in a shorter development length than would be required by the proposed coefficient for headed bars. For headed bars to retain their advantages, the required development length should be no more than that required for hooked bars.

8.6.2: Head-Dominated Bars

The head-dominated specimens are not as simple. As indicated in Table 10, the model with the lowest standard deviation (the code model) had an extremely high test-capacity to model-capacity ratio of 183%, and the other models were not any better. In an attempt to develop a model for head-dominated bars from this test program, the capacities of the head-dominated bars are plotted against cover (see Figure 100), and head bearing area (see Figure 101). Bond length is left out because all the specimens

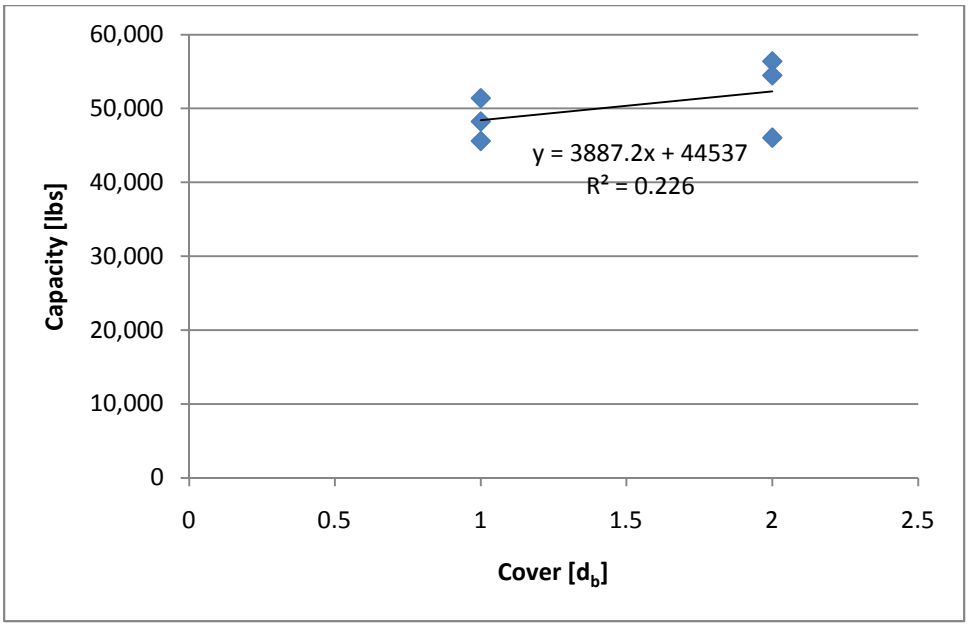

Figure 100: Specimen Capacities by Cover.

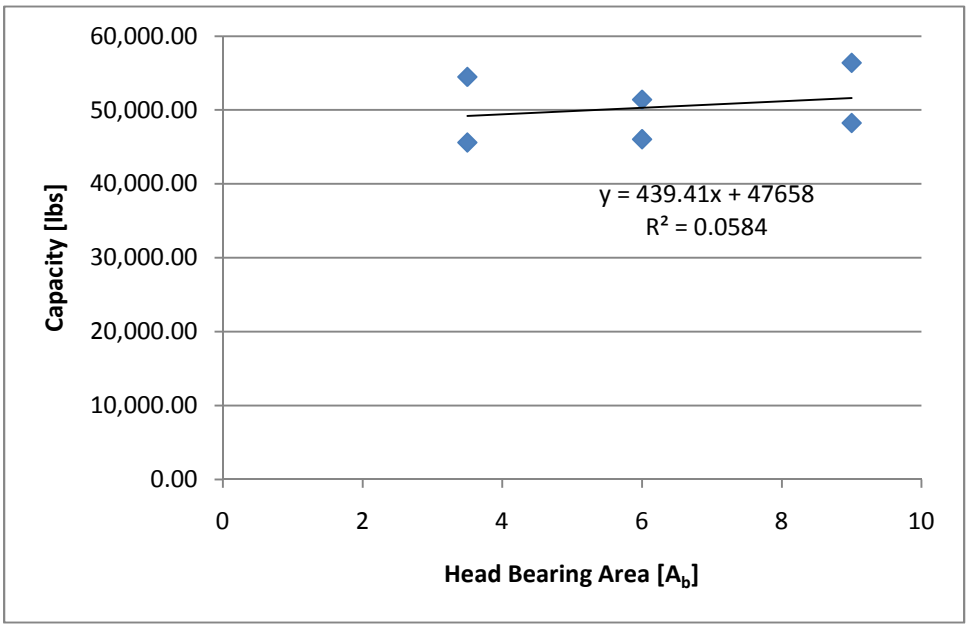

Figure 101: Specimen Capacities by Head Bearing Area.

have 8" bond length. Neither graph, however, provides great assistance in developing a capacity model because in each graph, the ranges of capacities for each variable value are approximately the same as indicated by the very small slope of the trend lines. Therefore, more data are necessary to develop a capacity model from this test program.

Chapter 9: Conclusion

The impacts of bond length, clear cover and head bearing area were studied to understand the behavior of the head and bond in resisting a tensile load on a headed bar. It was found that the contributions of the head and bond follow two distinct patterns dependent on the bond length. Where there is sufficient bond length, the bar is dominated by the bond capacity, and where there is little bond length, the bar is dominated by the head capacity. As such, in a design scenario, different models should be used to determine required development length and head size. The clear cover also had a very consistent impact on the head and bond contributions, although the difference was not nearly as dramatic as from the bond. In all specimens, the head resisted more force when there was $1d_b$ of cover than compared to $2d_b$ of cover. The head bearing had little impact on the head and bond contributions and it was determined that the addition of the head was more important than the size of the head.

From comparing the test specimens to the models proposed in the articles reviewed in this project and the ACI 318-08 code models, it was determined that none of the models accurately represented the general population of the specimens. It was found, however, that with minor modification, the code equation could be a good fit for specimens that are dominated by the bond. An attempt was made to develop a model from the data collected in this report for specimens that were dominated by the head; however, it was determined that there were insufficient data available. Therefore, to develop a model for head-dominated bars, more testing should be conducted.

References

[1] DeVries, Richard A. December 1996. “Anchorage of Headed Reinforcement in Concrete.” Ph.D., University of Texas at Austin.

[2] Chun, Sung-Chui, Bohwan Oh, Sung-Ho Lee and Clay J. Naito. September-October 2009. “Anchorage Strength and Behavior of Headed Bars in Exterior Beam-Column Joints.” *ACI Structural Journal* Vol. 106(5), pp. 579-590.

[3] Zimdahl, Jamie L. May 2009. “The Behavior of Headed Reinforcement in Concrete Members with an Applied Tensile Load.” Master’s Thesis, Milwaukee School of Engineering.

[4] Thompson, Michael K. May 2002. “The Anchorage Behavior of Headed Reinforcement in CCT Nodes and Lap Splices.” PhD diss., University of Texas at Austin.

[5] American Concrete Institute (ACI). 2008. *Building Code Requirements for Structural Concrete (ACI 318-08) and Commentary.* ACI 318-08. Farmington Hills, Michigan: American Concrete Institute.

[6] Bolda, Jacob. 2010. Untitled Capstone Report in Progress about Straight and Hooked Reinforcing Bars. Master’s thesis, Milwaukee School of Engineering.

Appendix A: Zimdahl's Specimens

Table A-1: Zimdahl's Specimen Details and Stiffness's[1].

Specimen	Stiffness (lb/in)	Average Specimen Designation	Average Stiffness (lb/in)	Adjusted Stiffness (lb/in)
1HB00M	161,153	1HB00	200,805	200,805
1HB00R-1	240,456			
1HB08M	1,444,178	1HB08	831,840	333,529
1HB08R-1	219,501			
1HB16M	387,760	1HB16	307,878	307,878
1HB16R-1	227,996			
2HB00M	1,798,045	2HB00	1,145,053	386,067
2HB00R-1	492,061			
2HB08M	785,914	2HB08	611,149	611,149
2HB08R-1	436,384			
2HB16M	614,377	2HB16	520,599	520,599
2HB16R-1	426,820			

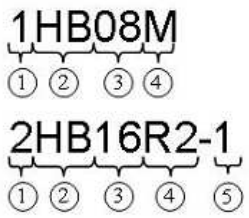

1. Clear Cover Depth (in d_b)
2. Headed Bar
3. Bonded Length (in Inches)
4. Testing Method (M = Monotonic, R = Repeated Loading, R2 = Repeated Loading)
5. Loading Cycle (for Repeated Loading only)

Figure 15 - Specimen Designation.

Figure A-1: Zimdahl's Specimen Name Description[2].

1 Zimdahl, Jamie L. May 2009. "The Behavior of Headed Reinforcement in Concrete Members with an Applied Tensile Load." Master's Thesis, Milwaukee School of Engineering.

2 Zimdahl, Jamie L. May 2009. "The Behavior of Headed Reinforcement in Concrete Members with an Applied Tensile Load." Master's Thesis, Milwaukee School of Engineering.

Structural Engineering

Capstone Report Approval Form

Master of Science in Structural Engineering – MSST

Milwaukee School of Engineering

This capstone report, titled “Head and Bond Contributions of a Headed Reinforcing Bar as used in Concrete Construction,” submitted by the student Andrew M. Blau, has been approved by the following committee:

Faculty Advisor: _____ Date: _____

Dr. Richard DeVries

Faculty Member: _____ Date: _____

Dr. Douglas Stahl

Faculty Member: _____ Date: _____

Chris Raebel